Electromagnetically induced transparency in multi-level atomic systems

A Thesis Submitted for the Degree of

DOCTOR OF PHILOSOPHY

By

AZEEM BAIG MIRZA

School of Physics

University of Hyderabad

Hyderabad 500 046

India

July 2016

Dedicated

to

My Sister

DECLARATION

I hereby declare that the matter embodied in this thesis entitled "**Electromagnetically induced transparency in multi-level atomic systems**" is the result of investigation carried out by me in the School of Physics, University of Hyderabad, Telangana, India, under the direct supervision of Prof. Suneel Singh. I hereby agree that my thesis can be deposited in Shodganga/INFLIBNET.

A report on plagiarism statistics from the University Librarian is enclosed.

(Azeem Baig Mirza)

Place: Hyderabad

Date:

CERTIFICATE

This is certified that the work contained in this thesis entitled "**Electromagnetically induced transparency in multi-level atomic systems"** has been carried out by Mr. Azeem Baig Mirza (Reg.No.09PHPH01), under my direct supervision and the same has not been submitted for any degree or diploma at this or any other University.

Place: Hyderabad
Date:

Prof. Suneel Singh

Dean
School of Physics

ACKNOWLEDGEMENTS

I would like to express my sincere gratitude to my supervisor, Prof. Suneel Singh for his continuous guidance, instigation and encouragement throughout my Ph.D programme.

I would like to thank Prof. D. Narayana Rao, Prof. P. Ananta Lakshmi and Dr. Ashok Vudayagiri for their valuable suggestions during the doctoral committee meetings. I convey my sincere thanks to Prof. R. Singh, Dean, School of Physics, former Deans Prof. S. Chaturvedi, Prof. S.P. Tewari, Prof. C. Bansal and faculty members for their co-operation in providing facilities in the School.

I would like to express my special thanks to my colleague (senior) Dr. M. Anil Kumar for his constant support, great encouragement and friendly nature. My special word of thanks to my friend D. Sanjeev Kumar for his help in computational techniques.

I convey my special thanks to my close friends Dr. G. Sriram, Shaik Ahmed for constantly supporting and encouraging me being throughout this period. I want thank my friends in this campus Dr. Aadi, Dr. Majji, Anji for their help, cheering chats and continuous support throughout the time.

I want to thank my VAX-lab seniors Dr. Sudha Nirmala and Dr. N. Shankaraiah for their support, encouragement and friendly lab atmosphere. It is my pleasure to express thanks to my Ph.D batch mates G.Thiupathi, J. Ananthaiah, Ch. Narasimha Raju, K. Rama Obulesu, K. Lakshun Naidu, G. Srinu, R.Kuladeep for their cheerful company.

It is my great pleasure to thank my childhood friends Santhosh, Harishankar and P. Rakesh for their suggestions, chats and continuous support throughout the course of my Ph.D.

I would like to thank T. Abraham, N. Shailaja, Prasad and other non-teaching staff for their help and support at various stages when needed. Financial assistance in the form of Ph.D fellowship from UoH (BBL fellowship), UGC-BSR (University Grants commission-Basic Science Research), is gratefully acknowledged.

The unconditional love of my family made me what I am today and I owe a lot to them. A simple thanks to you all my family is not enough and this dissertation is dedicated to you all.

..... **Azeem**

Abstract

Electromagnetically induced transparency (EIT) is a phenomenon in which one resonant laser beam propagating through the medium will get absorbed, but when two resonant laser beams propagate simultaneously through the same medium, neither will be absorbed due to the quantum interference between them, and the opaque medium is turned into transparent one. The aim of this dissertation is to develop general theoretical models to study the modification of EIT and its applications in both homogeneous (radiative) and Doppler broadened media comprising multilevel systems such as those formed with inclusion of one or more additional levels and additional fields in the basic three level lambda (Λ), vee (V) and cascade (ladder- Ξ) systems. In Chapter 2 we study wavevector mismatch effects (arising due to counter propagating probe-coupler wavevector mismatch along v_z direction) on EIT in four-level Y-type (dual-ladder) system. In Chapter 3, we explore the feasibility of attaining simultaneous dual electromagnetically induced transparency and efficient nonlinear generation in different configurations of Doppler broadened diamond (double-cascade) systems. In Chapter 4, we propose a simple and easy to implement scheme for superluminal (and subluminal) light propagation of both probe and signal fields in a radiative and Doppler broadened medium comprising highly symmetric double ladder (◊) systems. Chapter 5 deals with study of effect of various wavevector mismatch regimes (depending upon choice of control field transitions) on EIT of a probe field in a Doppler broadened five-level (K-type) and in four-level (Y-type, inverted Y-type) systems of ^{87}Rb atomic medium. Summary and conclusions are presented in Chapter 6.

Table of Contents

Chapter 1

Introduction

1.1. Introduction

Absorption and dispersion properties of a monochromatic light (probe) whose frequency is near resonance with frequency separation between two levels of an atomic transition can change drastically if transitions to other atomic levels are also included. This is the case, for instance, in three level atoms where an additional transition to either a meta-stable ground (Λ- configuration) or stable upper state (Ξ - configuration) is driven by a relatively strong laser (control) field. Under these circumstances it was found that the absorption of the resonant probe laser is highly reduced as it propagates through an otherwise opaque medium. This phenomenon, termed electromagnetically induced transparency (EIT) [1, 2] is actually a manifestation of laser-field-induced atomic coherences and interference effects. For a given (two-level) transition process it is seen to arise from destructive interference between alternative laser-induced atomic transition amplitudes (or atomic coherences) when the frequencies of the two applied laser beams fulfill two-photon (or Raman) resonance condition. For near resonance lasers, this two-photon resonance condition can be achieved by letting a frequency detuning of one laser from its resonant transition be equal to a frequency detuning of the other laser.

The foundations of EIT were laid in an early work of Tewari and Agarwal [3] who in 1986 and the later works of Kocharovskaya and Khanin in 1988 where they

reported “Coherent amplification of an ultrashort pulse in a three level medium without population inversion” [4] and Steven Harris and coworkers who reported “Lasers without Inversion: Interference of Lifetime Broadened Resonances” in 1989 [5]. However the first experimental observation and theoretical formulation of actual EIT in optically opaque strontium vapor was done by the Harris group in 1991 [1].

The basic interaction schemes of atomic levels and laser fields initially employed for studying EIT effect are the simple three level lamda (Λ), vee (V) and cascade (ladder - Ξ) systems in which the resonant one-photon (probe) transition takes place between states of opposite parity. The interaction schemes however are somewhat different in each of these three level systems. For example in Λ- scheme [1, 6, 7] two ground states are coupled by two fields through a common single upper level. Whereas in V- scheme [8] two higher levels are coupled by two fields via a single ground level and in ladder or cascade (Ξ) scheme [9] an upper level is coupled with the ground level through an intermediate level. Obviously these atomic systems display EIT effects under distinct actions of driving fields. All the above mentioned three or higher level schemes can readily be realized in various media such as, the alkali vapors [2] semiconductors [10] and in solids [11].

The immense interest in laser-field-induced coherences and the ensuing interference effects stems from the fact that they may serve as very useful and important tools in atomic physics and optical physics [2, 12, 13] for both their fundamental features and potential applications. In addition to electromagnetically induced transparency [1, 2] laser-induced coherence and interference effects on the two-photon Raman transition also give rise to many other interesting phenomena such as coherent population trapping [14] lasing without inversion [4, 5, 15] electromagnetically induced focusing and defocusing [16] and quantum computation, communication [17]. Apart from nearly zero absorption at resonance, strong dispersion near resonance is also equally interesting as the steepness of the dispersion function [18] near resonance plays the key role for reduction of group velocity of light pulse in the medium [19] and is directly related to the line width of the EIT resonance. Furthermore EIT can be also used for enhancing nonlinear optical processes including nonlinear frequency conversion [20] and high-resolution spectroscopy [21]. In

addition, EIT can be used in squeezed-light generation [22], low-light-level photon switching [23] and in entanglement generation [24]. Very narrow EIT resonances are also of immense interest for important applications in sensitive magnetometer [25], precision spectroscopy [26] and frequency standards [27].

1.2. Motivation

As mentioned above the early works on EIT primarily focused on one-photon transitions between states of opposite parity in simple three level lamda (Λ), vee (V) and cascade (ladder - Ξ) systems. It is natural to expect that higher (than three) or more involved levels structure of atomic system might generate further interesting effects. More complicated level structures such as four-level double Lambda (N) configuration [28], four-level atomic system of diamond (◊) configuration [29], tripod type four-level system [30], the Y [31] and inverted-Y systems [32], and the N-type system [33] etc., are formed by inclusion of an additional fourth level in three level atomic systems which creates additional controllable optical channel. This additional controllable optical channels provides the double-EIT for controlling two independent probe channels [28], four-wave mixing (FWM) process and enhanced frequency conversion [34], polarization qubit phase gate[35] and Five level schemes are also proposed to generate double-EIT and optimal cross phase modulation [36]. The formation of double EIT windows [37] in these is of interest for its applications in six-wave mixing processes [38], storage of light pulse in two channels [39], quantum switching [40], and entanglement generation [41]. Hence it is evident that currently there is considerable interest in the study of EIT and its effect on nonlinear optical interactions in multilevel systems of various configurations.

There however appears to be no explicit study of EIT especially when the systems are Doppler broadened. It would be of interest and important such an analysis, since gaseous atomic media are often used for experimental investigations of the EIT and nonlinear optical processes associated with it. Residual Doppler width of two-photon coherence as well as the Doppler broadening of one-photon coherences arising due to random thermal motion of atoms in a gaseous medium can significantly affect EIT and the associated nonlinear processes. It is therefore essential to examine

EIT as well as the other nonlinear processes such as for example four wave mixing in various Doppler broadened four-level atomic system driven by two additional (pump and coupler) fields.

Our aim to studying modification of EIT and its applications in multilevel systems such as with inclusion of an additional levels in three level lamda (Λ), vee (V) and cascade (ladder- Ξ) systems in both homogeneous(radiative) and Doppler broadened medium. In *radiative broadened medium* the finite lifetime of the excited state leads to a broadening of the spectral line. In *Doppler broadened medium* the random thermal motion of the atoms gives rise to Doppler shifts in the observed frequencies, which leads to a broadening of both two-photon coherence as well as the one-photon coherences which then causes line broadening. We considered different multilevel atomic systems such as four-level Y-type atomic system driven by two strong laser (coupling) fields for study of EIT of a weak probe field in negative residual Doppler broadened medium. A four-level double ladder atomic system consider for study of simultaneous EIT (DEIT) and propagation characteristics of probe and signal generated via nonlinear optical processes such as four wave mixing. The same double ladder configuration is used for studying subluminal and superluminal light propagation for both probe and signal fields in extended Doppler broadened medium. Finally we studied the absorption properties of a probe field in five-level K-type atomic system interacting with three additional strong coherent coupling (control) laser fields with ^{87}Rb atomic medium.

1.3. Interaction of electromagnetic wave with matter

The theoretical explanation of light and the interaction between light and matter is given by Maxwell's electromagnetic theory and the quantum. The combined theory is known as quantum electrodynamics. We present the general methods to describe the basic interaction process between the light and atoms.

1.3.1. Maxwell's equation for the propagation dynamics of a classical EM wave

The electromagnetic field radiation propagation through the medium is governed by Maxwell's equations [42]

$$\vec{\nabla} \cdot \vec{D} = 0 \tag{1.1}$$

$$\vec{\nabla} \cdot \vec{B} = 0 \tag{1.2}$$

$$\vec{\nabla} \times \vec{E} = -\frac{1}{c}\frac{\partial \vec{B}}{\partial t} \tag{1.3}$$

$$\vec{\nabla} \times \vec{H} = \frac{1}{c}\frac{\partial \vec{D}}{\partial t} \tag{1.4}$$

Here $\vec{D}$ is the electric displacement, $\vec{E}$ is the electric field, $\vec{H}$ is the magnetic field and c is the speed of light in vacuum. The electric displacement $\vec{D}$ and the magnetic induction $\vec{B}$ are defined as

$$\vec{D} = \vec{E} + 4\pi\vec{P}, \vec{B} = \vec{H} + 4\pi\vec{M} \tag{1.5}$$

where $\vec{P}$ and $\vec{M}$ is the macroscopic polarization and magnetization of the medium respectively. If the systems consider under non-magnetic medium, implying $\vec{M} = 0$. In this case $\vec{B} = \vec{H}$. Now make the curl of equations Eq.(1.3) and using the Eqs.(1.4) (1.5), we get

$$\vec{\nabla} \times \vec{\nabla} \times \vec{E} + \frac{1}{c^2}\frac{\partial^2}{\partial t^2}\left(\vec{E} + 4\pi\vec{P}\right) = 0 \tag{1.6}$$

Moreover, in isotropic media $\vec{D} = \varepsilon\vec{E}$, where ε is the permittivity of the medium. Therefore from Eq.(1.1), we get $\vec{\nabla} \cdot \vec{E} = 0$. By applying this condition in the above (triple product) Eq.(1.6), then the equation reduced to

$$\nabla^2\vec{E} - \frac{1}{c^2}\frac{\partial^2\vec{E}}{\partial t^2} = \frac{4\pi}{c^2}\frac{\partial^2\vec{P}}{\partial t^2} \tag{1.7}$$

In the following calculations we consider a plane wave, propagating along the z-direction in the medium

$$\vec{E}(z,t) = \vec{\varepsilon}(z,t)e^{i(kz-\omega t)} + c.c., \tag{1.8}$$

where $\vec{\varepsilon}(z)$ is the amplitude of the field with frequency ω, propagation wave vector $\vec{k}$ ($k = |\vec{k}|$). For continues wave laser, the time dependent of $\vec{\varepsilon}$ is negligible. If the electric field is written as in Eq.(1.8) then the response of medium is given by the polarization

$$\vec{P}(z,t) = \vec{p}(z,t)e^{i(kz-\omega t)} + c.c., \tag{1.9}$$

where $\vec{p}$ is a slow varying function of position and time. From Eq.(1.7) with the field propagation along z-direction as in Eq.(1.8), the corresponding equation can be rewritten as

$$\frac{\partial^2 \vec{E}}{\partial z^2} - \frac{1}{c^2}\frac{\partial^2 \vec{E}}{\partial t^2} = \frac{4\pi}{c^2}\frac{\partial^2 \vec{P}}{\partial t^2} \tag{1.10}$$

From Eq.(1.8 and 1.9) the slowly varying variables, $\vec{\varepsilon}(z,t)$ and $\vec{p}(z,t)$, vary at a rate much slower than the carrier frequency ω and $k = c\omega$ is the propagation constant at this frequency. These quantities vary slowly in both time and space such that the following relations are satisfied:

$$k^2|\varepsilon(z,t)| >> k\left|\frac{\partial \varepsilon(z,t)}{\partial z}\right| >> \left|\frac{\partial^2 \varepsilon(z,t)}{\partial z^2}\right|, \; k^2|p(z,t)| >> k\left|\frac{\partial p(z,t)}{\partial z}\right| >> \left|\frac{\partial^2 p(z,t)}{\partial z^2}\right|$$

$$\omega_i^2|\varepsilon(z,t)| >> \omega_i\left|\frac{\partial \varepsilon(z,t)}{\partial t}\right| >> \left|\frac{\partial^2 \varepsilon(z,t)}{\partial t^2}\right|, \; \omega_i^2|p(z,t)| >> \omega_i\left|\frac{\partial p(z,t)}{\partial t}\right| >> \left|\frac{\partial^2 p(z,t)}{\partial t^2}\right|$$

This is called the slowly-varying envelope approximation (SVEA). Using the SVEA Eq.(1.10) reduces from a second-order to a first order partial differential equation,

$$\frac{\partial \varepsilon}{\partial z} + \frac{1}{c}\frac{\partial \varepsilon}{\partial t} = 2i\pi k p \tag{1.11}$$

1.3.2. Formulation: Density matrix equations of motion

To study EIT effect in atomic systems interacting with coherent fields, we followed a semi classical approximation (where electromagnetic fields are treated classically and atom is a quantum object) through which density matrix analysis is considered. This allows us to examine the quantum mechanical atomic coherences and interference effects with the incorporation of various depahsing processes occurring in the atomic medium. As the atomic susceptibility is directly related to atomic coherence established between the levels, it is possible to investigate the absorption and dispersion properties of the system.

Interaction Hamilton:

The Hamiltonian for the combined atom and field system is $H = H_0 + V$, where H_0 is the unperturbed Hamiltonian with the property

$$H_0|j\rangle = W_j|j\rangle \tag{1.12}$$

W_j being the energy of the level $|j\rangle$ and the field-atom interaction term V is given in the electric dipole approximation as

$$V = -\vec{\mu}_{ij} \cdot \vec{E}(t) \tag{1.13}$$

Here, the total electric field $\vec{E}(t)$ can be written as

$$\vec{E}(t) = \sum_\ell \vec{E}_\ell(t) = \sum_\ell \left[\vec{\varepsilon}_\ell \, e^{i(\vec{k}_\ell \cdot \vec{r} - \omega_\ell t)} + c.c. \right] , \tag{1.14}$$

where ω_ℓ ($\vec{\varepsilon}_\ell$) is the frequency (amplitude) and $\vec{k}_\ell$ is the wave vector of the field $\vec{E}_\ell(t)$, and $\vec{\mu}_{ij}$ is the electric dipole matrix element is given by $\vec{\mu}_{ij} = \langle i|\vec{\mu}|j\rangle$.

The interaction Hamiltonian V in the interaction picture (denoted V^{int}) is given by

$$V^{int} = e^{\left(\frac{i}{\hbar}\right)H_0 t}(-\vec{\mu}_{ij} \cdot \vec{E})e^{-\left(\frac{i}{\hbar}\right)H_0 t} \tag{1.15}$$

The time evolution of the density matrix of the system in the interaction representation is

$$\dot{\rho} = \left(\frac{i}{\hbar}\right)\left[\rho, V^{int}\right] = \left(\frac{i}{\hbar}\right)(\rho V^{int} - V^{int}\rho) \tag{1.16}$$

The equation of motion of ij-th element of the density matrix is

$$\dot{\rho}_{ij} = \left(\frac{i}{\hbar}\right)\left[\langle i|[\rho, V^{int}]|j\rangle\right] = \left(\frac{i}{\hbar}\right)(\langle i|\rho V^{int}|j\rangle - \langle i|V^{int}\rho|j\rangle) \tag{1.17}$$

Inserting an orthonormal set of states $|m\rangle$ that, obey the completeness property $\sum_m |m\rangle\langle m| = 1$ between ρ and V^{int} (V^{int} and ρ) in the above equation, we get

$$\dot{\rho}_{ij} = \left(\frac{i}{\hbar}\right)\sum_m \left\{\rho_{im} V^{int}_{mj} - V^{int}_{im}\rho_{mj}\right\} \tag{1.18a}$$

where $\rho_{ij} = \langle i|\rho|j\rangle$ and $V^{int}_{mn} = \langle m|V^{int}|n\rangle$ (1.18b)

The equation of motion Eq.(1.16) can be generalized further to include the various incoherent processes as

$$\dot{\rho}_{ij} = \left(\frac{i}{\hbar}\right)\sum_m \left\{\rho_{im} V^{int}_{mj} - V^{int}_{im}\rho_{mj}\right\} + (\rho_{ij})_{relax} \tag{1.19}$$

Here the term $(\rho_{ij})_{relax}$ includes various relaxation process such as the spontaneous decays (γ_{ij}) of levels, radiative decay and collisional depahsing of off-diagonal

elements ($\gamma_{ij}; i \neq j$), line width of probe (γ_p) and pump (γ_c) lasers etc. that lead to homogeneous broadening. Inhomogeneous broadening caused by Doppler shift of atomic resonance owing to thermal motion of atoms can be incorporated by replacing the derivative $\dot{\rho}_{ij}$ on the left-hand side of Eq.(1.19) as

$$\dot{\rho}_{ij} \rightarrow \left\{\frac{\partial}{\partial t} + \vec{v}.\vec{\nabla}\right\}\rho_{ij} \tag{1.20}$$

where $\vec{v}$ is the atomic velocity.

Incorporating the effect of atomic motion in Eq.(1.19), the density matrix equation of motion can be written as,

$$\left(\frac{\partial}{\partial t} + \vec{v}\cdot\vec{\nabla}\right)\rho_{ij} = \left(\frac{i}{\hbar}\right)\sum_m\left\{\rho_{im}V_{mj}^{int} - V_{im}^{int}\rho_{mj}\right\} + (\rho_{ij})_{relax} \tag{1.21}$$

Eq.(1.21) describes dynamic equation of motion with inclusion of effects of atomic velocity and other relaxation processes. The dynamics of light-atom interaction can be fully described by Eq.(1.21) together with Eq.(1.11).

1.3.3. Induced macroscopic polarization

The density matrix elements can be used for calculating the expectation values of all operators (measurable quantities) such as population, absorption and refractive index. This is because the density matrix can be related to macroscopic polarization i.e., the ensemble average of the induced dipole moment per unit volume in a medium of atomic number density N. Thus in terms of density matrix elements, the macroscopic polarization P can be expressed as

$$P = NTr(\mu\rho) = N\sum_{i,j=1}^{n}\mu_{ji}\rho_{ij} \tag{1.22}$$

where μ_{ji} is the dipole matrix element for the transition from level i to j. This shows that since $\mu_{ii} = 0$, the induced (macroscopic polarization) in the medium is proportional to coherences (off-diagonal elements) ρ_{ij}.

In a Doppler broadened medium, all moving atoms regardless of their velocity or their places of excitation contribute to the macroscopic polarization induced in a medium consisting of moving atoms. Therefore, it is necessary to include averaging over their velocity distribution in addition to the times of excitation. Hence, assuming

the velocity distribution along the line of the axis (taken to be the z-axis) defined by the Maxwellian, we define the density matrix elements by integration over the velocity distribution. The macroscopic polarization P in a Doppler broadened medium can be given as,

$$P = N\,Tr(\mu < \rho >) = N\sum_{i,j=1}^{n} \mu_{ji} < \rho_{ij} > \tag{1.23}$$

Here angular brackets < > denote averaging over thermal velocities i.e.,$< \rho_{ij} > = \int \rho_{ij}(v)dv$.

The induced macroscopic polarization $\vec{P}(z,t)$ in Eq. (1.9) can be rewritten as

$$\vec{P}(z,t) = \chi\,\vec{\varepsilon}(z,t)e^{i(kz-\omega t)} + c.c \tag{1.24}$$

where χ is the electric susceptibility and $\vec{\varepsilon}(z,t)$ is the optical field strength inducing the polarization. Equating equations (1.22) or (1.23) with (1.24) allows the susceptibility related to the density matrix elements.

The susceptibility of the medium is related to the one-photon coherence (velocity averaged) is given as,

$$\chi = \frac{4\pi N|\mu_{ji}|^2}{\hbar}\frac{<\rho_{ij}>}{\Omega} \tag{1.25}$$

where $\Omega = \vec{\mu}_{ij}\cdot\varepsilon/\hbar$ is the Rabi frequency of the field. It is well know that the imaginary part of the susceptibility gives the absorption and real part gives the dispersion of the weak probe field.

1.4. Line Broadening Mechanisms in EIT

The term line broadening is used to denote the finite spectral width of the resonance of atomic system to electromagnetic fields. The radiation emitted in atomic transitions is not perfectly monochromatic. The shape of the emission line is described by the spectral lineshape function. The most important parameter of the lineshape function is the full width at half maximum (FWHM) $\Delta\omega$, which quantifies the width of the spectral line.

The main line broadening mechanisms that can occur in gases, namely:

- Homogeneous broadening
- Inhomogeneous broadening

In *homogeneous broadening* case, all the individual atoms behave in the same way and produce the same spectrum, the cause of homogeneous broadening in EIT is due to spontaneous transitions or nonradiative transitions, broadening due to the interaction with an electromagnetic field (power broadening), phase perturbing (elastic) collisions, laser line *widths etc.* Physically this would correspond to experiments carried out in either a 'cold' atomic sample (Bose Einstein condensate, optical trap) or in an atomic beam. In *inhomogeneous broadening* case, the individual atoms behave differently and contribute to different parts of the spectrum, inhomogeneous broadening occurring in EIT resonance is due to Doppler shift of atomic resonance (Doppler broadening) caused by thermal motion of atoms in a gas medium. The spectral lineshapes are different in both the broadening cases, that homogeneous mechanisms generally give rise to Lorentzian lineshapes, while inhomogeneous processes tend to produce Gaussian spectral lines.

1.4.1. Lifetime (radiative) broadening

Light is emitted when an electron in an excited state drops to a lower level by spontaneous emission. The rate at which this occurs is determined by the radiative lifetime τ. The finite lifetime of the excited state leads to a broadening of the spectral line in accordance with the energy-time uncertainty principle:

$$\Delta E\, \Delta t \geq \hbar \tag{1.26}$$

On setting $\Delta t = \tau$, we then deduce that the amount of broadening in angular-frequency units must satisfy:

$$\Delta\omega = \frac{\Delta E}{\hbar} \geq \frac{1}{\tau} \tag{1.27}$$

Since this broadening mechanism is intrinsic to the transition, it is alternatively called natural broadening or simply radiative broadening. In radiative broadening the FWHM is given by:

$$\gamma = \Delta\omega_{\text{lifetime}} = \frac{1}{\tau} \tag{1.28}$$

1.4.2. Doppler broadening

Doppler broadening originates from the random motion of the atoms in the gas. The random thermal motion of the atoms gives rise to Doppler shifts in the observed frequencies, which then causes line broadening. The broadening caused by the Doppler mechanism can be quantified by considering the light emitted by an atom moving with velocity component v_z towards the observer. If the transition frequency in the rest frame of the atom is ω_0, the observed frequency will be Doppler shifted to:

$$\omega = \omega_0 \left(1 + \frac{v_z}{c}\right) \tag{1.29}$$

The Maxwellian velocity distribution of atoms with velocity between v_z and $v_z + dv_z$ is given by,

$$M(v_z) = \sqrt{\ln 2/(\pi \bar{v}^2)} \exp(-\ln 2\, {v_z}^2/\bar{v}^2), \tag{1.30}$$

where $\bar{v} = \sqrt{\ln 2}\, v_{th}$ and $v_{th} = \sqrt{2k_B T/m_a}$ is the most probable thermal velocity at a temperature T of an atom of mass m_a. In Doppler broadening medium the FWHM is given by,

$$\gamma_D = k_p v_z = \Delta\omega_{Doppler} = 2\omega_0 \left(\frac{(2\ln 2)k_B T}{mc^2}\right)^{1/2} = \frac{4\pi}{\lambda}\left(\frac{(2\ln 2)k_B T}{m}\right)^{1/2} \tag{1.31}$$

If an experiment is carried out in a gas cell, we must include the effects of Doppler broadening as we would expect that Doppler broadened line shape is much broader than that of the homogeneous line shape. The Doppler linewidth in a gas at STP is usually much larger than the natural linewidth. For example, the Doppler linewidth of the 589.0 nm line of Sodium at 300K works out to be 1.3 GHz, which is about two orders of magnitude larger than the 10 MHz natural broadening due to the radiative lifetime of 16 ns. The dominant broadening mechanism in low-pressure gases at room temperature is therefore usually Doppler broadening, and the lineshape is closer to Gaussian than Lorentzian.

1.4.3. Effect of wave-vectors mismatch on probe transparency (or absorption)

In Doppler broadened (hot) atomic vapors, particularly at low densities, the availability of large mean-free path for thermal motion of atoms can lead to a substantial Doppler broadening of one and two-photon transitions. In Doppler broadened medium the probe transparency (or absorption) characteristics are governed by nature of the residual (two-photon) Doppler broadening and mismatch $k_p - k_c$, of applied probe and coupling field wave-vectors k_p and k_c respectively. This is because realizing perfect Doppler-free two-photon transition in real atomic (EIT) systems is not feasible due to a rather large dissimilarity between the wavelengths (or wave-vectors) of the (upper) transition driven by strong coupling field(s) and the (lower) transition connected by the weak probe field. As EIT requires two laser beams, ideally the beam geometry should be set so that the Doppler shifts for the probe and coupling beams cancel. However based on that (beam geometry) the two-photon Doppler broadening can be reduced to a large extent with the use of counter propagating pump and probe geometry in ladder-type systems and co-propagating pump and probe geometry in lamda-type systems.

It therefore would be of interest to assess the influence of the various regimes of wave vector mismatches in the Doppler broadening medium on probe transparency (absorption) characteristics in various systems. The three different mismatch regimes which occurs in the Doppler broadening medium are,

(i) $k_p = k_c$

(ii) $k_p < k_c$

(iii) $k_p > k_c$

Although residual (two photon) Doppler broadening effect can be significant in experiments on EIT in atomic vapors, it was found that the nature of EIT in (a three-level ladder) atomic system depends critically on the sign of the two photon residual Doppler width $\delta k = (k_p - k_c)$ which, depending on the probe and pump (control) field wave-vector mismatch, is either positive ($k_p > k_c$) or negative ($k_p < k_c$) and is markedly dissimilar in these two cases. Gea-Banacloche *et al.*, [43] Shepherd *et al.*, [44] and Boon *et al.* [45] theoretically and experimentally studied the role of two-

photon residual broadening in EIT in ladder-type inhomogeneously broadened media and identified ways to optimize the absorption reduction effect for various regimes of coupler and probe wavelength (or wave-vector) mismatch.

1.5. Organization of the thesis

Chapter 1: Introduces the phenomenon of electromagnetically induced transparency (EIT) along with its applications to some associated nonlinear optical processes. The motivation for the work and the basic formulation of the problem in the framework of density matrix formalism is presented.

Chapter 2: This chapter deals with a comprehensive study of the electromagnetically induced transparency of a probe field in four-level atomic system of Y-configuration, driven by two strong laser (coupling) fields. Both homogenously (radiative) and Doppler broadening in the systems are considered. Emphasis is on examining the effect of residual Doppler broadening on EIT for various cases of wave-vector mismatches. Depending upon the energy-level separations, these occur when the wavenumber (frequency) of the coupling field is either equal ($k_c = k_p$), larger ($k_c > k_p$), or lesser ($k_c < k_p$) than that of the probe field. It is found that in the $k_c > k_p$ wave-vector mismatch case, the negative residual Doppler broadening is actually conducive for the observation of electromagnetically induced transparency in Doppler broadened four level Y-type atomic systems. Finally the dependence of the width, depth and location of the probe absorption profile of on system and field parameters is also examined.

Chapter 3: In this chapter we investigate the feasibility of attaining simultaneous electromagnetically induced transparency (DEIT) and efficient nonlinear generation in different configurations of Doppler broadened diamond systems such as, the frequency up-conversion, nearly degenerate and degenerate scheme. We show that EIT and nonlinear generation efficiency depend critically on the type of residual Doppler broadening present in each of the two cascade subsystems constituting the diamond system. Furthermore it is observed that nonlinear generation with perfect EIT simultaneously in both subsystems is not possible as the process of nonlinear generation actually tends to oppose EIT. Yet in an

extended medium, we observe that with suitable choice of the driving field strengths, sufficiently large nonlinear gain can be produced to offset the high absorption losses and create a steady state (equilibrium) situation in the medium. Under these conditions both probe and the signal fields propagate in the medium without further attenuation or gain.

Chapter 4: Here we propose an easy to implement simple scheme for subluminal (or superluminal) light propagation of both probe and signal fields in a radiative and Doppler broadened double ladder system driven by two strong laser fields. The proposed scheme is easier to implement compared with other schemes as it is based on generation of nonlinear gain large enough to compensate for the absorption losses. This can be done simply by appropriate choice of strengths of the two strong laser fields. Further we observe that the under suitable choice of driving field strengths both the fields probe (signal) are matched in intensity and create a steady state (equilibrium) situation in the medium. Finally we presented the propagation measurements for the two weak fields probe (signal) and observed simultaneous slow and superluminal light propagation.

Chapter 5: This chapter deals with the electromagnetically induced transparency (EIT) of a probe field in a Doppler broadened five-level(K-type) ^{87}Rb atomic medium where the intermediate level in a ladder-type atom is coupled with a higher-excited and ground levels by two strong laser (coupling) fields. This configuration can be regarded as being composed of *three* sub-systems of Λ-type three-level systems and *two* sub-systems of ladder-type three-level systems. Effect of wave-vector mismatch occurring when the coupling field frequency is higher than that of the probe field frequency ($\lambda_c < \lambda_p$) are considered. Under the influence of the coherent coupling fields, we observe the unusual EIT behavior (at resonance) of the probe field or double (triple) EIT windows (at near resonance) depending on the amplitude and the detuning of the coupling fields.

Chapter 6: Finally, this chapter contains a summary and conclusion of the results obtained in this thesis along with exploration of further possible studies of EIT and its applications.

1.6. References

1. K. J. Boller, A. Imamoglu and S. E. Harris, Phys. Rev. Lett. **66**, 2593 (1991).

2. S. E. Harris, G.Y. Jain, M. Jain, H. Xia and A. J. Merriam, Phil. Trans. R. Soc. London. A **335**, 2291 (1997); A. Joshi, M. Xiao, in; Progress in Optics, 49 (2000) E. Wolf, (Ed.) Elsevier; M. D. Lukin, P. Hemmer and M. O. Scully Adv. At. Mol. Opt. Phys. **42**, 347 (2000).

3. S. P. Tewari and G. S. Agarwal, Phys. Rev. Lett. **56**, 17 (1986).

4. O. A. Kocharovskaya and Y. I. Khanin, Jetp Lett. **48**, 630 (1988).

5. S. E. Harris Phys. Rev. Lett. **62**, 1033 (1989).

6. J. E. Field, K. H. Hahn and S. E. Harris, Phys. Rev. Lett. **67**, 3062 (1991).

7. S. E. Harris, Phys. Today **50**, 36 (1997).

8. J. R. Boon, E. Zekou, D. J. Fulton and M. H. Dunn, Phys. Rev. A **57**, 1323 (1998); G. R. Welch, G. G. Padmabandu, E. S. Fry, M. D. Lukin, D. E. Nikonov, F. Sander, M. O. Scully, A. Weis and F. K. Tittel, Foundations of Physics **28**, 621 (1998).

9. M. Xiao, Y. Q. Li, S.Z. Jin and J. Gea-Banacloche, Phys. Rev. Lett. **74**, 666 (1995); Y. Q. Li, S. Z. Jin and M. Xiao, Phys. Rev. A **51**, R1754 (1995).

10. H. Schmidt, K. L. Campman, A. C. Gossard and A. Imamoglu, Appl. Phys. Lett. **70**, 3455 (1997); H. Schmidt and A. Imamoglu, Opt. Commun. **131**, 333 (1996); H. Schmidt and R. J. Ram, Appl. Phy. Lett. **76**, 3173 (2000).

11. B. E. Ham, M. S. Shahriar, P. R. Hemmer, Opt. Lett. **22**, 1138 (1997); Y. Zhao, C. Wu, B.S. Ham, M. K. Kim and E. Awadl, Phys. Rev. Lett. **79**, 641 (1997).

12. M. O. Scully and M. S. Zubairy, Quantum Optics (1997) (Cambridge: Cambridge University Press).

13. M. D. Lukin, Rev. Mod. Phys. **75**, 457 (2003); M. Fleischhauer, A. Imamoglu and J. P. Marangos, Rev. Mod. Phys. **77**, 633 (2005).

14. E. Arimondo, Progress in Optics **35**, 257 (1996) E. Wolf, (Ed.) Elsevier; H. R. Gray, R. M. Whitley and C. R. Stroud, Opt. Lett. **3**, 218 (1978).

15. M. O. Scully, S. Y. Zhu and A. Gavrielides, Phys. Rev. Lett. **62**, 2813 (1989); O. Kocharovskaya, Phys. Rep. **219**, 175 (1992); E. S. Fry, X. F. Li, D. Nikonov, G. G. Padmabandu, M. O. Scully, A. V. Smith, F. K. Tittel, C. Wang, S. R. Wilkinson and S. Y. Zhu, Phys. Rev. Lett. **70**, 3235 (1993).

16. R. R. Moseley, S. Shepherd, D. J Fulton, B.D. Sinclair and M. H. Dunn, Phys. Rev. Lett. **74**, 670 (1995).

17. J. P. Marangos, J. Mod. Opt. **45**, 471 (1998); M. D. Lukin and A. Imamoglu, Nature **413**, 273 (2001); Z. Ficek and S. Swain, J. Mod. Opt. **49**, 3 (2002).

18. L. V. Hau, S. E. Harris, Z. Dutton and C. H. Behroozi, Nature (London) **397**, 594 (1999); D. Budker, D. F. Kimball, S. M. Rochester and V. V. Yashchuk, Phys. Rev. Lett. **83**, 1767 (1999); C. Liu, Z. Dutton, C. H. Behroozi and L. V. Hau, Nature (London) **409**, 490 (2001).

19. S. E. Harris, J. E. Field and A. Kasapi, Phys. Rev. A **46**, R29 (1992); O. Schmidt, R. Wynands, Z. Hussein and D. Meschede, Phys. Rev. A **53**, R27 (1996).

20. K. Hakuta, L. Marmet and B. P. Stoicheff, Phys. Rev. Lett. **66**, 596 (1991); R. R. Moseley, S. Shepherd, D. J. Fulton, B. D. Sinclair and M. H. Dunn, Phys. Rev. A **50**, 4339 (1994); M. Jain. H. Xia, G. Y. Yin, A. J Merriam and S. E. Harris, Phys. Rev. Lett. **77**, 4326 (1996).

21. M. D. Lukin, S. F. Yelin, M. Fleischhauer and M. O. Scully, Phys. Rev. A **60**, 3225 (1999); A. M. Akulshin, S. Barreiro and A. Lezama, Phys. Rev. A **57**, 2996 (1998).

22. M. D. Lukin, A. B. Matsko, M. Fleischhauer and M. O. Scully, Phys. Rev. Lett. **82**, 1847 (1999).

23. S. E. Harris, Y. Yamomoto, Phys. Rev. Lett. **81**, 3611 (1998); A. Imamoglu, H. Schmidt, G. Woods and M. Deutsch, Phys. Rev. Lett. **79**, 1467 (1997).

24. M. D. Lukin and A. Imamoglu, Phys. Rev. Lett. **84**, 1419 (2000); M. G. Payne and L. Deng, Phys. Rev. Lett. **91**, 123602 (2003).

25. I. Novikova, A. B. Matsko and G. R. Welch, Opt. Lett. **26**, 1016 (2001); V. A. Sautenkov, M. D. Lukin, C. J. Bednar, I. Novikova, E. Mikhailov, M. Fleischhauer, V. I. Velichansky, G. R.Welch and M. O. Scully, Phys. Rev. A **62**, 023810 (2000).

26. R. Wynands and A. Nagel, Appl. Phys. B **68**, 1 (1998).

27. S. Knappe, R. Wynands, J. Kitching, H. G. Robinson and L. Hollberg, J. Opt.Soc. Am. B **18**, 1545 (2001).

28. D. P. Katz, J. Donoghue, M. Cronin-Golomb, M. S. Shariar, P. R. Hemmer and P. Kumar, Opt. Lett. **20**, 769 (1995); W. H. Burkett, B. Lu and M. Xiao, Opt. Lett. **23**, 804 (1998).

29. A. K. Patnaik and G. S. Agarwal, Opt. Comm. **199**, 127 (2001); G. Morigi, S. Franke-Arnold and Gian-Luca Oppo, Phys. Rev. A **66**, 053409 (2002).

30. S. Rebic, D. Vitali, C. Ottaviani, P. Tombesi, M. Artoni, F. Cataliotti and R. Corbalan, Phys. Rev. A **70**, 032317 (2004); S. Li, X. Yang, X. Cao, C. Zhang, C. Xie and H. Wang, Phys. Rev. Lett. **101**, 073602 (2008).

31. G. S. Agarwal and W. Harshawardhan, Phys. Rev. Lett. **77**, 1039 (1996); J. Y. Gao, S. H. Yang, D. Wang, X. Z. Guo, K. X. Chen, Y. Jiang and B. Zhao, Phys. Rev. A **61**, 023401 (2000).

32. A. Joshi and M. Xiao, Phys. Rev. A **72**, 062319 (2005); A. Joshi and M. Xiao, Eur. Phys. J. D **30**, 431(2004).

33. H. Schmidt, A. Imamoglu, Opt. Lett. **21**, 1936 (1996); W. J. Munro, R.G. Beausoleil and T. P. Spiller, J. Mod. Opt. **51**, 1559 (2004).

34. S. E. Harris, J. E. Field and A. Imamoglu, Phys. Rev. Lett. **64**,1107 (1990)*;* P. R. Hemmer, D. P. Katz, J. Donoghue, M. Cronin-Golomb, M. S. Shahriar and P. Kumar, Opt. Lett. **20,** 982 (1995).

35. C. Ottaviani, D. Vitali, M. Artoni, F. Cataliotti and P. Tombesi, Phys. Rev. Lett. **90**, 197902 (2003).

36. Z. Wang, K. Marzlin and B. C. Sanders, Phys. Rev. Lett. **97**, 063901(2006).

37. Y. Zhang, A.W. Brown and M. Xiao, Phys. Rev. Lett. **99**, 123603 (2007); S. Li, X. Yang, X. Cao, C. Zhang, C. Xie and H. Wang, Phys. Rev. Lett. **101**, 073602 (2008).

38. Y. Chen, X. G. Wei and B.S. Ham, J. Phys. B: At. Mol. Opt. Phys. **42**, 065506 (2009).

39. A. Raczynski, M. Rzepecka, J. Zaremba and S. Zielinska-Kaniasty, Opt. Commun. **260**, 73 (2006).

40. B.S. Ham and P.R. Hemmer, Phys. Rev. Lett. **84**, 4080 (2000).

41. M.G. Payne and L. Deng, Phys. Rev. Lett. **91**, 123602 (2003); S. A. Moiseev and B.S. Ham, Phys. Rev. A **71**, 053802 (2005).

42. J. D. Jackson, "Classical Electrodynamics" 3rd Ed., Wiley, New York (1962).

43. J. Gea-Banacloche, Y. Q. Li, S. Z. Jin and M. Xiao, Phys. Rev.A **51**, 576 (1995).

44. S. Shepherd, D. J. Fulton and M. H. Dunn, Phys. Rev. A **54**, 5394 (1996).

45. J. R. Boon, E. Zekou, D. McGloin and M. H. Dunn, Phys. Rev. A **59**, 4675 (1999).

Chapter 2

EIT in Four-Level Y-type System

In this chapter we study the transparency of a weak probe field in a four-level Y-type atomic system with dual ladder-type EIT scheme, interacting with two strong laser (coupling) fields. Both cold atomic vapor (radiative) and hot atomic vapor (Doppler broadened) are considered. The crucial dependence of the nature of EIT on the type of the wave-vector mismatch, originating from the wavelength (frequency) difference between the probe and coupling fields in Doppler broadening medium is illustrated in detail. We found that negative residual Doppler broadening case (i.e.,$k_c > k_p$) is actually conducive for the observation of transparency in Doppler broadened four level Y-type atomic systems. The absorption profile of a weak probe field displays very wide and almost complete single or double EIT windows whose width, depth can be controlled by manipulating the parameters of the coupling fields. Analytical results are also obtained to explain these interesting features.

2.1. Introduction:

As mentioned earlier electromagnetically induced transparency (EIT) [1] is one of the many unusual and interesting phenomena produced by atomic coherence and interference effects that enable propagation (without significant attenuation) of light through an otherwise opaque atomic medium. The four-level Y-type atomic system with dual ladder-type EIT scheme in recent times has been utilized in several studies by many authors [2-9]. The dual ladder-type EIT (Y-type) system interacting

with two strong laser (coupling) fields and a low-intensity probe field as shown in Figure 2.1.

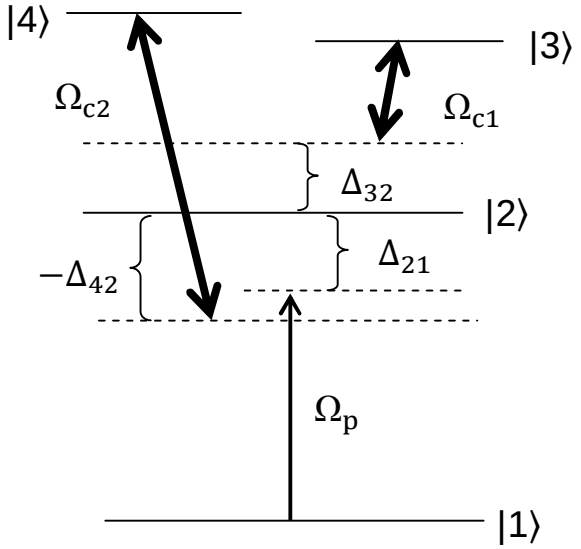

Figure 2.1: EIT scheme in Four-level Y-type atomic system with dual ladder-type EIT. Here Ω_p is Rabi frequency of the (weak) probe and Ω_{c1}, Ω_{c2} are (strong) coupling fields Rabi frequencies. The detunings of the probe and coupling fields from their respective atomic transitions are $\Delta_{21} = \omega_{21} - \omega_p$, $\Delta_{32} = \omega_{32} - \omega_{c1}$ and $\Delta_{42} = \omega_{42} - \omega_{c2}$ respectively.

As stated earlier, (Chapter 1 section **1.4.3**) in atomic vapors the probe transparency (or absorption) characteristics are governed by nature of the residual (two photon) Doppler broadening originating from thermal motion of atoms and mismatch $k_p - k_c$, of applied probe and coupling field wave-vectors k_p and k_c respectively [10,11,12]. It is the usual belief that a Doppler-free medium is essential for observing reduced probe absorption at much lower coupling (or pump) laser power. Hence most experiments tend to utilize a two-photon Doppler free geometry where the coupling and probe beams are counter-propagating and have similar frequencies so that $k_p = k_c$ and the residual Doppler width vanishes. Realizing perfect Doppler free two-photon transition in real atomic systems is not feasible due to rather large dissimilarity between the wavelengths (or wave vectors) of the (upper) transition driven by coupling field(s) and the lower transition connected by the probe field. For example, even the often utilized nearly Doppler free two-photon process involving the $5S_{1/2} \rightarrow 5P_{3/2} \rightarrow 5D_{5/2}$ (or $5D_{3/2}$) transition in Rb [7, 8] has a nonzero ($k_p < k_c$) residual

width of 1.6 MHz [11] which is much larger than the dephasing rate (0.4 MHz) of two photon transition and thus can significantly affect the probe transparency. On the other hand it was found that the $k_p < k_c$ case is actually conducive to observation of reduced probe absorption [10, 12]. It therefore would be of interest to assess the influence of the various broadening mechanisms and different regimes of wave vector mismatches in the inhomogeneous broadening case (particularly when $k_p < k_c$) on probe transparency (absorption) characteristics in a Y-type four level system.

We study transparency of a weak probe field in a Doppler broadened four level Y-type system interacting with two strong laser (coupling) fields. For comparison and contrasting, analysis for a homogeneously (radiatively) broadened four level Y-type systems is also presented. Here we deals with density matrix formulation, solve for the steady-state density matrix-equations for the Y-type system to first order in amplitude of a (weak) probe field. Expressions are derived for one-photon (probe) coherence, susceptibility and absorption coefficient from which absorption and dispersion characteristics of the probe field can be determined. Analytical results are derived so as to explain the influence of various broadening mechanisms as well the velocity selective nature of the probe transparency in different regimes of wave vector mismatch. It is shown that depending on the amplitude and the detuning of the coupling lasers, the absorption profile of a weak probe field shows single or double EIT windows whose location, width, and depth can be controlled by manipulating the parameters of the coupling fields. Present the numerical results for probe absorption and dispersion considering the transitions $3S_{1/2} \rightarrow 3P_{3/2} \rightarrow 4D_{3/2}$ ($3S_{1/2} \rightarrow 3P_{3/2} \rightarrow 4D_{5/2}$) in sodium atom. These are compared with analytical results and good agreement is obtained.

2.2. Theory for the four level Y system

2.2.1. Formulation

We consider a dual ladder Y-type four-level atomic system interacting with three laser fields $\vec{E}_p$, $\vec{E}_{c1}$ and $\vec{E}_{c2}$ as shown in Figure 2.1. The spontaneous emission rates from the two nearly degenerate upper states $|4\rangle$, $|3\rangle$ respectively to intermediate

level $|2\rangle$ are $2\gamma_{42}$, $2\gamma_{32}$ and that from level $|2\rangle$ to ground level $|1\rangle$ is $2\gamma_{21}$. The three laser fields are given by $\vec{E}_p=\vec{\varepsilon}_p \exp\left[i\left(\vec{k}_p.\vec{r}-\omega_p t\right)\right]+c.c.$, $\vec{E}_{c1}=\vec{\varepsilon}_{c1}\exp\left[i\left(\vec{k}_{c1}.\vec{r}-\omega_{c1}t\right)\right]+c.c$ and $\vec{E}_{c2}=\vec{\varepsilon}_{c2}\exp\left[i\left(\vec{k}_{c2}.\vec{r}-\omega_{c2}t\right)\right]+c.c.$ The weak probe laser field $\vec{E}_p$ of frequency ω_p, wave vector $\vec{k}_p$ and Rabi frequency $\Omega_p=(\vec{\mu}_{21}.\vec{\varepsilon}_p)/\hbar$ is applied to the $|1\rangle\rightarrow|2\rangle$ transition. The transition $|2\rangle\rightarrow|3\rangle(|2\rangle\rightarrow|4\rangle)$ is being driven by coupling laser field $\vec{E}_{c1}(\vec{E}_{c2})$ of frequency $\omega_{c1}(\omega_{c2})$, wave vector $\vec{k}_{c1}(\vec{k}_{c2})$ and Rabi frequency $\Omega_{c1}=(\vec{\mu}_{32}.\vec{\varepsilon}_{c1})/\hbar$ $(\Omega_{c2}=(\vec{\mu}_{42}.\vec{\varepsilon}_{c2})/\hbar)$. Here $\vec{\mu}_{21}$, $\vec{\mu}_{32}$and $\vec{\mu}_{42}$ are dipole moments of $|2\rangle\rightarrow|1\rangle$, $|3\rangle\rightarrow|2\rangle$ and $|4\rangle\rightarrow|2\rangle$ transitions respectively.

2.2.2. Interaction Hamiltonian:

Using Eq.(1.15) the interaction Hamiltonian in the interaction picture and under rotating wave approximation is obtained as

$$V^{int}=-\hbar[\Omega_p e^{i(\vec{k}_p.\vec{r}+\Delta_{21}t)}|2\rangle\langle 1|+\Omega_{c1}e^{i(\vec{k}_{c1}.\vec{r}+\Delta_{32}t)}|3\rangle\langle 2| +\Omega_{c2}e^{i(\vec{k}_{c2}.\vec{r}+\Delta_{42}t)}|4\rangle\langle 2|+H.c.], \quad (2.1)$$

where $\Delta_{21}=\omega_{21}-\omega_p$, $\Delta_{32}=\omega_{32}-\omega_{c1}$ and $\Delta_{42}=\omega_{42}-\omega_{c2}$ denote the detuning of probe and coupling fields frequencies from the atomic resonance frequencies ω_{21}, ω_{32} and ω_{42} respectively and $|i\rangle\langle j|$, (i, j =1, 2, 3, 4) are the atomic raising or lowering operators.

2.2.3. Density matrix-equations of motion

The equations describing time evolution of the slowly varying components of the density matrix elements $\tilde{\rho}_{jk}$ can now be written using Eqs.(2.1) and (1.18b) in Eq. (1.21) and appropriate transformations to eliminate fast oscillating (exponential) terms as,

$$\dot{\tilde{\rho}}_{21}=-[i(\Delta_{21}+\vec{k}_p.\vec{v})+\gamma_{21}]\tilde{\rho}_{21}+i\Omega_p(\rho_{11}-\rho_{22})+i\Omega_{c1}^{*}\tilde{\rho}_{31}+i\Omega_{c2}^{*}\tilde{\rho}_{41} \quad (2.2a)$$

$$\dot{\tilde{\rho}}_{31}=-[i(\Delta_{21}+\Delta_{32}+(\vec{k}_p+\vec{k}_{c1}).\vec{v})+\gamma_{32}]\tilde{\rho}_{31}+i\Omega_{c1}\tilde{\rho}_{21}-i\Omega_p\tilde{\rho}_{32}, \quad (2.2b)$$

$$\dot{\tilde{\rho}}_{41}=-[i(\Delta_{21}+\Delta_{42})+(\vec{k}_p+\vec{k}_{c2}).\vec{v})+\gamma_{42}]\tilde{\rho}_{41}+i\Omega_{c2}\tilde{\rho}_{21}-i\Omega_p\tilde{\rho}_{42}, \quad (2.2c)$$

$$\dot{\tilde{\rho}}_{32}=-[i\Delta_{32}+\vec{k}_{c1}.\vec{v}+(\gamma_{21}+\gamma_{32})]\tilde{\rho}_{32}-i\Omega_p^{*}\tilde{\rho}_{31}+i\Omega_{c1}(\rho_{22}-\rho_{33})-i\Omega_{c2}\tilde{\rho}_{34}, \quad (2.2d)$$

$$\dot{\tilde{\rho}}_{42}=-[i\Delta_{42}+\vec{k}_{c2}.\vec{v}+(\gamma_{21}+\gamma_{42})]\tilde{\rho}_{42}+i\Omega_{c2}(\rho_{22}-\rho_{44})-i\Omega_p^{*}\tilde{\rho}_{41}-i\Omega_{c1}\tilde{\rho}_{43}, \quad (2.2e)$$

$$\dot{\tilde{\rho}}_{43}=-[i(\Delta_{42}-\Delta_{32})+(\vec{k}_{c2}-\vec{k}_{c1}).\vec{v})+(\gamma_{42}+\gamma_{32})]\tilde{\rho}_{43}-i\Omega_{c1}^{*}\tilde{\rho}_{42}+i\Omega_{c2}\tilde{\rho}_{23}, \quad (2.2f)$$

$$\dot{\rho}_{11}=2\gamma_{21}\rho_{22}+i\Omega_{p}^{*}\tilde{\rho}_{21}-i\Omega_{p}\tilde{\rho}_{12}, \quad (2.2g)$$

$$\dot{\rho}_{22}=2\gamma_{42}\rho_{44}+2\gamma_{32}\rho_{33}-2\gamma_{21}\rho_{22}+i\Omega_{p}\tilde{\rho}_{12}-i\Omega_{c1}\tilde{\rho}_{23}+i\Omega_{c2}\tilde{\rho}_{24}-i\Omega_{p}^{*}\tilde{\rho}_{21}+i\Omega_{c1}^{*}\tilde{\rho}_{32}-i\Omega_{c2}^{*}\tilde{\rho}_{42} \quad (2.2h)$$

$$\dot{\rho}_{33}=-2\gamma_{32}\rho_{33}+i\Omega_{c1}\tilde{\rho}_{23}+i\Omega_{c1}^{*}\tilde{\rho}_{32}, \quad (2.2i)$$

$$\dot{\rho}_{44}=-2\gamma_{42}\rho_{44}-i\Omega_{c2}^{*}\tilde{\rho}_{42}+i\Omega_{c2}\tilde{\rho}_{24}, \quad (2.2j)$$

Our aim is to determine the velocity averaged first-order one-photon coherence $I_{21}=\int\tilde{\rho}_{21}(v)dv^{3}$; the imaginary and the real parts of which describes probe absorption and dispersion respectively, in dual ladder Y-type four level system. We solve the above set of density-matrix equations in the usual limit of a weak probe and an arbitrarily strong coupling (or 'control') fields using the following approach. Initially all the population is in the ground level $|1\rangle$ with a Maxwellian velocity distribution. We assume the probe to be sufficiently weak so as not to induce any population transfer to upper levels. Thus the zeroth-order solution obtained from Eq.(2.2) in the absence of probe (i.e., putting $\Omega_{p}=0$) is

$$\rho_{11}^{0}=M(v), \quad (2.3)$$

and all other zeroth-order matrix elements vanish.

where

$$M(v)=\frac{1}{\bar{v}}\sqrt{\frac{\ln 2}{\pi}}\exp(-\ln 2\frac{v^{2}}{\bar{v}^{2}}), \quad (2.4)$$

is the Maxwellian velocity distribution of atoms with $\bar{v}=\sqrt{\ln 2}\,v_{th}$ and $v_{th}=\sqrt{\frac{2k_{B}T}{m_{a}}}$ is the most probable thermal velocity at a temperature T of an atom of mass m_{a}.The relevant first-order (i.e., to leading order in probe amplitude) density-matrix equations are found as

$$\tilde{\rho}_{21}^{(1)}=-[i(\Delta_{21}+\vec{k}_{p}.\vec{v})+\gamma_{21}]\tilde{\rho}_{21}+i\Omega_{p}\rho_{11}^{(0)}+i\Omega_{c1}^{*}\tilde{\rho}_{31}^{(1)}+i\Omega_{c2}^{*}\tilde{\rho}_{41}^{(1)}, \quad (2.5a)$$

$$\tilde{\rho}_{31}^{(1)}=-[i(\Delta_{21}+\Delta_{32}+(\vec{k}_{p}+\vec{k}_{c1}).\vec{v})+\gamma_{32}]\tilde{\rho}_{31}+i\Omega_{c1}\tilde{\rho}_{21}^{(1)}, \quad (2.5b)$$

$$\tilde{\rho}_{41}^{(1)}=-[i(\Delta_{21}+\Delta_{42})+(\vec{k}_{p}+\vec{k}_{c2}).\vec{v})+\gamma_{42}]\tilde{\rho}_{41}+i\Omega_{c2}\tilde{\rho}_{21}^{(1)}, \quad (2.5c)$$

The steady-state solution obtained by setting the time derivates to zero on the left-hand side of Eq.(2.5) yields the velocity averaged one-photon coherence as

$$I_{21}^{(1)} = \int \tilde{\rho}_{21}^{(1)}(v)\, dv^3 = i\Omega_p \int \frac{A_{31}(v)A_{41}(v)M(v)dv^3}{A_{21}(v)A_{31}(v)A_{41}(v)+A_{31}(v)|\Omega_{c2}|^2+A_{41}(v)|\Omega_{c1}|^2}, \quad (2.6)$$

where

$$A_{21}(v) = i(\Delta_{21} + \vec{k}_p.\vec{v}) + \gamma_{21}, \quad (2.7a)$$

$$A_{31}(v) = i\{(\Delta_{21} + \Delta_{32} + (\vec{k}_p + \vec{k}_{c1}).\vec{v})\} + \gamma_{32}, \quad (2.7b)$$

$$A_{41}(v) = i\{(\Delta_{21} + \Delta_{42}) + (\vec{k}_p + \vec{k}_{c2}).\vec{v}\} + \gamma_{42}, \quad (2.7c)$$

In the above equations $2\gamma_{ij}$ are the spontaneous emission rates from level $|i\rangle \rightarrow |j\rangle$ (i, j =1- 4). In EIT-experimental situations typically one considers an arrangement of probe and coupler fields counter-propagating along z axis. For this experimental configuration we can henceforth set the terms $(\vec{k}_p + \vec{k}_{cj}).\vec{v} = (k_p - k_{cj})v_z$ (j = 1, 2) in and $\vec{k}_p.\vec{v} = k_p v_z$ in Eq.(2.7) and consequently the velocity integration in Eq.(2.6) reduces to a one dimensional integral over velocity v_z .

2.2.4. Susceptibility and Absorption coefficient

The susceptibility of the medium (Chapter 1 section **1.3.3**) is related to the velocity averaged one-photon coherence as follows:

$$\chi = N\frac{|\mu_{21}|^2}{\hbar\gamma_D}\left(\frac{I_{21}^{(1)}}{\Omega_p/\gamma_D}\right), \quad (2.8)$$

where N is the atomic density of the vapor and $\gamma_D (= k_p\bar{v})$ is the Doppler width in the system. As is well known, the imaginary ($Im(\chi)$) and real ($Re(\chi)$) parts respectively of the susceptibility χ give the absorption and dispersion of the probe field.

Transmission of the probe beam through a vapor cell of length L is governed by

$$I_p(L)/I_p(0) = \exp(\alpha_p L). \quad (2.9a)$$

where I(L) and I(0) respectively, are the output (at z = L) and input (at z = 0) probe beam intensities and the probe absorption coefficient is given by

$$\alpha_p = -\frac{8\pi^2}{\lambda_p} Imag(\chi). \quad (2.9b)$$

2.3. Analytical Results

2.3.1. Radiatively (homogenously) broadened medium

We analyze probe absorption (transparency) characteristics to arrive at conditions for EIT in a radiatively (homogenously) broadened medium. Result for this case can be derived from Eq.(2.8) by dropping velocity dependent terms and performing the velocity integration using Eq.(2.4) as follows:

$$\frac{I_{21}^{(1)}}{\Omega_p} = \frac{i}{\gamma_{21} + i\,\Delta_{21} + \frac{|\Omega_{c1}|^2}{\gamma_{32} + i\,(\Delta_{21}+\Delta_{32})} + \frac{|\Omega_{c2}|^2}{\gamma_{42} + i\,(\Delta_{21}+\Delta_{42})}} \quad . \tag{2.10}$$

The above expression reveals the existence of *two* two-photon resonances in probe absorption profile as a function of probe detuning. Evidently the one occurring at $\Delta_{21} = -\Delta_{32}$ corresponds to the transition $|1\rangle \rightarrow |2\rangle \rightarrow |3\rangle$ whereas the other occurring at $\Delta_{21} = -\Delta_{42}$ corresponds to $|1\rangle \rightarrow |2\rangle \rightarrow |4\rangle$ transition of the four level Y system. Thus the four level Y system derives contributions from two distinct three-level cascade subsystems which can be strongly coupled or decoupled by manipulating the coupling field detunings or Rabi frequencies.

For instance let us consider the case, in which both the coupling fields have same detuning given by, $\Delta\ (= \Delta_{32} = \Delta_{42})$. In this case a single two photon resonance that occurs at $\Delta_{21} = -\Delta$ has contributions from both subsystems. For this case it is also clear from expression (2.10) that if the Rabi frequencies of the coupling fields are sufficiently large, so that the following criterion is met:

$$\gamma_{21} \ll \frac{|\Omega_{c1}|^2}{\gamma_{32}} + \frac{|\Omega_{c2}|^2}{\gamma_{42}}, \tag{2.11}$$

the probe absorption is considerably reduced at the position of the two photon resonance $\Delta_{21} = -\Delta$. Furthermore, in the exact resonance case, that is, when the coupling fields are tuned to exact resonance $\Delta_{32} = \Delta_{42} = 0$, the EIT resonance is centered around the probe detuning $\Delta_{21} = 0$. Implementation of the criterion specified in Eq.(2.11) would require choosing either very large $|\Omega_{c1}|^2$, $|\Omega_{c2}|^2$ or very small γ_{32} and γ_{42}.

Since at higher powers of the coupling fields, resolution of the Autler Townes (AT) doublet [13] which arise from splitting of the intermediate level $|2\rangle$ tends to obfuscate EIT effects, it is essential to choose systems in which two photon dephasing parameters γ_{32} and γ_{42} are very small in order to enable observation of EIT.

On the other hand when detuning of both the coupling fields are different, $\Delta_{32} \neq \Delta_{42}$ the two subsystems are decoupled [2, 7, 8] because tuning the probe frequency detuning to a particular two-photon resonance will render the other non-resonant with a large detuning. Eq.(2.10) shows that then the contribution from non-resonant term can be ignored and consequently the Y system reduces to a single three level cascade system with absorption and dispersion properties governed by the Rabi frequency and two-photon dephasing rate in that system.

2.3.2. Doppler broadened medium

When the medium is Doppler broadened the two photon detuning is affected by residual Doppler broadening. The result for a Doppler broadened Y system is obtained from Eqs.(2.6) and Eq.(2.7) for counter-propagating (along z axis) coupling and probe fields configuration as

$$\frac{I_{21}^{(1)}}{\Omega_p} = \int dv_z\, M(v_z) \times \frac{i}{\gamma_{21}+i\left(\Delta_{21}+k_p v_z\right)+\frac{|\Omega_{c1}|^2}{\gamma_{32}+i(\Delta_{21}+\Delta_{32})+i(k_p-k_{c1})v_z}+\frac{|\Omega_{c2}|^2}{\gamma_{42}+i(\Delta_{21}+\Delta_{42})+i(k_p-k_{c2})v_z}}. \quad (2.12)$$

Comparing above result (Eq.(2.12)) with that of a radiatively broadened case given by Eq.(2.10), we can draw the following inferences:

(A). Various wave-vector mismatch regime

If we consider a system from Figure 2.1 in which the upper levels $|3\rangle$ and $|4\rangle$ are very close with similar level separation wavelength with intermediate level $|2\rangle$, we can approximately write $k_c\ (= k_{c1} \cong k_{c2})$

(i) $k_c = k_p$ case:

For the case of perfect wave-vector matching the two photon resonances are Doppler free, $(k_p - k_{c1})v_z = (k_p - k_{c2})v_z = 0$. The criterion for observing of probe transparency at the location of two photon resonance is still given by Eq.(2.11) but with radiative width γ_{21} replaced by the Doppler width γ_D, i. e.,

$$\gamma_D \ll \frac{|\Omega_{c1}|^2}{\gamma_{32}} + \frac{|\Omega_{c2}|^2}{\gamma_{42}}. \tag{2.13}$$

(ii) $k_c \neq k_p$ case:

It however remains to be seen what happens when the probe and coupling wave-vectors differ from each other. Inspection of Eq.(2.12) shows that if we consider a system in which the upper levels $|3\rangle$ and $|4\rangle$ are very close with similar decay rates, we can approximately write Δ_c $(= \Delta_{32} \cong \Delta_{42})$, k_c $(= k_{c1} \cong k_{c2})$ and γ_c $(= \gamma_{32} \cong \gamma_{42})$. Using these facts in Eq.(2.7) and through Eq.(2.6) we obtain

$$\frac{I_{21}^{(1)}}{\Omega_p} = \int dv_z\, M(v_z)\, \frac{i[\gamma_c + i(\Delta_{21}+\Delta_c) + i(k_p - k_c)v_z]}{[\gamma_{21} + i(\Delta_{21} + k_p v_z)][\gamma_c + i(\Delta_{21}+\Delta_c) + i(k_p - k_c)v_z)] + |\Omega_{c1}|^2 + |\Omega_{c2}|^2}. \tag{2.14}$$

Eq.(2.14) resembles the typical result for a three level cascade system [10] whose upper transition is driven by a coupling field of effective Rabi frequency $\Omega_c = \sqrt{|\Omega_{c1}|^2 + |\Omega_{c2}|^2}$.

To understand the effect of velocity on probe transparency (absorption) around two-photon resonance we rewrite, by factorizing, the denominator of Eq.(2.14) in the following form:

$$\frac{I_{21}^{(1)}}{\Omega_p} = \int dv_z\, M(v_z) \times \frac{(\Delta_{21}+\Delta_c) + (k_p - k_c)v_z - i\gamma_c}{\left[(\Delta_{21}+\Delta_c) + (k_p - k_c)v_z - i\gamma_c - \frac{\{\Delta_c - k_c v_z + i(\gamma_{21} - \gamma_c)\}}{2}\right]^2 - \left[\sqrt{|\Omega_{c1}|^2 + |\Omega_{c2}|^2 + \frac{\{\Delta_c - k_c v_z + i(\gamma_{21} - \gamma_c)\}^2}{4}}\right]^2}. \tag{2.15}$$

Let us first analyze the above result (Eq.(2.15)) for the matched wave vectors $k_c = k_p$ case. For this case it is easily seen that at the location of exact two-photon resonance

when $\Delta_{21} = -\Delta_c$ is very close to zero, the remaining velocity and radiative width dependent (curly brackets) terms contained in the first square bracket cancel out similar (curly brackets) terms of the second square bracket of the denominator of Eq.(2.15) (assuming negligible γ_c). Thus a narrow two photon Doppler free transparency resonance is formed around $\Delta_{21} + \Delta_c = 0$. This cancellation can no longer occur when the (nonzero) probe frequency detuning Δ_{21} is tuned away from the two photon resonance. The residual Doppler broadening terms can then cause probe detuning Δ_{21} to shift into resonance with the absorbing Autler-Townes (AT) doublet [12, 13] components arising from the terms (in second square bracket) of the denominator. Consequently in the matched wave-vector case, except in a narrow region around the two photon resonance $\Delta_{21} + \Delta_c = 0$, at other frequencies within the region between the AT doublet, the probe is absorbed due to velocity shifting into absorbing AT doublet components.

On the other hand it is evident that if $k_p < k_c$ the residual broadening terms in first square bracket in the denominator tend to cancel out and thus eliminate the velocity shift of probe frequencies into absorbing AT peaks. In the extreme case of $k_c = 2k_p$ (which is feasible in atomic systems), the first (square bracket) term in the denominator (Eq.(2.15)) becomes Doppler free. In other words as the probe detuning is varied the probe does not experience any (velocity dependent) absorption for all frequencies in the entire region enclosed between the AT doublet. The frequency range over which the probe is transparent thus can be determined from the location of the AT doublet which occur at (for the particular case when $k_c = 2k_p$)

$$\Delta_{21} = -\frac{\Delta_c}{2} \pm \sqrt{|\Omega_{c1}|^2 + |\Omega_{c2}|^2 + \frac{\{\Delta_c - k_c v_z\}^2}{4}} \quad . \qquad (2.16)$$

Thus we further observe that if the coupling fields are tuned to exact resonance $\Delta_c = 0$ the location of the two AT peaks is symmetric on either side of the probe resonance $\Delta_{21} = 0$. Nonzero pump detuning causes asymmetry in the AT peak positions. As is well known when the coupling fields are large compared with the Doppler width, the AT doublet will be fully resolved. This is the usual AT regime. In the typical EIT regime however, the coupling Rabi frequencies are much small compared with the Doppler width and hence the AT doublet are not resolved.

Consequently the probe absorption profile should display a very broad resonance. Yet the above discussion leading to Eq.(2.16) shows that for $k_p < k_c$ it is possible to observe a wide transparency window even in the otherwise absorbing region between the AT peaks.

(B). Detuning of the coupling fields

(i) When detuning of both the coupling fields are same (exact resonance case), that is, when the coupling fields are tuned to exact resonance $\Delta_{32} = \Delta_{42} = 0$, the EIT resonance is centered around the probe detuning $\Delta_{21} = 0$.

(ii) When detuning of both the coupling fields are different, $\Delta_{32} \neq \Delta_{42}$ the two subsystems are decoupled. The probe absorption profile then displays two distinct two-photon resonances corresponding to the individual cascade systems.

2.3.3. Qualitative analysis of the problem

The foregoing explanation provides only a qualitative analysis in terms of the velocity selectivity of the EIT process associated with various wavevector mismatch cases. We now present an analysis to obtain quantitative information regarding the nature of width and depth of the transparency resonance and parameter dependence of the EIT process. For this purpose the denominator of Eq.(2.14) can be factorized for velocity as:

$$k_p v_z = -(\eta + \xi)/2 \pm \sqrt{[\eta - \xi]^2/4 + [|\Omega_{c1}|^2 + |\Omega_{c2}|^2]/\alpha} \ , \qquad (2.17)$$

where

$$\xi = \Delta_{21} - i\gamma_{21}, \qquad (2.18a)$$

$$\eta = (\Delta_{21} + \Delta_c - i\gamma_c)/\alpha \ , \qquad (2.18b)$$

$$\alpha = (k_p - k_c)/k_p \neq 0 \ . \qquad (2.18c)$$

For the particular case of $k_p < k_c$ wave-vector mismatch, the sign of the residual Doppler width $(k_p - k_c)\bar{v}$ is negative. For this case we denote

$$\Phi = |k_p - k_c|/k_p = -\alpha \ , \qquad (2.19)$$

Using Eq.(2.17) along with Eq.(2.19) in Eq.(2.14) we obtain

$$\frac{I_{21}^{(1)}}{\Omega_p} = \int \frac{dv_z\, M(v_z)}{[\Delta_{21}+k_p v_z - i\,\gamma_{21}]}$$

$$\times \left[1 - \frac{[|\Omega_{c1}|^2+|\Omega_{c2}|^2]/\Phi}{\{k_p v_z+\frac{(\eta+\xi)}{2}+i\sqrt{\frac{[|\Omega_{c1}|^2+|\Omega_{c2}|^2]}{\Phi}-\frac{[\eta-\xi]^2}{4}}\}\{k_p v_z+\frac{(\eta+\xi)}{2}-i\sqrt{\frac{[|\Omega_{c1}|^2+|\Omega_{c2}|^2]}{\Phi}-\frac{[\eta-\xi]^2}{4}}\}}\right]. \qquad (2.20)$$

In this case it can be seen from the second term in the bracket that two poles exist, one each in the upper and lower complex (velocity) planes as long as the condition

$$\mathrm{Re}[\eta-\xi]^2/4 < [|\Omega_{c1}|^2 + |\Omega_{c2}|^2]/\Phi\,, \qquad (2.21a)$$

is fulfilled together with

$$\gamma_{21}/2\,,\ \gamma_c/2\Phi < \sqrt{|\Omega_{c1}|^2 + |\Omega_{c2}|^2/\Phi}\,. \qquad (2.21b)$$

another pole exits in the upper half plane (from term outside brackets). Furthermore if all the parameters are so chosen as to be much small compared with the Doppler width γ_D, we can approximate, $M(v) \approx \sqrt{\ln 2/\pi\,\bar{v}^2}$ in Eq.(2.20) which can then be evaluated using the method of contour integration to obtain the result

$$\frac{I_{21}^{(1)}}{\Omega_p/\gamma_D} = i\sqrt{\pi \ln 2}\left[1 + \frac{4\Phi[|\Omega_{c1}|^2+|\Omega_{c2}|^2]/\{\sqrt{4\Phi[|\Omega_{c1}|^2+|\Omega_{c2}|^2]-[(\eta-\xi)\Phi]^2}\}}{\{i(\eta-\xi)\Phi-\sqrt{4\Phi[|\Omega_{c1}|^2+|\Omega_{c2}|^2]-[(\eta-\xi)\Phi]^2}\}}\right]. \qquad (2.22)$$

Furthermore using the condition Eq.(2.21b) to ignore γ_c, $\Phi\gamma_{21}$ in η and ξ (defined in Eq.(2.18)) the above result, Eq.(2.22) is recast in terms of real and imaginary parts as

$$\frac{I_{21}^{(1)}}{\Omega_p/\gamma_D} = i\sqrt{\pi \ln 2}\left[1 + \frac{i(\Delta_{21}+\Delta_c+\Delta_{21}\Phi)-\sqrt{4\Phi[|\Omega_{c1}|^2+|\Omega_{c2}|^2]-[\Delta_{21}+\Delta_c+\Delta_{21}\Phi]^2}}{\sqrt{4\Phi[|\Omega_{c1}|^2+|\Omega_{c2}|^2]-[\Delta_{21}+\Delta_c+\Delta_{21}\Phi]^2}}\right]. \qquad (2.23)$$

The above result shows that the probe absorption described by the imaginary part of Eq.(2.23) is zero as long as the condition $(\Delta_{21} + \Delta_c + \Delta_{21}\Phi) < \sqrt{4\Phi[|\Omega_{c1}|^2 + |\Omega_{c2}|^2]}$ (stipulated by Eq.(2.21a) is fulfilled. Clearly full width of this transparency region is given by

$$\gamma_t = 2\sqrt{4\Phi[|\Omega_{c1}|^2 + |\Omega_{c2}|^2]}\,. \qquad (2.24)$$

It is interesting to note that the width of the transparency region depends upon the wavevector mismatch and increases as $\sqrt{\Phi}$ for given coupling field powers. Thus if $\Phi = 1$ which correspond to the wave-vector mismatch situation of $k_c = 2k_p$, almost entire region between the AT doublet can be rendered transparent (see also discussion preceding Eq.(2.16)). Eqs.(2.24) and (2.22) are the main new results of the present work which allow us to estimate the depth and width of the transparency windows for a cascade type three level system in which $k_c < k_p$.

2.4. Numerical results and discussions

As mentioned above (in section **2.1**) for counter-propagating probe and coupling waves, nature of EIT in a three level cascade system depends critically on the relative sign of the residual Doppler width $(k_p - k_c)\bar{v}$ which, depending on the probe and coupling field wave-vector mismatch can be positive ($k_p > k_c$) or negative ($k_p < k_c$) and is markedly dissimilar from each other. If the wave-vectors k_p and k_c are the same in magnitude ($k_p = k_c$), the residual Doppler width vanishes, and usually the medium is considered to be Doppler free.

Keeping in view the essential criterion Eq.(2.13) for observation of EIT as well as the wave-vector mismatch condition (2.19), (i.e., ($k_p < k_c$) the sign of the residual Doppler width $(k_p - k_c)\bar{v}$ is negative). For our numerical calculations we have chosen an atomic system in which $k_p < k_{ci}$ (or $\lambda_p > \lambda_{ci}$), (where ci = c1, c2) so the sign of the residual Doppler width is negative. This situation can be realized, for example, considering the transitions $3S_{1/2} \rightarrow 3P_{3/2} \rightarrow 4D_{3/2}$ ($3S_{1/2} \rightarrow 3P_{3/2} \rightarrow 4D_{5/2}$) in sodium atom. These transitions form a four-level dual cascade (Y-type) EIT configuration with one stable ground state $3S_{1/2}$, an intermediate level $3P_{3/2}$ and two nearly degenerate upper states $4D_{3/2}$ and $4D_{5/2}$. The level separation wavelength of the lower and intermediate levels is λ_p = 5890Å (D2 transition) and those of the intermediate and upper transitions are $\lambda_{c1} \cong \lambda_{c2}$ = 5688Å. The large wavelength mismatch between the counter-propagating coupling and probe fields in this dual ladder EIT system introduces a residual Doppler width $(k_p - k_c)\bar{v} / k_p\bar{v} \simeq -0.04$. For comparison purpose the other case of matched ($k_p = k_c$) (and positive ($k_p > k_c$))

wave-vector mismatch is also considered hypothetically for this four-level Y-type atomic system. In our numerical calculation all parameters are expressed in units of Doppler width $\gamma_D/2\pi$ = 1GHz, i.e., $2\gamma_{21}/\gamma_D$ = 0.01, $2\gamma_{32}/\gamma_D$ = 0.0003 and $2\gamma_{42}/\gamma_D$ = 0.0019.

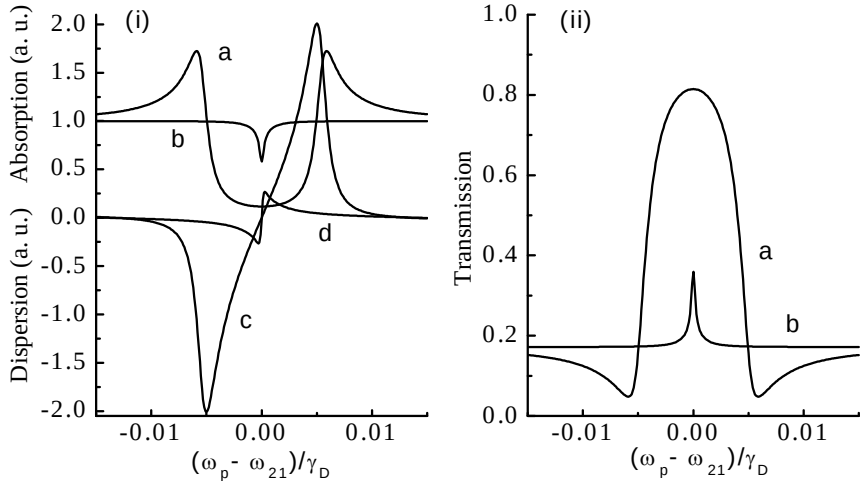

Figure 2.2: (i) Probe absorption (curves a, b) and dispersion (curves c, d) in arbitrary units (a. u) as a function of probe field detuning ($\omega_p - \omega_{21})/\gamma_D$ with coupling field Rabi frequencies $\Omega_{c1} = \Omega_{c2} = 10\,(2\pi \times MHz)$ and for various wave-vector mismatch cases for $k_p - k_c = -0.04k_p$ (curves a and c) and $k_p = k_c$ (curves b and d). The coupling fields are on resonance ($\Delta_{32} = \Delta_{42} = 0$). (ii) Probe transmission ($I_p(L)$ /$I_p(0)$) as a function of the probe detuning for wave-vector mismatch $k_p - k_c = -0.04k_p$ (curve a) and $k_p = k_c$ (curve b). Thus the values unity and zero on y-axis (in this and subsequent Figures) correspond respectively, to maximum ($I_p(L)=I_p(0)$) and minimum ($I_p(L)=0$) transmission of probe intensity. The density-length product (used in Eqs.(2.9)) is $NL = 2\times10^{11}$ atoms/cm^2 and other parameters are the same as in (i).

In above Figure 2.2(i) probe absorption ($\mathrm{Im}(I_{21}^{(1)}\gamma_D/\Omega_p)$) and dispersion ($\mathrm{Re}(I_{21}^{(1)}\gamma_D/\Omega_p)$) profiles are shown as a function of the probe detuning for various cases of coupling and probe field wave-vector mismatches. The coupling fields are on resonance ($\Delta_{32} = \Delta_{42} = 0$) and the Rabi frequencies are chosen equal ($\Omega_{c1} = \Omega_{c2}$) and of same magnitude as the spontaneous emission rate of the probe transition $2\gamma_{21}$(= $2\pi \times 10$ MHz). No transparency is found to exist for $k_p > k_c$ wave-vector mismatch case (hence results not shown). There is no perfect EIT even in the exact wave-vector

matching ($k_p = k_c$) case (curves b and d). It should be noted that for these values ($2\pi \times 10$ MHz) of the coupling field Rabi frequencies the criterion for observing EIT specified by Eq.(2.13) is not fulfilled. Yet a very wide and almost complete transparency window appears in the case when $k_p < k_c$ (curves a and c). The width of this resonance is in good agreement with the analytical result given by Eq.(2.24). The EIT resonance and the dispersion curves for $k_p = k_c$ case are narrower than those observed for $k_p < k_c$ since in the former case it is governed mainly by the two photon dephasing rate alone for small values of coupling Rabi frequencies whereas in the latter it depends (see Eq.(2.24)) upon the mismatch factor $k_p - k_c$ and the Rabi frequency of the coupling fields. Figure 2.2(ii) shows the probe transmission (using Eqs.(2.9)) as a function of the probe detuning for the same parameters as in Figure 2.2(i). The density length product used is NL = 2×10^{11} atoms/cm^2. The transmission at line center for $k_p < k_c$ (curve a) is very high as compared with the matched $k_p = k_c$ case (curve b).

We now consider the finite detuning case when the coupling fields are detuned on either side of the intermediate level.

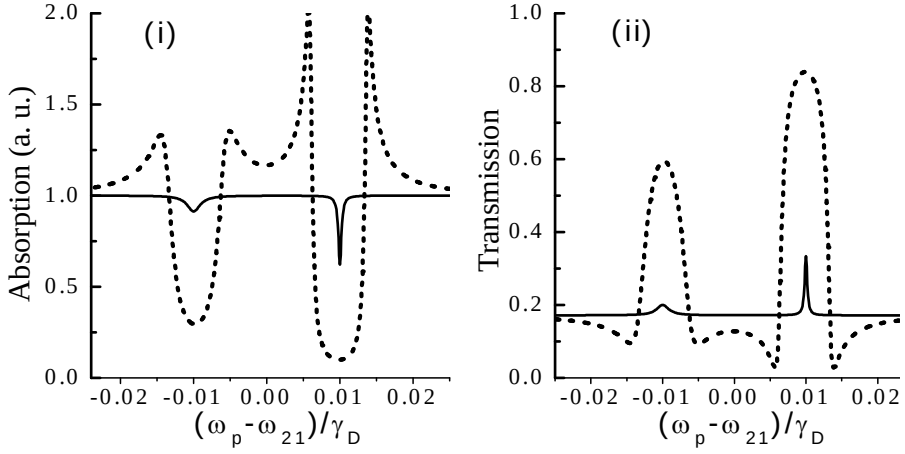

Figure 2.3: (i) Probe absorption (a. u.) as a function of the probe field detuning ($\omega_p - \omega_{21})/\gamma_D$ for the coupling field Rabi frequencies $\Omega_{c1} = \Omega_{c2} = 10\,(2\pi \times MHz)$ and various wave-vector mismatch cases, $k_p - k_c = -0.04k_p$ (dashed line) and $k_p = k_c$ (solid line). The coupling fields detuning chosen are, $\Delta_{42} = -\Delta_{32} = 10\,(2\pi \times MHz)$. (ii) Probe transmission ($I_p(L)/I_p(0)$) as a function of the probe detuning for density-length product, NL = 2×10^{11} atoms/cm^2 and the same parameters as in (i).

Figure 2.3(i) shows the probe absorption ($\mathrm{Im}(I_{21}^{(1)}\gamma_D/\Omega_p)$) variation as the probe frequency is tuned through the coupling field detuning. The probe absorption profile for this case splits into two distinct transparency windows corresponding to two distinct cascade subsystems. The transparency window occurring at the two photon resonance $\Delta_{21} + \Delta_{32} = 0$ corresponds to the $3S_{1/2} \rightarrow 3P_{3/2} \rightarrow 4D_{3/2}$ transition, whereas the other occurring at $\Delta_{21} + \Delta_{42} = 0$ corresponds to the $3S_{1/2} \rightarrow 3P_{3/2} \rightarrow 4D_{5/2}$ transition. Since these two cascade subsystems are decoupled, the depth and width of each transparency window is now governed by the two-photon depahsing rate parameter and the coupling field Rabi frequency in that particular subsystem. The asymmetry in the depth of the transparency in the two windows occurs as the two-photon decay rates in the two subsystems are dissimilar in the present Y system. The probe transmission shown in Figure 2.3(ii) also displays similar features.

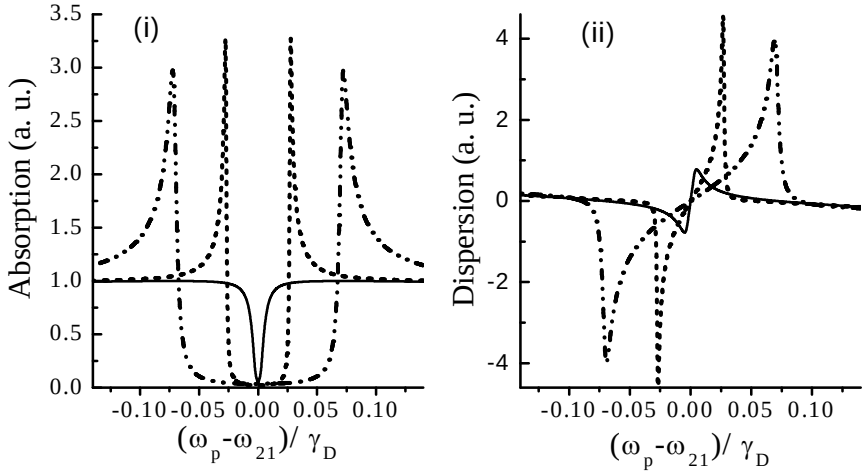

Figure 2.4: Probe (i) absorption and (ii) dispersion (a. u.) as a function of the probe field detuning $(\omega_p - \omega_{21})/\gamma_D$ for strong coupling field Rabi frequencies $\Omega_{c1} = \Omega_{c2} = 50\,(2\pi \times MHz)$ and various wave-vector mismatch cases, $k_p - k_c = -0.04k_p$ (dashed line) and $k_p = k_c$ (solid line). Also shown is the case when $k_c = 2k_p$ (dashed-dot-dot line).

Finally in Figure 2.4 we show the probe absorption and dispersion profile choosing values of the coupling field Rabi frequencies $\Omega_{c1} = \Omega_{c2} = 50\,(2\pi \times \mathrm{MHz})$ which fulfill the criterion Eq.(2.13) for observing large absorption reduction at line center. The coupling fields are on resonance ($\Delta_{32} = \Delta_{42} = 0$). As usual in the

matched wave-vector ($k_c = k_p$) case we observe a narrow resonance and complete transparency at the probe line center. For illustration purpose also shown is the result when $k_c = 2k_p$ (hypothetical case). In this case it is evident that the width of the transparency window (as predicted by Eq.(2.23)) is same as the separation between the AT peaks and hence the entire region between the AT doublet is rendered transparent.

2.5. Conclusion

In conclusion, we have studied electromagnetically induced transparency (EIT) of a probe field in both homogenously (radiative) and Doppler broadened four level Y-type atomic system driven by two strong laser (coupling) fields. Influence of residual Doppler broadening on two-photon resonances were assessed for various wave-vector mismatches occurring when the frequency of coupling fields is higher ($k_c > k_p$), equal ($k_c = k_p$), or lesser ($k_c < k_p$) than that of the probe field frequency. Contrary to the usual belief it is found that in the $k_c > k_p$ wave-vector mismatch case the residual Doppler broadening is actually conducive for the observation of transparency in Doppler broadened four level Y-type atomic systems. In this case, the probe absorption profile displays very wide and almost completely transparent single or double EIT windows whose width, depth and location depend upon the wave vector mismatch, Rabi frequencies and atom field detuning of the coupling fields. Thus it is possible to attain almost complete transparency over a broad range of frequencies which may be essential for propagation of very short light pulses through an inhomogeneously broadened medium. Analytical results derived to explain the velocity selective nature of transparency (absorption) and width of resonances are in good agreement with computed results.

2.6. References

1. J. E. Field, K. H. Hahn and S. E. Harris, Phys. Rev. Lett. **67**, 3062 (1991);

S. E. Harris, Phys. Today **50**, 36 (1997).

2. G. S. Agarwal and W. Harshawardhan, Phys. Rev. Lett. **77**, 1039 (1996).

3. J. Y. Gao, S. H. Yang, D. Wang, X. Z. Guo, K. X. Chen, Y. Jiang and B. Zhao, Phys. Rev. A **61**, 23401 (2000).

4. D. Wang, J. Y. Gao, J. H. Xu, G. La Rocca and F. Bassani, Europhys. Lett. **54**, 456 (2001); J. H. Xu, G. C. La Rocca, F. Bassani, D. Wang and J. Y. Gao, Opt. Commun. **216**, 157 (2003).

5. R. Arun, Phys. Rev. A **77**, 033820 (2008).

6. B. P. Hou, S. J. Wang, W. L. Yu and W. L. Sun, Phys. Rev. A **69**, 053805 (2004); B. K. Dutta and P. K. Mahapatra, J. Phys. B: At. Mol. Opt. Phys. **41**, 055501 (2008).

7. Y. Zhang, A. W .Brown and M. Xiao, Phys. Rev. Lett. **99**, 123603 (2007).

8. Y. Zhang, B. Anderson, A. W .Brown and M. Xiao, Appl. Phys. Lett. **91**, 061113 (2007).

9. L. G. Si, X. Y. Lu, X. Hao and J. H. Li, J. Phys. B: At. Mol. Opt. Phys. **43**, 065403 (2010).

10. J. Gea-Banacloche, Y. Q. Li, S. Z. Jin and M. Xiao, Phys. Rev.A **51**, 576 (1995).

11. D. J. Fulton, S. Shepherd, R. R. Moseley, B. D. Sinclair and M. H. Dunn, Phys. Rev. A **52**, 2302 (1995).

12. S. Shepherd, D. J. Fulton and M. H. Dunn, Phys. Rev. A **54**, 5394 (1996); J. R. Boon, E. Zekou, D. McGloin and M. H. Dunn, Phys. Rev. A **59**, 4675 (1999).

13. S. H. Autler and C. H. Townes, Phys. Rev. **100**, 703 (1955).

Chapter 3

EIT and Nonlinear Generation in Four-Level Double-Ladder System

In this chapter we explore the feasibility of attaining simultaneous electromagnetically induced transparency (DEIT) and efficient nonlinear generation in different configurations of Doppler broadened diamond (double-cascade) systems such as, the frequency up-conversion, nearly degenerate and degenerate scheme. Presented systematic study of the influence of various system parameters (dipole moments, level decay rates, transition frequencies) and driving (pump and coupling) field strength and wavenumber mismatch on absorption (loss) and nonlinear generation (gain) coefficients, which govern the propagation dynamics of the weak (probe and signal) fields in the Doppler broadened medium. We show that EIT and nonlinear generation efficiency depend critically on the type of residual Doppler broadenings present in each of the two cascade subsystems constituting the diamond system. Further it is observed that nonlinear generation with perfect EIT simultaneously in both subsystems is not possible as the process of nonlinear generation actually tends to oppose EIT. Furthermore we show how with suitable choice of the driving field strengths, sufficiently large nonlinear gain can be produced to offset the high absorption losses and create a steady state (equilibrium) situation in the medium. Under these conditions both probe and the signal fields propagate in the medium without further attenuation or gain.

3.1. Introduction

As mentioned earlier early works on EIT primarily focused on one-photon transitions between states of opposite parity in simple three level lamda (Λ), vee (V) and cascade (ladder - Ξ) systems. It is expected that more complicated levels structure of atomic system might generate further interesting effects. Accordingly studies involving modification of EIT and its applications with inclusion of an additional fourth level are also widely reported in literature. Many of these were initially carried out in closed-loop four-level system of a double Lambda (N) configuration. For example, doubly electromagnetically induced transparency (double-EIT) [1, 2]. Four-wave mixing (FWM) process and enhanced frequency conversion [3]. Using EIT technique in double Lambda configuration possible to explore quantum nonlinear optics and quantum information processes [4]. Relevant to this work's in four-level double Lambda (N) configuration, a four-level atomic system of diamond (◊) configuration (shown in Figure 3.1) which has also attracted considerable attention in recent years.

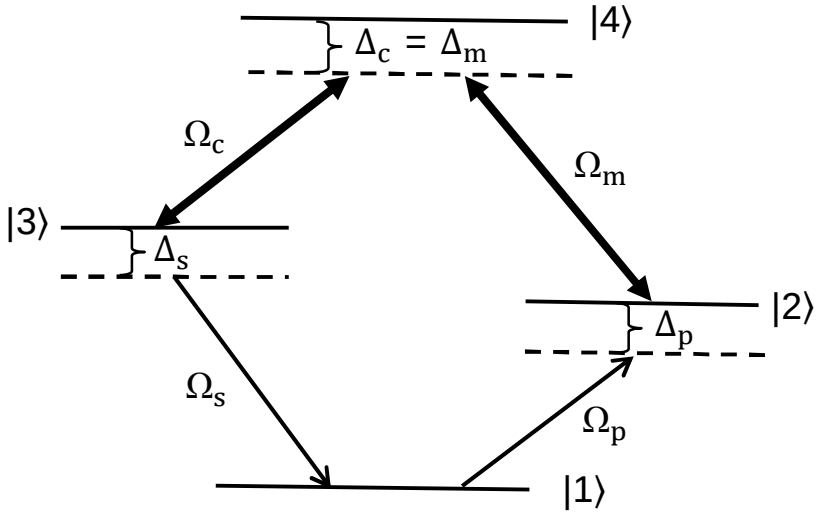

Figure 3.1: EIT and nonlinear generation scheme in double ladder configuration. Here Ω_p and Ω_s respectively, are Rabi frequencies of the weak probe and signal fields. Rabi frequencies of the strong pump and coupler fields are Ω_m and Ω_c respectively. The probe (signal) and pump (coupler) field frequency detuning from their respective atomic transitions are $\Delta_p = \omega_p - \omega_{21}$ ($\Delta_s = \omega_s - \omega_{31}$) and $\Delta_m = \omega_m - \omega_{42}$ ($\Delta_c = \omega_c - \omega_{43}$) respectively.

Four level ◊ scheme in recent times has been utilized in several studies by many authors [5-16]. Four level diamond (◊) systems that can be regarded as two three-level ladder subsystems sharing a common ground and highest upper levels. Coupling of these subsystems is caused by strong driving (coupler and pump) fields which connect the common upper level to (two) distinct intermediate states in each ladder subsystems as shown in Figure 3.1. In literature earlier studies of four level diamond (◊) systems appears to be no consistent theoretical formulation of EIT especially when the system is Doppler broadened. Such an analysis is important since experimental investigations of the EIT phenomenon and nonlinear optical processes aided by it are mostly performed in atomic vapours. Earlier studies show that the nature of the residual Doppler width of two-photon coherence arising due to wave-vector mismatch of the field and thermal motion of atoms in an atomic vapour can drastically affect EIT [16, 17] and the associated nonlinear processes. Since a diamond system essentially consists of two ladder subsystems, analysis and interpretation of these experiments would require examining EIT of both probe as well as the signal field generated via nonlinear mixing in a Doppler broadened ◊ system driven by two additional (pump and coupler) fields. Obviously, the weak signal approximation used in the existing theoretical formulations [12, 13] breaks down when the generated (signal) field grows sufficiently strong and one can no longer ignore its back reaction on the other (probe) field [9]. Accordingly one has to then simultaneously explore the conditions of EIT and gain by considering the coupled Maxwell's equations for both the weak (probe and signal) fields. Finally solution of Maxwell's Equations under the optimal conditions of EIT and gain will determine the propagation characteristics of the probe and signal fields in an extended medium consisting of four level diamond systems.

The aim of the work is to develop a theoretical formulation with the incorporation of all the aspects mentioned above. We deal with density matrix formulation, solve for the steady-state density matrix-equations for this system using first order perturbation in probe and generated (signal) fields. Expressions are derived for the one-photon as well as three-photon coherences which describe respectively, the absorption and gain properties of the probe and generated field resulting from

resonant nonlinear mixing. Neglecting depletion of the strong pump fields and under slowly varying amplitude condition, we also derive the coupled wave equations for the probe and generated signal fields from Maxwell equations. We present analytical and numerical calculations for EIT and propagation characteristics of the weak probe and signal fields as a function of the strong coupler and pump field amplitudes.

3.2. Four level atomic system-electromagnetic field interaction

3.2.1. Formulation

We consider a gas of atoms of mass m, in a thermal distribution at temperature T. The resonance response of each atom to laser light is modeled as a four-level system in a ◊ (diamond) configuration which has been experimentally realized in most alkali (Rb, Na) atoms. As shown schematically in Figure 3.1, the ground ($|1\rangle$) intermediate ($|2\rangle$) and the uppermost ($|4\rangle$) levels are in a three-level ladder configuration. Similarly, the intermediate level ($|3\rangle$), together with levels $|1\rangle$ and $|4\rangle$, forms another three-level ladder configuration. So the ◊ configuration can be regarded as a composite system of two (coupled) ladder configuration subsystems that share a common ground and uppermost states. An arbitrarily strong pump laser field $\vec{E}_m$ and a weak probe field $\vec{E}_p$ respectively, couple the dipole transitions $|2\rangle \rightarrow |4\rangle$ and $|1\rangle \rightarrow |2\rangle$ of one ladder subsystem. Coupling between the two subsystems is provided by application of another arbitrarily strong coupler laser field $\vec{E}_c$ to the dipole transitions $|3\rangle \rightarrow |4\rangle$ which also results in the generation of a fourth field $\vec{E}_s$ on the dipole transitions $|1\rangle \rightarrow |3\rangle$ via the process of four wave mixing $|1\rangle \rightarrow |2\rangle \rightarrow |4\rangle \rightarrow |3\rangle$ For this frequency matched process $\omega_p + \omega_m - \omega_c - \omega_s = 0$, the required phase-matching condition is given by $\Delta\vec{k} = \vec{k}_p + \vec{k}_m - \vec{k}_c - \vec{k}_s = 0$. Thus we have to formulate a theory for a four-level atomic system in ◊ (diamond) configuration interacting with four laser fields in closed-loop geometry.

The total electric field can be written as

$$\vec{E}(t) = \sum_\ell \vec{E}_\ell(t) = \sum_\ell [\,\vec{\varepsilon}_\ell\, e^{i(\vec{k}_\ell\cdot\vec{r}-\omega_\ell t)} + c.c.\,] \ , (\ell = p, s, c, m), \qquad (3.1)$$

where $\omega_\ell\,(\vec{\varepsilon}_\ell)$ is the frequency (amplitude) and $\vec{k}_\ell$ is the wavevector of the field $\vec{E}_\ell(t)$, (ℓ = p, s, c, m).

3.2.2. Interaction Hamiltonian

Using Eq.(1.15) the interaction Hamiltonian in the interaction picture and under rotating wave approximation is obtained as

$$V^{\text{int}} = -\hbar[\Omega_p e^{i(\vec{k}_p\cdot\vec{r}-\Delta_p t)}\,|2\rangle\langle 1| + \Omega_s e^{i(\vec{k}_s\cdot\vec{r}-\Delta_s t)}\,|3\rangle\langle 1| + \Omega_c e^{i(\vec{k}_c\cdot\vec{r}-\Delta_c t)}\,|4\rangle\langle 3| + \Omega_m e^{i(\vec{k}_m\cdot\vec{r}-\Delta_m t)}\,|4\rangle\langle 2| + \text{H.c.}]. \quad (3.2)$$

Here $\Omega_\ell = \vec{\mu}_{ij}\cdot\varepsilon_\ell/\hbar$, ($\ell$ = p, s, c, m) are the Rabi frequencies and $|i\rangle\langle j|$, (i, j =1, 2, 3, 4) are the atomic raising or lowering operators. The dipole operator matrix element is given by $\vec{\mu}_{ij} = \langle i|\vec{\mu}|j\rangle$, (i, j = 1, 2, 3, 4). The detuning of the field frequencies from atomic resonance frequencies are denoted $\Delta_p = \omega_p - \omega_{21}$, $\Delta_s = \omega_s - \omega_{31}$, $\Delta_m = \omega_m - \omega_{42}$ and $\Delta_c = \omega_c - \omega_{43}$.

3.2.3. Density matrix-equations of motion

Time evolution of the slowly varying components of the density matrix elements $\tilde{\rho}_{jk}$can now be written using Eqs.(3.2) and (1.18b) in Eq.(1.21) and the following transformations with the frequency matching condition $\omega_p + \omega_m - \omega_c - \omega_s = 0 (= \Delta_p + \Delta_m - \Delta_s - \Delta_c)$ to eliminate fast oscillating (exponential) terms as,

$$\tilde{\rho}_{21}^{(\Omega_p)} = \rho_{21}^{(\Omega_p)} e^{-i\vec{k}_p\cdot\vec{r}+i\Delta_p t}, \quad (3.3a)$$

$$\tilde{\rho}_{31}^{(\Omega_s)} = \rho_{31}^{(\Omega_s)} e^{-i\vec{k}_s\cdot\vec{r}+i\Delta_s t}, \quad (3.3b)$$

$$\tilde{\rho}_{41}^{(\Omega_p)} = \rho_{41}^{(\Omega_p)} e^{-i(\vec{k}_p+\vec{k}_m)\cdot\vec{r}+i(\Delta_p+\Delta_m)t}, \quad (3.3c)$$

$$\tilde{\rho}_{41}^{(\Omega_s)} = \rho_{41}^{(\Omega_s)} e^{-i(\vec{k}_s+\vec{k}_c)\cdot\vec{r}+i(\Delta_s+\Delta_c)t}, \quad (3.3d)$$

$$\tilde{\rho}_{21}^{(\Omega_s)} = \rho_{21}^{(\Omega_s)} e^{-i(\vec{k}_s+\vec{k}_c-\vec{k}_m)\cdot\vec{r}+i\Delta_p t}, \quad (3.3e)$$

$$\tilde{\rho}_{31}^{(\Omega_p)} = \rho_{31}^{(\Omega_p)} e^{-i(\vec{k}_p+\vec{k}_m-\vec{k}_c)\cdot\vec{r}+i\Delta_s t}. \quad (3.3f)$$

With phenomenological incorporation of the spontaneous decay in the equations of motion for diagonal matrix elements and relaxation due to spontaneous emission

process in off-diagonal (coherence) elements, the equations for time evolution of the slowly varying components of the density matrix $\rho(v)$ for atoms with velocity $\vec{v}$ are obtained as,

$$\dot{\tilde{\rho}}_{21}=-[i(-\Delta_p + \vec{k}_p.\vec{v})+\gamma_{21}]\tilde{\rho}_{21}-i\Omega_p(\rho_{22}-\rho_{11})- i\Omega_s\tilde{\rho}_{23}+ i\Omega_m^*\tilde{\rho}_{41}, \quad (3.4a)$$

$$\dot{\tilde{\rho}}_{31}=-[i(-\Delta_s + \vec{k}_s.\vec{v})+\gamma_{31}]\tilde{\rho}_{31}-i\Omega_s(\rho_{33}-\rho_{11})- i\Omega_p\tilde{\rho}_{32}+ i\Omega_c^*\tilde{\rho}_{41}, \quad (3.4b)$$

$$\dot{\tilde{\rho}}_{41}=-[i(-\Delta_p - \Delta_m + (\vec{k}_p + \vec{k}_m).\vec{v}) + \Gamma_{41}]\tilde{\rho}_{41}$$
$$-i\Omega_s\tilde{\rho}_{43}\ i\Omega_m\tilde{\rho}_{21}-i\Omega_p\tilde{\rho}_{42} + i\Omega_c\tilde{\rho}_{31}, \quad (3.4c)$$

$$\dot{\tilde{\rho}}_{32}=-[i(-\Delta_s - \Delta_p + (\vec{k}_s + \vec{k}_p).\vec{v})+ \gamma_{32}]\tilde{\rho}_{32}-i\Omega_p^*\tilde{\rho}_{31} + i\Omega_s\tilde{\rho}_{12}+i\Omega_c^*\tilde{\rho}_{42}-i\Omega_m\tilde{\rho}_{34}, \quad (3.4d)$$

$$\dot{\tilde{\rho}}_{42}=-[i(-\Delta_m + \vec{k}_m.\vec{v})+\gamma_{42}]\tilde{\rho}_{42}-i\Omega_m(\rho_{44}-\rho_{22})+ i\Omega_c\tilde{\rho}_{32}- i\Omega_p^*\tilde{\rho}_{41}, \quad (3.4e)$$

$$\dot{\tilde{\rho}}_{43}=-[i(-\Delta_c + \vec{k}_c.\vec{v})+\gamma_{43}]\tilde{\rho}_{43}-i\Omega_c(\rho_{44}-\rho_{33})+ i\Omega_m\tilde{\rho}_{23}- i\Omega_s^*\tilde{\rho}_{41}, \quad (3.4f)$$

$$\dot{\rho}_{11}= i(\Omega_p^*\tilde{\rho}_{21}-c.c)+ i(\Omega_s^*\tilde{\rho}_{31}-c.c)+2\gamma_{21}\rho_{22}+2\gamma_{31}\rho_{33}, \quad (3.4g)$$

$$\dot{\rho}_{22}= i(\Omega_p\tilde{\rho}_{12}-c.c)+i(\Omega_m^*\tilde{\rho}_{42}-c.c)+2\gamma_{42}\rho_{44}-2\gamma_{21}\rho_{22}, \quad (3.4h)$$

$$\dot{\rho}_{33}= i(\Omega_s\tilde{\rho}_{13}-c.c)+i(\Omega_c^*\tilde{\rho}_{43}-c.c) +2\gamma_{43}\rho_{44}-2\gamma_{31}\rho_{33}, \quad (3.4i)$$

$$\dot{\rho}_{44}= i(\Omega_m\tilde{\rho}_{24}-c.c)+i(\Omega_c\tilde{\rho}_{34}-c.c)-2\gamma_{42}\rho_{44}-2\gamma_{43}\rho_{44}. \quad (3.4j)$$

These equations (Eq.(3.4)) can be solved under the usual EIT conditions of arbitrarily strong pump and coupler fields in the following manner. In the standard limit of weak amplitudes of probe, Ω_p and signal, Ω_s fields all the population initially, is in the ground level $|1\rangle$ with a Maxwellian velocity distribution $M(v) = [\ln 2/(\pi\bar{v}^2)]^{3/2} \exp(-\ln 2\, \vec{v}\cdot\vec{v}/\bar{v}^2)$ where $\bar{v} = \sqrt{\ln 2}\, v_{th}$ and $v_{th} = \sqrt{2k_BT/m_a}$ is the most probable thermal velocity at a temperature T of an atom of mass m_a and k_B is the Boltzmann constant. Thus the zero-order solution of density matrix elements in the absence of probe (i.e., putting $\Omega_p = \Omega_s = 0$) is given simply by $\rho_{11}^0 = M(v)$ and all other zeroth-order matrix elements vanish. The probe (and signal) field are assumed to be sufficiently weak so as not to induce any population transfer to upper levels. Thus the relevant first-order (i.e., to leading order in probe Ω_p, signal Ω_s amplitude) slowly varying components of the density matrix elements are obtained as follows:

$$\dot{\tilde{\rho}}_{21}^{(\Omega_p)} = -\{i(-\Delta_p + \vec{k}_p \cdot \vec{v}) + \gamma_{21}\}\tilde{\rho}_{21}^{(\Omega_p)} + i\Omega_p M(v) + i\Omega_m^* \tilde{\rho}_{41}^{(\Omega_p)}, \quad (3.5a)$$

$$\dot{\tilde{\rho}}_{31}^{(\Omega_s)} = -\{i(-\Delta_s + \vec{k}_s \cdot \vec{v}) + \gamma_{31}\}\tilde{\rho}_{31}^{(\Omega_s)} + i\Omega_s M(v) + i\Omega_c^* \tilde{\rho}_{41}^{(\Omega_s)}, \quad (3.5b)$$

$$\dot{\tilde{\rho}}_{41}^{(\Omega_p)} = -\{i[(-\Delta_p - \Delta_m + (\vec{k}_p + \vec{k}_m) \cdot \vec{v}] + \Gamma_{41}\}\tilde{\rho}_{41}^{(\Omega_p)} + i\Omega_c \tilde{\rho}_{31}^{(\Omega_p)} + i\Omega_m \tilde{\rho}_{21}^{(\Omega_p)}, \quad (3.5c)$$

$$\dot{\tilde{\rho}}_{41}^{(\Omega_s)} = -\{i[(-\Delta_s - \Delta_c) + (\vec{k}_s + \vec{k}_c) \cdot \vec{v}] + \Gamma_{41}\}\tilde{\rho}_{41}^{(\Omega_s)} + i\Omega_c \tilde{\rho}_{31}^{(\Omega_s)} + i\Omega_m \tilde{\rho}_{21}^{(\Omega_s)}, \quad (3.5d)$$

$$\dot{\tilde{\rho}}_{21}^{(\Omega_s)} = -\{i[-\Delta_p + (\vec{k}_s + \vec{k}_c - \vec{k}_m) \cdot \vec{v}] + \gamma_{21}\}\tilde{\rho}_{21}^{(\Omega_s)} + i\Omega_m^* \tilde{\rho}_{41}^{(\Omega_s)}, \quad (3.5e)$$

$$\dot{\tilde{\rho}}_{31}^{(\Omega_p)} = -\{i[-\Delta_s + (\vec{k}_P + \vec{k}_m - \vec{k}_c) \cdot \vec{v}] + \gamma_{31}\}\tilde{\rho}_{31}^{(\Omega_p)} + i\Omega_c^* \tilde{\rho}_{41}^{(\Omega_p)}. \quad (3.5f)$$

In the above equations $2\gamma_{ij}$ are the spontaneous emission rates from level $|i\rangle \rightarrow |j\rangle$ (i, j =1- 4) and $\Gamma_{41} = \gamma_{42} + \gamma_{43}$ is the dephasing rate of the two-photon coherence established by probe and pump (or signal and coupler) fields between the states $|1\rangle \rightarrow |4\rangle$.

From the transformation equations (Eq.(3.3)) with the frequency matching condition $\omega_p + \omega_m - \omega_c - \omega_s = 0$ $(= \Delta_p + \Delta_m - \Delta_s - \Delta_c)$ were used to obtain set of equations (Eqs.(3.5a) through Eqs.(3.5f)) describing time evolution of the slowly varying components of the density matrix elements $\tilde{\rho}_{jk}$. As mentioned above, the closed loop FWM configuration of the double ladder system depicted in Figure 3.1, is formed via generation of a fourth field due to application of any three fields, and the phase matching conditions $\Delta\vec{k} = 0$ can be used to further determine the wave vectors of the generated signal as $\vec{k}_s = \vec{k}_p + \vec{k}_m - \vec{k}_c$ (see Eq.(3.5f)) and that of the generation of the probe field due to back reaction of the signal and coupler and pump fields as $\vec{k}_p = \vec{k}_s + \vec{k}_c - \vec{k}_m$ (see Eq.(3.5e)). Moreover in experiments, typically a nearly collinear geometry in which the probe and pump (signal and coupler) beams counter-propagate (along z-axis) is used in order to maximize two-photon Doppler cancellation. Accordingly we henceforth put $\vec{k}_s = \hat{z}\, k_s$, $\vec{k}_c = -\hat{z}\, k_c$, $\vec{k}_p = \hat{z}\, k_p$ and $\vec{k}_m = -\hat{z}\, k_m$ where $k_j = \omega_j / c$, $(j = p, m, s, c)$ are the wavenumbers. As $\vec{k}_j \cdot \vec{v} = k_j v_z$, $(j = p, m, s, c)$ the Maxwellian velocity distribution reduces to one-dimensional form $M(v_z)$ involving only the v_z component.

3.2.4. Linear and nonlinear coherences: steady-state solutions

The above density matrix elements ρ_{jk} are in the interaction picture and they are related to their counterparts ρ^{s}_{kj} in the Schrodinger picture via the relation $\rho_{jk} = \rho^{s}_{jk} e^{i\omega_{jk}t}$. Hence the steady-state solution obtained by setting the time derivates zero on the left-hand side of Eq.(3.5) yields the velocity averaged one-photon coherences in the Schrodinger picture (dropping superscript s and subscript z in v_z for brevity) as

$$I_{21}^{(\Omega_p)} = e^{-i(k_p z-\omega_p t)} \int \rho_{21}^{(\Omega_p)}(v)\, dv = i\Omega_p \int dv\, M(v) \frac{\left(\xi_s(v)\phi_{pm}(v)+|\Omega_c|^2\right)}{\xi_p(v)\xi_s(v)\phi_{pm}(v)+|\Omega_m|^2\xi_s(v)+|\Omega_c|^2\xi_p(v)} \quad (3.6a)$$

$$I_{31}^{(\Omega_s)} = e^{-i(k_s z-\omega_s t)} \int \rho_{31}^{(\Omega_s)}(v)\, dv = i\Omega_s \int dv\, M(v) \frac{\left(\xi_p(v)\eta_{sc}(v)+|\Omega_m|^2\right)}{\xi_p(v)\xi_s(v)\eta_{sc}(v)+|\Omega_m|^2\xi_s(v)+|\Omega_c|^2\xi_p(v)}. \quad (3.6b)$$

The real and imaginary parts of Eq.(3.6) describe dispersion and absorption of the probe and generated FWM signal in the inhomogeneous double ladder system. The generation of four wave mixing field and probe is governed by the nonlinear coherences, which in the Schrodinger picture (dropping superscript s and subscript z in v_z for brevity) as

$$I_{21}^{(\Omega_s)} = e^{-i(k_p z-\omega_p t)} \int \rho_{21}^{(\Omega_s)}(v)dv = -i\Omega_s \int dv\, M(v) \frac{|\Omega_m||\Omega_c|}{\xi_p(v)\xi_s(v)\eta_{sc}(v)+|\Omega_m|^2\xi_s(v)+|\Omega_c|^2\xi_p(v)}, \quad (3.7a)$$

$$I_{31}^{(\Omega_p)} = e^{-i(k_s z-\omega_s t)} \int \rho_{31}^{(\Omega_p)}(v)dv = -i\Omega_p \int dv\, M(v) \frac{|\Omega_m||\Omega_c|}{\xi_p(v)\xi_s(v)\phi_{pm}(v)+|\Omega_m|^2\xi_s(v)+|\Omega_c|^2\xi_p(v)} \quad (3.7b)$$

where

$$\xi_p(v) = i\left[k_p v - \Delta_p\right] + \gamma_{21}, \quad (3.8a)$$

$$\xi_s(v) = i[k_s v - \Delta_s] + \gamma_{31}, \quad (3.8b)$$

$$\phi_{pm}(v) = i\left[(k_p - k_m)v - \Delta_p - \Delta_m\right] + \Gamma_{41}, \quad (3.8c)$$

$$\eta_{sc}(v) = i[(k_s - k_c)v - \Delta_s - \Delta_c] + \Gamma_{41}. \quad (3.8d)$$

A diamond system can be regarded as a combination of two Doppler broadened three-level cascade subsystems which share a common ground and a highest upper level. A typical three-level cascade system interacting with a probe and pump fields (termed subsystem-I) exhibits perfect EIT for probe at certain values of pump field strength. This can be seen from Eq.(3.6a) which in the limit of zero coupling field, $\Omega_c = 0$, reduces to the usual EIT result for three-level cascade system. Let us recall that EIT in an isolated (three level ladder) subsystem-I occurs due to destructive interference between two channels: (i) a one-photon (direct) probe absorption path $|1\rangle \rightarrow |2\rangle$ and (ii) another (indirect) three-photon path $|1\rangle \rightarrow |4\rangle \rightarrow |2\rangle$. Note that the transition $|1\rangle \rightarrow |4\rangle$ involved (in the three-photon process) is the two-photon transition created by probe and pump fields, the strength of which (and hence the three-photon path) can be controlled by varying the pump field strength.

Now application of another strong (coupling) field Ω_c to an adjacent transition involving the common upper but different intermediate level (of subsystem-II) couples the two subsystems and modifies the EIT response of the probe field. This is evident from the appearance of an additional coupling field dependent (second) term in the numerator (and also in the denominator) in Eq.(3.6a) which results in enhanced probe absorption. Physically this effect can be interpreted in terms of incomplete destructive interference brought about by an additional two-photon transition $|1\rangle \rightarrow |4\rangle$ created by the coupling and signal fields as follows: Application of the coupling field Ω_c gives rise to generation of a fourth weak (signal) field on the ground to intermediate transition (in the cascade subsystem-II) through a nonlinear coherence $I_{31}^{(\Omega_p)}$ (see Eq.(3.7b)) created by mixing of the probe, pump and coupler fields. In this manner, the other three-level cascade EIT system interacting with a signal and coupling fields (termed subsystem-II) is formed. We note from Eq.(3.7) that the nonlinear coherences $I_{31}^{(\Omega_p)}$(and $I_{21}^{(\Omega_s)}$) depend on the strength of drive fields and hence can be suitably enhanced by varying the strength of both the fields. Thus as the strength of the coupling field is varied (for a fixed initially applied pump field strength), the generated signal field can grow strong enough to mix with the coupling and pump field and cause regeneration of the probe field through a nonlinear

coherence $I_{21}^{(\Omega_s)}$. This extra channel formed by the three photon transition $|1\rangle \rightarrow |4\rangle \rightarrow |2\rangle$ for reaching the intermediate state $|2\rangle$ (which is the excited state for probe absorption transition) tends to destroy the usual EIT that existed in the subsystem-I before application of the coupling field.

Let us now examine the influence of (two-photon) residual Doppler broadening arising due to wavenumber mismatch of probe and pump (or coupling and signal) fields. We observe from Eq.(3.6) that the EIT of probe (and signal) field depend upon the residual broadening through the factors $\phi_{pm}(v)$ (and $\eta_{sc}(v)$). It is usually expected that EIT will be observable when the field strength dependent terms in the denominator of Eq.(3.6) are very large compared with the residual Doppler broadening dependent terms. However as we shall show later, through numerical calculations, this is not true in general and that EIT and nonlinear generation critically depend upon the nature of the residual broadening.

3.2.5. Signal-probe generation and propagation characteristics

To investigate the generation and transmission characteristics of the weak fields we consider propagation of the signal and probe waves through an extended medium composed of double ladder systems. Propagation of a field of the plane wave form given by Eq.(3.1) is described by the Maxwell's wave equation

$$(\nabla^2 - \frac{1}{c^2}\frac{\partial^2}{\partial t^2})E_\ell = \frac{4\pi}{c^2}\frac{\partial^2}{\partial t^2}(P_\ell^L + P_\ell^{NL}) \ , \ (\ell = s, p). \qquad (3.9)$$

where P_ℓ^L and P_ℓ^{NL} respectively, are the macroscopic linear and nonlinear polarizations associated with and aligned along the direction of the field $\vec{E}_\ell$. In general the macroscopic polarization P, i.e., the ensemble average of the induced dipole moment per unit volume in a medium of atomic number density N is given by (as mentioned in Chapter 1 section **1.3.3**)

$$P = N\,Tr(\mu < \rho >) = N\sum_{j,k=1}^{4}\mu_{jk} < \rho_{kj} >$$
$$= N\mu_{12} < \rho_{21} > + N\mu_{13} < \rho_{31} > + c.c. \qquad (3.10)$$

Here angular brackets < > denote averaging over thermal velocities i.e.,$< \rho_{ij} > = \int \rho_{ij}(v)dv$. We thus have

$$P_{31} = P_s^L + P_s^{NL} = N\mu_{13}\left(I_{31}^{(\Omega_s)} + I_{31}^{(\Omega_p)}\right)e^{i(k_s z-\omega_s t)} + c.c. \ , \qquad (3.11a)$$

$$P_{21} = P_p^L + P_p^{NL} = N\mu_{12}\left(I_{21}^{(\Omega_p)} + I_{21}^{(\Omega_s)}\right)e^{i(k_p z-\omega_p t)} + c.c. \ . \qquad (3.11b)$$

Substituting Eqs.(3.11a) and (3.11b) along with Eq.(3.1) in Eq.(3.9) and assuming no depletion of the driving fields and the validity of the slowly-varying amplitude approximation, we get the following coupled waves equations for signal and probe field amplitudes:

$$\frac{\partial}{\partial z}\varepsilon_s = \frac{\alpha_s}{2}\varepsilon_s + \frac{\beta_s}{2}\varepsilon_p \ , \qquad (3.12a)$$

$$\frac{\partial}{\partial z}\varepsilon_p = \frac{\alpha_p}{2}\varepsilon_p + \frac{\beta_p}{2}\varepsilon_s \ . \qquad (3.12b)$$

The second term β_j , (j = s, p) on the right-hand side of Eqs.(3.12a) and (3.12b) arise from the nonlinear polarization and give rise to generation of the signal and probe fields via four wave mixing. The first terms α_j (j = s, p) originate from the linear polarization and describe EIT absorption (EIT) and dispersion properties of the atomic medium. These are given by

$$\alpha_s = i\frac{4\pi N}{\hbar\gamma_D}k_s|\mu_{31}|^2\left(\frac{I_{31}^{(\Omega_s)}}{\Omega_s/\gamma_D}\right), \beta_s = i\frac{4\pi N}{\hbar\gamma_D}k_s|\mu_{31}||\mu_{21}|\left(\frac{I_{31}^{(\Omega_p)}}{\Omega_p/\gamma_D}\right), \qquad (3.13a)$$

$$\alpha_p = i\frac{4\pi N}{\hbar\gamma_D}k_p|\mu_{21}|^2\left(\frac{I_{21}^{(\Omega_p)}}{\Omega_p/\gamma_D}\right), \beta_p = i\frac{4\pi N}{\hbar\gamma_D}k_p|\mu_{31}||\mu_{21}|\left(\frac{I_{21}^{(\Omega_s)}}{\Omega_s/\gamma_D}\right). \qquad (3.13b)$$

It should be noted that since $\alpha_s \propto iI_{31}^{(\Omega_s)}$, the *real* and *imaginary* parts of α_s (α_p) respectively, describe absorption and dispersion properties of the generated signal (probe) field in the medium. The dispersion vanishes at line center since the imaginary part of α_s (α_p) is zero at exact resonance. Thus it can be shown and verified numerically that the coefficients α_j and β_j (j = s, p) given by Eqs.(3.13) are purely real at line center. For this particular case in which all the fields are on-resonance and using the boundary condition at the input $\varepsilon_p(z = 0) = \varepsilon_p(0)$ and

$\varepsilon_s(z = 0) = 0$, the coupled set of Eqs.(3.12) can be solved to obtain the field amplitudes for the signal, $\varepsilon_s(z)$ and the probe wave, $\varepsilon_p(z)$ in the medium as

$$\varepsilon_s(z) = \varepsilon_p(o)\frac{\beta_s}{2\Phi}\exp\left\{\left(\frac{\alpha_p+\alpha_s}{4}\right)z\right\}\sinh(\Phi z)\,, \tag{3.14a}$$

$$\varepsilon_p(z) = \varepsilon_p(o)\exp\left\{\left(\frac{\alpha_p+\alpha_s}{4}\right)z\right\}\left(\cosh(\Phi z) + \frac{(\alpha_p-\alpha_s)}{4\Phi}\sinh(\Phi z)\right)\,, \tag{3.14b}$$

where

$$\Phi = \sqrt{\beta_s\beta_p/4 + (\alpha_p/4 - \alpha_s/4)^2}\quad . \tag{3.15}$$

It is also evident from Eqs.(3.14) and (3.15) that an optimal case for signal generation is when Φ attains a minimum value. This occurs when the (on-resonance) absorption coefficients (for the probe and signal) in both the ladder subsystems become equal i.e.,

$$\alpha_p = \alpha_s(= -\alpha). \tag{3.16}$$

Using Eq.(3.16) in Eq.(3.15) we obtain the following expression for the relative (to incident probe intensity) signal and probe intensities

$$\frac{I_s(z)}{I_p(o)} = \frac{|\varepsilon_s(z)|^2}{|\varepsilon_p(o)|^2} = \frac{\beta_s}{\beta_p}\,\frac{1}{4}\left(e^{[\sqrt{\beta_s\beta_p}\,-\alpha]z} + e^{-[\sqrt{\beta_s\beta_p}\,+\alpha]z} - 2e^{-\alpha z}\right)\,, \tag{3.17a}$$

$$\frac{I_p(z)}{I_p(o)} = \frac{|\varepsilon_p(z)|^2}{|\varepsilon_p(o)|^2} = \frac{1}{4}\left(e^{[\sqrt{\beta_s\beta_p}\,-\alpha]z} + e^{-[\sqrt{\beta_s\beta_p}\,+\alpha]z} + 2e^{-\alpha z}\right). \tag{3.17b}$$

Clearly the first terms in Eq.(3.17) govern the propagation characteristics of the signal and probe fields, as the second and third terms (depending upon the values of α and β_s, β_p) will vanish at some propagation distance z in the medium. Interestingly now the field propagation characteristics are determined by competition between the nonlinear generation (effective gain) coefficient $(\beta_s\beta_p)^{1/2}$ and the absorption (loss) coefficient α. Hence the fields may exhibit gain, $((\beta_s\beta_p)^{1/2} > \alpha)$, attenuation $((\beta_s\beta_p)^{1/2} < \alpha)$ or matching $((\beta_s\beta_p)^{1/2} = \alpha)$ in the course of propagation in the medium. Furthermore we observe from Eq.(3.17a) that the generated signal field intensity can be larger, equal to or less than that of the probe field. In order to

determine the values of the system and field parameters required for fulfilling above conditions we find through Eqs.(3.13) the ratios of the absorption and gain coefficients as

$$\frac{\beta_s}{\beta_p} = \frac{k_s}{k_p} \times \frac{I_{31}^{(\Omega_p)}/\Omega_p}{I_{21}^{(\Omega_s)}/\Omega_s}, \tag{3.18a}$$

$$\frac{\alpha_s}{\alpha_p} = \frac{k_s}{k_p} \times \frac{|\mu_{31}|^2}{|\mu_{21}|^2} \times \frac{I_{31}^{(\Omega_s)}/\Omega_s}{I_{21}^{(\Omega_p)}/\Omega_p}. \tag{3.18b}$$

Obviously the absorption and nonlinear generation coefficients (through $I_{m1}^{(\Omega_j)}$ (j = s, p; m = 2, 3)) depend upon system and field parameters such as the level decay rates γ_{ij} (i, j = 1- 4), the field strength ($|\Omega_c|^2$, $|\Omega_m|^2$). These also depend through the factor $\eta_{sc}(v)$ (and $\phi_{pm}(v)$), on the residual Doppler broadening caused by the two-photon wave-vector mismatch $k_s - k_c$ (and $k_p - k_m$) between the signal and coupler (probe and pump) fields. In this regard the two possible regimes of pump and probe frequencies are:

(i) Non-degenerate case, $k_s \neq k_p$:

The first nondegenerate frequency case would essentially involve excitation of different intermediate levels for the probe and signal transitions in the two ladder subsystems. Thus the spontaneous decay rates, the dipole moments μ_{ij} $(i, j = 1 - 3)$ of the transitions and the wavenumber k_j (j = s, p) mismatches may vastly differ for the probe and signal transitions. This can be seen for instance in the frequency upconversion schemes [7] where $\omega_s \gg \omega_p$. In this particular case $k_s \gg k_c$ in the subsystem-I formed by the transition ($5S_{1/2} \rightarrow 6P_{3/2} \rightarrow 5D_{5/2}$) and therefore the wavenumber mismatch $k_s - k_c$ has a positive sign and is very large compared with the (one-photon) Doppler width of the probe transition. Whereas $k_p \approx k_m$ in the other subsystem-II formed by the transition $5S_{1/2} \rightarrow 5P_{3/2} \rightarrow 5D_{5/2}$ and the wavenumber mismatch has a small negative value. A positive and large wavenumber mismatch is known to have a detrimental effect on the EIT phenomenon in ladder systems [17]. Thus absorption in each of the two ladder subsystem will differ considerably leading to violation of the condition, $\alpha_p = \alpha_s$. Although the adverse effect of wavenumber

mismatch on EIT can also be offset by applying higher drive field intensities, in this case coupling field amplitudes much larger than the Doppler width (beyond EIT regime) may be needed. Thus in Doppler broadened diamond systems the possibility of large frequency up-conversion using EIT does not seem feasible.

(ii) Degenerate case, $k_s = k_p$:

In contrast for degenerate probe and signal frequencies ($\omega_s = \omega_p$), $k_s = k_p$ and therefore the residual Doppler broadening in the two subsystems will be equal. But the dipole moments μ_{ij} and the spontaneous decay rates γ_{ij} of the signal and probe transitions may still be dissimilar. In this situation, the ratios $\frac{\beta_s}{\beta_p}$ and $\frac{\alpha_s}{\alpha_p}$ will depend (see Eq.(3.18)) only on the nature of the wavenumber mismatch and the strength of the drive fields.

(iii) Nearly degenerate case:

It remains to be seen what happens in the second case of nearly degenerate signal and probe frequency ($\omega_s \sim \omega_p$) involving excitation of different intermediate transitions ($\mu_{13} \neq \mu_{12}$) for signal and probe in each ladder subsystem. Let us consider a case when k_s (k_p) does not differ much from k_c (k_m). It is then expected that if the applied driving fields strengths are much large compared with the wavenumber mismatch ϕ_{pm}, η_{sc} and level decay rates γ_{21}, γ_{31} etc., so that the first term in the numerator and denominator of Eqs.(3.6) and (3.7) are negligible compared to the field strength ($|\Omega_c|^2$, $|\Omega_m|^2$) dependent terms, the relations Eqs.(3.18) will reduce to the form

$$\frac{\beta_s}{\beta_p} \cong \frac{k_s}{k_p}\,, \tag{3.19a}$$

$$\frac{\alpha_s}{\alpha_p} \cong \frac{k_s}{k_p} \times \frac{|\mu_{31}|^2}{|\mu_{21}|^2} \times \frac{|\Omega_m|^2}{|\Omega_c|^2}\,. \tag{3.19b}$$

The above mentioned nearly degenerate situation may arise for instance, in typical alkali atoms when using D_1 (D_2) lines as intermediate levels. In this situation if the probe and signal fields are generated respectively, on the D_1 and D_2 transitions, the

wavenumbers are nearly equal ($k_s \cong k_p$) but the transition strength is $|\mu_{31}|^2 = 2|\mu_{21}|^2$. Using these values in Eq.(3.19) we find that for a given pump amplitude Ω_m, the value of pump amplitude Ω_c at which absorption coefficients for probe and signal in both ladder subsystems becomes equal ($\alpha_s = \alpha_p = \alpha$) is obtained as

$$|\Omega_c| = \sqrt{2}|\Omega_m| \,. \tag{3.20a}$$

Moreover the nonlinear coefficients for the probe and signal generation satisfy the relation

$$\beta_s \cong \beta_p, \tag{3.20b}$$

which in conjunction with Eq.(3.19) implies that $\sqrt{\beta_s \beta_p} - \alpha = 0$ (see Eq.(3.17) and the discussion succeeding it). Hence we have shown that even for a nearly degenerate probe- signal scheme, with proper choice of the coupler and pump field amplitude it may be possible to observe matched propagation of the signal and probe waves through the medium with no further attenuation or gain.

In certain degenerate probe and signal frequencies ($k_s = k_p$) schemes where the intermediate levels belong to the same electronic level or manifold; such as, for transitions involving Zeeman levels of D2 transition in Cs atoms [12,13] the dipole moments μ_{ij} and the spontaneous decay rates γ_{ij} of the signal and probe transitions may be similar. In such a case Eq.(3.19) shows that the absorption (and nonlinear) coefficients for probe and signal in both ladder subsystems become equal when $|\Omega_c| = |\Omega_m|$.

3.3. Numerical results and discussions

For this diamond (double ladder) configuration the numerical results are obtained by performing numerically, one-dimensional velocity, v_z averaging in Eqs.(3.6) and (3.7) which subsequently are used through Eq.(3.13) and (3.15), for further numerical evaluation of Eq.(3.14). The theory is applied to an alkali-metal atomic vapor in which the coupled double-ladder (◊) configuration of Figure 3.1 can

easily be realized. For illustration, let us consider a ^{87}Rb atom in which a weak 795 nm (probe) laser is tuned to the $5^2S_{1/2} \rightarrow 5^2P_{1/2}$ (D_1 line) transition and a strong 762 nm (pump) laser driving the transition $5^2P_{1/2} \rightarrow 5^2D_{3/2}$ form a three level ladder subsystem-I. The other ladder subsystem-II is formed by an applied strong 776 nm coupler laser on the transition $5^2D_{3/2} \rightarrow 5^2P_{3/2}$ and the internally generated weak signal field on the 780 nm, $5^2P_{3/2} \rightarrow 5^2S_{1/2}$ transition (D_2 line). Since $k_p < k_m (k_s < k_c)$, in this double ladder scheme, the sign of the wavenumber mismatch between the probe and pump fields $(k_p - k_m)$ in subsystem-I and that between the generated signal and coupling fields $(k_s - k_c)$ in the other ladder subsystem-II are negative. These wavenumber mismatches introduces a residual Doppler width of the order 11(MHz×2π) in subsystem-I and 1.3(MHz×2π) in subsystem-II. Furthermore, to facilitate comparison we also show numerical results for the other two (hypothetical) cases of, perfect wavenumber matching $k_p = k_m (k_s = k_c)$ and positive mismatch which occurs when $k_p > k_m (k_s > k_c)$. In our numerical calculations both drive fields (pump and coupler) are fixed on resonance with their respective transitions, $\Delta_{42} = \Delta_{43} = 0$ and all other parameters are expressed in units of the Doppler width $\gamma_D (= k_p \bar{v})$, i. e., $2\gamma_{21}/\gamma_D = 2\gamma_{31}/\gamma_D = 0.024$, $\Gamma_{41}/\gamma_D = (\gamma_{42} + \gamma_{43})/\gamma_D = 0.001$. The Doppler width (half width at half maximum) γ_D chosen is 250 (MHz × 2π).

We first study probe EIT characteristics by plotting imaginary part of the coherence $I_{21}^{(\Omega_p)}/(\frac{\Omega_p}{\gamma_D})$ as a function of the probe detuning Δ_p/γ_D. Figure 3.2 illustrates the influence of coupling field on probe EIT characteristics for various cases of pump-probe wavenumber mismatch. From Figure 3.2, in the absence of the coupling field ($\Omega_m = 0$), we obtain the result for an isolated three-level cascade subsystem-I (see Figure 3.2(i) and (iii)). It is the general belief that perfect two-photon Doppler cancellation i.e., $k_p = k_c$ is essential for attaining EIT in a Doppler broadened medium. Because in that case the EIT resonance is Doppler free and we can deduce from Eq.(3.6a) and (3.8) the following criterion (in subsystem-I, for example) for observation of EIT

$$\Omega_m >> \sqrt{\gamma_D \times \gamma_{42}} \quad (\text{or} \quad \Omega_m >> 8\text{MHz} \times 2\pi), \tag{3.21}$$

as against the requirement for the wavenumber mismatch case

$$\Omega_m >> \sqrt{\gamma_D \times |k_p - k_m|\bar{v}} \quad (\text{or } \Omega_m >> 50\text{MHz} \times 2\pi), \qquad (3.22)$$

where $|k_p - k_m|\bar{v}$ is the (magnitude) of the residual Doppler width due to the wavenumber mismatch between the pump-probe fields.

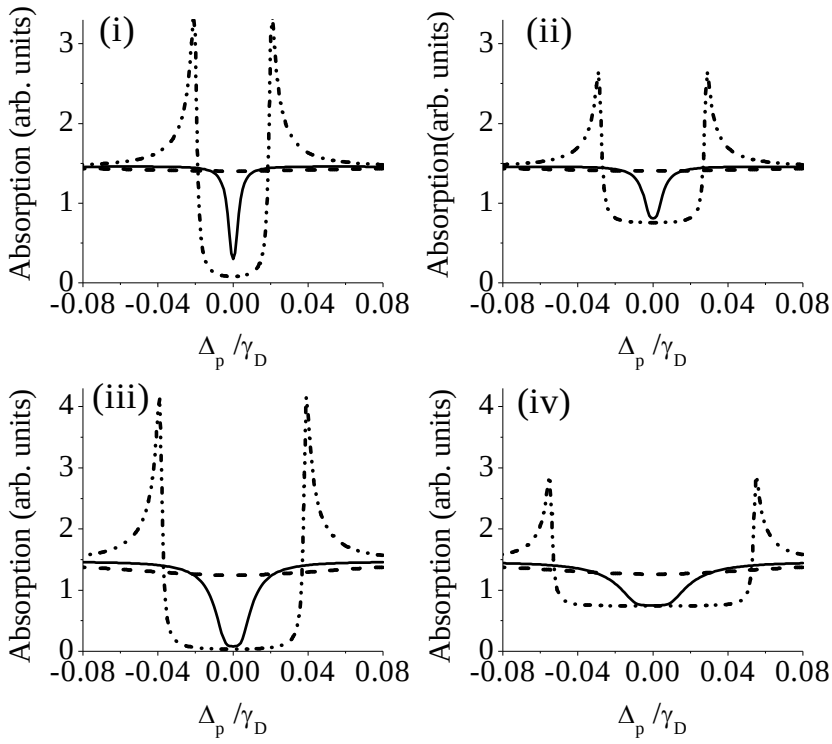

Figure 3.2: Influence of wave-vector mismatch on probe EIT [Im $(I_{21}^{(\Omega_p)}\gamma_D/\Omega_p)$] as function of probe detuning Δ_p/γ_D for various values of the coupler and pump field Rabi frequencies, (i) $\Omega_c = 0.0, \Omega_m = 0.05\gamma_D$ (ii) $\Omega_c = \Omega_m = 0.05\gamma_D$ (iii) $\Omega_c = 0.0, \Omega_m = 0.1\gamma_D$ (iv) $\Omega_c = \Omega_m = 0.1\gamma_D$. The wavenumber mismatch, $k_p - k_m$ are $-0.04\,k_p$ (dash-dot-dot curves), 0 (solid curves) and $+0.04\,k_p$ (dashed curves).

It should also be noted that the same criterion as Eq.(3.21) holds in the stationary atom (radiatively broadened) case, but with γ_D replaced by the one-photon (homogeneous) dephasing rate γ_{21} of the probe transition. In the present case we estimate from the criteria Eq.(3.21) and Eq.(3.22) that in order to observe EIT of the probe, the pump amplitude Ω_m/γ_D should be much greater than 0.03 (for $k_p = k_m$)

and 0.2 (for the wavenumber mismatch) case. It is for this reason we observe *no EIT in the positive mismatch* case (dashed curves in Figure 3.2(i)-(iv)) when Ω_m/γ_D = 0.05 and 0.1. Moreover for Ω_m/γ_D = 0.05 the complete two-photon Doppler cancellation ($k_p = k_m$) case (solid curve in Figure 3.2(i)) also does not show perfect EIT. However we find that the negative wavenumber mismatch case shows an almost complete and wide EIT resonance (dash-dot-dot curve in Figure 3.2(i)) at even this value of pump amplitude (Ω_m/γ_D = 0.05) which does not fulfil the criterion Eq.(3.22) for observing EIT. Furthermore, the width of the EIT window is also found to depend upon the values of wavenumber mismatch and the pump amplitude [18]. Figure 3.2(ii) and (iv) show that application of a coupling field Ω_c results in further power broadening of the EIT resonances. In addition, its effect is seen as a rise in the absorption level by a constant value through entire probe detuning regime. As discussed in Section **3.2.4** this reduction of EIT (or rise in absorption) arises due to incomplete destructive interference and is determined by the coupling field power dependent second term in Eq.(3.6a).

The drive (pump and coupling) fields actually play a dual role: the first is in the generation of the signal (or conversely the probe) via nonlinear mixing of any three fields and the second is in causing the EIT of the weak fields connected to the ground state. The mechanism of generation and propagation characteristics of the signal and probe was discussed analytically in Section **3.2.5** and numerical results for the same will be presented below. At present assuming that significant generation of the signal field occurs, we examine the simultaneous effect of the coupling and pump fields on the EIT of the generated signal and probe fields.

In Figure 3.3 we show the EIT characteristics for both the probe and generated signal fields including the actual residual Doppler broadening existing in each subsystem. As seen in Figure 3.2 above, for zero or weak coupling field amplitudes Ω_c the probe transparency is maximum whereas the signal field does not exist. As the coupling field amplitude Ω_c increases, coupling between the two ladder subsystems occurs (see the discussion in Section **3.2.4**). Consequently, the probe EIT diminishes (or absorption increases) whereas the signal field EIT increases. The probe and signal

fields display equal amount of EIT (or absorption) when the drive field amplitudes are equal $\Omega_c = \Omega_m$ (curves b in Figure 3.3) and for coupler field amplitude larger than the pump ($\Omega_c > \Omega_m$), signal EIT is higher than the probe EIT.

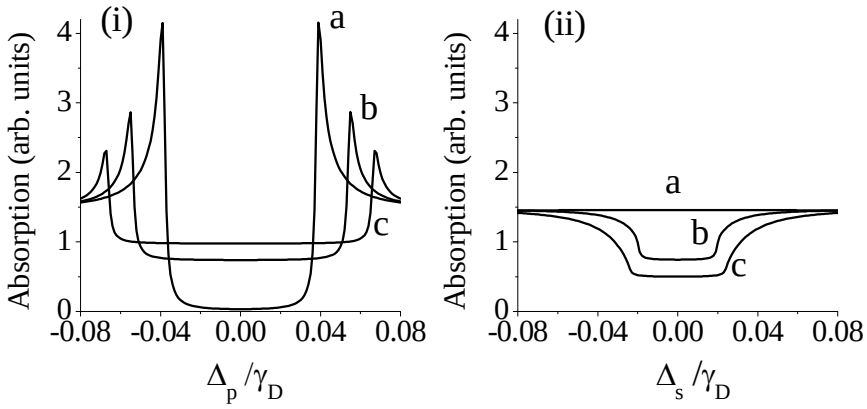

Figure 3.3: EIT of (i) probe [Im $(I_{21}^{(\Omega_p)}\gamma_D/\Omega_p)$] and (ii) generated signal [Im $(I_{31}^{(\Omega_s)}\gamma_D/\Omega_s)$] as a function of the probe (signal) field detuning Δ_p/γ_D (Δ_s/γ_D) for various coupling field Rabi frequencies $\Omega_c = 0$ (curve a), $\Omega_c = \Omega_m$ (curve b) and $\Omega_c = \sqrt{2}\Omega_m$ (curve c). The value of the pump field Rabi frequency is fixed at $\Omega_m/\gamma_D = 0.1$. Only the actual wavenumber mismatch cases for the probe ($k_p - k_m = -0.04\,k_p$) and signal ($k_s - k_c = -0.005\,k_p$) fields are plotted.

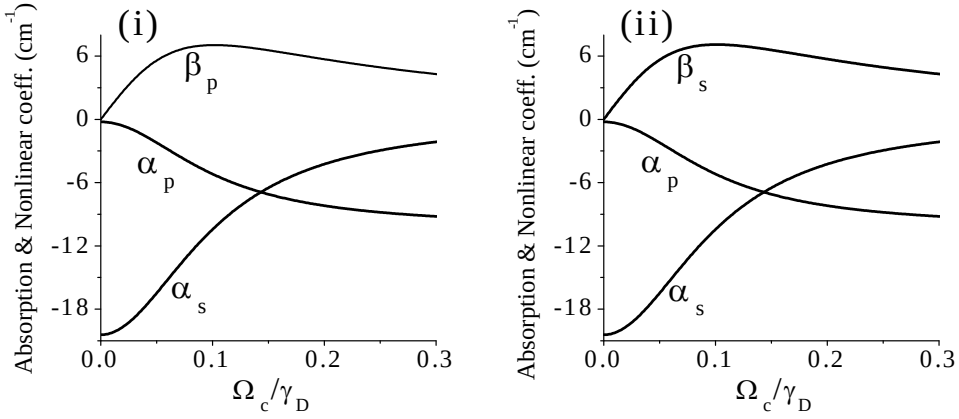

Figure 3.4: On-resonance ($\Delta_p = \Delta_m = \Delta_c = 0$) absorption (nonlinear) coefficient values of the probe α_p (β_p) and signal α_s (β_s) as a function of the coupler amplitude, Ω_c/γ_D. The value of the pump amplitude is fixed at, $\Omega_m/\gamma_D = 0.1$. The atomic density of the vapor is N=2×10^{11} atoms-cm^{-3}. It should be noted that for the given pump amplitude ($\Omega_m/\gamma_D = 0.1$) the absorption and nonlinear coupling coefficients for the signal and probe fields are equal when $\Omega_c/\gamma_D = \sqrt{2}\,\Omega_m/\gamma_D = 0.1414$.

We now explore numerically, the field generation process and propagation characteristics of the signal and probe fields, using Eqs.(3.13) and (3.14). For this purpose shown in Figure 3.4 are the values of on-resonance (i.e.,$\Delta_p = \Delta_s = 0$) absorption coefficient, $\alpha_p(\alpha_s)$ as well as the nonlinear coefficients, $\beta_p(\beta_s)$ for probe (signal) field as a function of the coupler field Rabi frequency Ω_c/γ_D for a fixed pump field Rabi frequency, $\Omega_m/\gamma_D = 0.1$. It is found, in accordance with our analysis in Section **3.2.5,** that absorption coefficients in both ladder subsystems become equal when $\Omega_c = \sqrt{2}\Omega_m$. Furthermore we find that when $\Omega_c = \sqrt{2}\Omega_m$ the absorption coefficients, $(\alpha_p = \alpha_s)$ and nonlinear coefficients, $(\beta_p = \beta_s)$ are also nearly equal. Under these conditions, it is expected that an equilibrium (steady-state) will be established where the propagation loss determined by absorption coefficient α is compensated for by the effective (nonlinear) gain given by β in the medium.

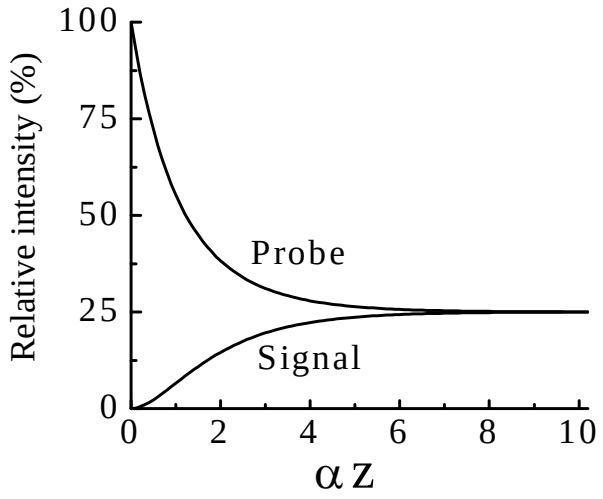

Figure 3.5: Variation of the relative intensity of the probe $\frac{|\varepsilon_p(z)|^2}{|\varepsilon_p(o)|^2}$ *(×100) and generated signal* $\frac{|\varepsilon_s(z)|^2}{|\varepsilon_p(o)|^2}$ *(×100) as a function of the dimensionless parameter αz where z is the propagation distance in the vapor and the value of* α_j *(and* β_j*),(j = p, s) are evaluated at line center (*$\Delta_p = \Delta_m = \Delta_c = 0$*) for* $\Omega_m/\gamma_D = 0.1$ *and* $\Omega_c = \sqrt{2}\Omega_m$ *.*

To illustrate this point, we show in Figure 3.5 the probe and signal propagation characteristics (using Eq.(3.14)) under the same conditions as in Figure 3.4, i.e., for $\Omega_c = \sqrt{2}\Omega_m$ (with $\Omega_m/\gamma_D = 0.1$) and $\alpha = \beta$. The relative signal (probe)

intensity given by $|\frac{\varepsilon_s(z)}{\varepsilon_p(o)}|^2$ ($|\frac{\varepsilon_p(z)}{\varepsilon_p(o)}|^2$) is plotted as a function of the dimensionless quantity αz, where z is the propagation distance in the medium. The product αz can be varied either by changing the atomic density (N) or length of the vapor cell. We observe from Figure 3.5 that initially the signal field is zero and probe is a maximum. As the fields propagate in the medium, generation of the signal field occurs (via nonlinear mixing) due to which the intensity of the probe decreases. However as the generated signal intensity grows sufficiently strong and comparable to the probe field strength, the reverse process also can occur in which the signal, coupler and the pump via nonlinear mixing regenerate the probe field. It is thus obvious that beyond a certain value of αz the generated signal and probe are amplitude (or intensity) matched, i.e., $\varepsilon_s(z)/\varepsilon_p(o) = \varepsilon_p(z)/\varepsilon_p(o) = 1/2$ and thus the signal (probe) intensity relative to the incident probe intensity is 25% [19]. As a consequence of this amplitude (or intensity) matching and since the condition $\alpha = \beta$ is also satisfied, the generated signal and probe continue to propagate through the medium without further attenuation or amplification.

3.4. Conclusion

In conclusion, we have studied the EIT and nonlinear generation process and propagation dynamics in Doppler broadened diamond systems that can be regarded as two three-level ladder subsystems sharing a common ground and highest upper levels. Coupling of these subsystems is caused by strong driving (coupler and pump) fields which connect the common upper level to (two) distinct intermediate states in each ladder subsystems. In the absence of one of the strong driving fields, for example the coupler field, the diamond system reduces to a Doppler broadened three-level cascade EIT scheme involving a weak probe and strong pump field. The applied coupling field Ω_c (by mixing with the probe and pump fields) generates a fourth weak (signal) field which affects the EIT of the probe field.

The influence of residual Doppler broadening arising from the wavenumber mismatch in the two cascade subsystems and the driving (pump and coupling) field strength, on probe and signal EIT is investigated. It is usually expected that a two-

photon Doppler free case will exhibit maximum EIT whereas a finite residual Doppler width (arising from wavenumber mismatch) will adversely affect the EIT. While this is observation is found to be true for the positive mismatch case, we observe that in the negative wavenumber mismatch case a much wider and deeper EIT window is obtainable at much lower pump amplitudes, compared with the $k_p = k_m$ case. Furthermore, in the negative wavenumber mismatch case, width of the EIT window depends upon the values of the pump amplitude and wavenumber mismatch. Application of a coupling field results in enhanced absorption and further power broadening of the EIT resonances. Physical interpretation of this effect is provided in terms of incomplete destructive interference between the absorption paths.

The two (relatively weak) fields, probe and internally generated signal field which connect ground states to intermediate states in each ladder subsystems are coupled, i.e., exchange energy through nonlinear polarization generated via nonlinear mixing process. The influence of various system parameters (dipole moments, level decay rates, transition frequencies) and driving (pump and coupling) field strength and wavenumber mismatch on absorption and nonlinear coefficients which govern the probe and signal field propagation dynamics in a Doppler broadened medium is also discussed. It is shown that the effective gain arising from the nonlinear polarization depends on the strength of drive fields and can be suitably enhanced to compensate for high absorption losses in the medium. Thus a steady state (equilibrium) situation is created under suitable conditions (parameters) of driving field strengths in which both the probe and signal fields propagate in an extended Doppler broadened partial EIT medium.

3.5. References

1. S. Babin, U. Hinze, E. Tinemann and B. Wellehehausen, Opt. Lett. **21**, 1186 (1996); S. E. Harris and Y. Yamamoto, Phys. Rev. Lett. **81**, 3611 (1998); B. Lu, W. H. Burkett and M. Xiao, Opt. Lett. **23**, 804 (1998);

   D. A. Braje, V. Balic, S. Goda, G. Y. Yin and S. E. Harris, Phys. Rev. Lett. **93**, 18360 (2004).

2. A. J. Merriam, S. J. Sharpe, M. Shverdin, D. Manuszak, G.Y. Yin and S. E. Harris, Phys. Rev. Lett. **84**, 5308 (2000).

3. S. E. Harris, J. E. Field and A. Imamoglu, Phys. Rev. Lett. **64**, 1107 (1990); P. R. Hemmer, D. P. Katz, J. Donoghue, M. Cronin-Golomb, M. S. Shahriar and P. Kumar, Opt. Lett. **20**, 982 (1995).

4. M. D. Lukin and A. Imamoglu, Nature **413**, 273 (2001).

5. A. K. Patnaik and G. S. Agarwal, Opt. Comm. **199**, 127 (2001).

6. G. Morigi, S. Franke-Arnold and Gian-Luca Oppo, Phys. Rev. A **66**, 053409 (2002); S. K. Schröder, G. Morigi, S. Franke-Arnold and Gian-Luca Oppo, Phys. Rev. A **75**, 013816 (2007).

7. A. S. Zibrov, M. D. Lukin, L. Hollberg and M. O. Scully, Phys. Rev. A **65**, 051801 (2002); A. M. Akulshin, R. J. McLean, A. I. Sidorov and P. Hannaford, Opt. Exp. **17**, 22861 (2009).

8. R. T. Willis, F. E. Becerra, L. A. Orozco and S. L. Rolston, Phys. Rev. A **79**, 033814 (2009).

9. Y. Zhang, A. W. Brown and M. Xiao, Phys. Rev. A **74**, 053813 (2006).

10. Bao-Quan Ou, Lin-Mei Liang and Cheng-Zu Li, Opt. Comm. **282**, 2870 (2009).

11. P. S. Hsu, G. R. Welch, J. R. Gord and A. K. Patnaik, Phys. Rev. A **83**, 053819 (2011).

12. P. S. Hsu, A. K. Patnaik and G. R. Welch, J. Mod. Opt. **55**, 3109 (2008).

13. P. S. Hsu, A. K. Patnaik and G. R. Welch, Opt. Lett. **33**, 381 (2008).

14. A. K. Patnaik, S. Roy and J. R. Gord, Opt. Lett. **36**, 3272 (2011).

15. X. Hao, J. Wu and Y. Wang, J. Opt. Soc. Am. B. **29**, 420 (2012).

16. A. Kolle, G. Epple, H. Kubler, R. Low and T. Pfau, Phys. Rev. A **85**, 063821 (2012).

17. J. Gea-Banachloche, Y.Q. Li, S. Z. Jin and M. Xiao, Phys. Rev. A **51**, 576 (1995); S. Shepherd, D. J. Fulton and M. H. Dunn, Phys. Rev. A **54**, 5394 (1996); J. R. Boon, E. Zekou, D. McGloin and M. H. Dunn, Phys. Rev. A **59**, 4675 (1999).

18. A. B. Mirza and Suneel Singh, Phys. Rev. A **85**, 053837 (2012).

19. This is consistent with the experimental observations for degenerate probe and signal (and equal spontaneous emission rates) case (see Fig.5 of Ref. 12 and Fig. 2 of Ref. 13) in which after the coupler filed is applied, the transmission intensity of the final signal and probe intensity are the same and equal to 25% of the initial probe intensity. A similar phenomenon of field matching has also been observed in Ref.4 in the context of pulse propagation in N type four-level systems.

Chapter 4

Subluminal and Superluminal Light Propagation in Double-Ladder System

In this chapter we demonstrate a scheme for generating subluminal as well as superluminal probe (and signal) light in a medium comprising coupled double ladder systems. This scheme can be realized in both homogeneously (radiative) as well as in inhomogeneously (Doppler) broadened atomic systems. We show how easily in this scheme the speed of weak probe (and signal) fields can be switched from subluminal to superluminal by simply varying the strengths of the coherent pump and coupling fields. Unlike more intricate earlier schemes, our scheme is based simply on steady-state propagation dynamics resulting from compensation of the inevitable absorption losses by large nonlinear gain generated through appropriate choice of the pump and coupling fields. Furthermore it is shown that under these conditions both the signal and probe fields are intensity matched and both propagate with the same subluminal (or superluminal) group velocity without suffering loss or gain for long distance in the medium.

4.1. Introduction

Since the discovery of EIT [1] especially after experimental demonstration of slow light propagation in cold [2], hot [3] and room temperature vapors [4] several proposals for generation of superluminal (fast) and subluminal (slow) light via EIT or

other types of interaction schemes [5-9] in various multilevel systems have emerged. These phenomena are of tremendous interest as they may offer a variety of important applications such as controllable optical delay lines, optical switching, optical data storage and optical memories [10].

However the question that has often cropped up since the early days of discovery of EIT and the accompanying slow light phenomenon is: would it be possible to observe slow light propagation under certain conditions of the system or field parameters and fast light propagation under some other conditions in a single system using the same EIT scheme? Because then it would provide a means for switching from one form to the other by simply varying those parameters. Many researchers [11-14] have attempted to address this issue over the past decade without much success because dispersion is normal (positive slope) and steep in EIT and hence it inherently is a slow light process. Whereas for fast (superluminal) light propagation, anomalous dispersion (negative slope) is required, that invariably is accompanied with considerable absorption near line centre [5, 6, 15, 16].

For this reason practically all the existing schemes for creation of fast light have to rely on some or the other gain mechanisms such as Raman gain [7, 17, 18-21] or incoherently pumped inverted medium [22, 23] and rf field coupling between two electric-dipole-transition-forbidden states to produce gain profile [24-27]. It may therefore appear that it would not be possible to achieve fast light propagation using the phenomenon of EIT.

In this communication we address this issue and show that it indeed is feasible to achieve fast light propagation using EIT. What is more we show that it is possible to achieve both slow and fast light in a single medium using EIT scheme and one can switch from one type of propagation to the other by simply varying the intensities of the control fields.

4.2. Theory for the four level double-cascade (◊) system

4.2.1. Formulation

For this purpose we consider EIT scheme in an alkali-metal atomic vapor in which the double-cascade (◊) configuration (as shown in Figure 4.1) can be realized by exciting the $6S_{1/2} \rightarrow 6P_{3/2} \rightarrow 8S_{1/2}$ transition in Cesium atom using polarized, strong pump (coupler) and weak probe (signal) laser fields. The combination of the beam polarizations and the Zeeman substructure of the intermediate state $6P_{3/2}$ renders the system a four-level double-cascade system [28, 29].

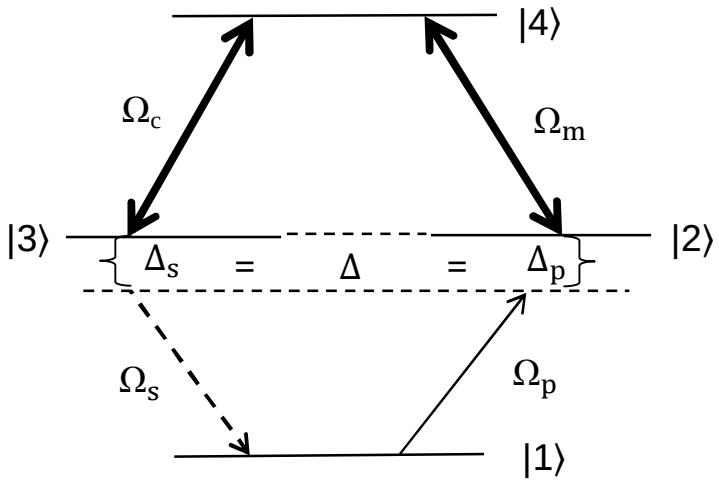

Figure 4.1: Schematic configuration of four-level double-ladder system, upper transitions of which are driven by strong pump (coupler) field of Rabi frequency Ω_m (Ω_c). The lower transitions are connected by weak probe (signal) field of Rabi frequency Ω_p (Ω_s). The detuning of the probe (signal) from the respective atomic transition is given by $\Delta = \Delta_p$ (Δ_s) = $\omega_{21} - \omega_p$ ($\omega_{31} - \omega_s$).

The theoretical formulation of the previous Chapter 3 is applicable here as this scheme is similar to the one studied there.

The total electric field can be written

$$\vec{E}(t) = \sum_\ell \vec{E}_\ell(t)\ , (\ell = p, s, c, m)\ , \tag{4.1}$$

where

$$\vec{E}_\ell(t) = \vec{\varepsilon}_\ell\, e^{i(\vec{k}_\ell.\vec{r}-\omega_\ell t)} + c.c\ ,\ (\ell = p, s, c, m)\ , \tag{4.2}$$

and ω_ℓ ($\vec{\varepsilon}_\ell$) is the frequency (amplitude) and $\vec{k}_\ell$ is the wave vector of the field $\vec{E}_\ell(t)$, (ℓ = p, s, c, m). The Rabi frequencies of the pump, coupler, probe and signal fields respectively, are $\Omega_m = \vec{\mu}_{42} \cdot \vec{\varepsilon}_m/\hbar$, $\Omega_c = \vec{\mu}_{43} \cdot \vec{\varepsilon}_c/\hbar$, $\Omega_p = \vec{\mu}_{21} \cdot \vec{\varepsilon}_p/\hbar$ and $\Omega_s = \vec{\mu}_{31} \cdot \vec{\varepsilon}_s/\hbar$ where the dipole operator matrix element is given by $\vec{\mu}_{ij} = \langle i|\vec{\mu}|j\rangle$, (i, j = 1, 2, 3, 4).

In this four-level coupled double-ladder system (Figure 4.1) the resonant pump (coupler) field with Rabi frequency Ω_m (Ω_c) drives the transition $|2\rangle \rightarrow |4\rangle$ ($|3\rangle \rightarrow |4\rangle$) at a wavelength 794.3 nm and wavevector $\vec{k}_m$ ($\vec{k}_c$). A weak probe (signal) field drives the transition $|1\rangle \rightarrow |2\rangle$ ($|1\rangle \rightarrow |3\rangle$) with Rabi frequency Ω_p (Ω_s) tuned at 852.2 nm and wavevector $\vec{k}_p$ ($\vec{k}_s$). The detuning of the field frequencies from atomic resonance frequencies are denoted $\Delta = \Delta_p(\Delta_s) = \omega_p - \omega_{21}(\omega_s - \omega_{31})$, $\Delta_m(\Delta_c) = \omega_m - \omega_{42}\ (\omega_c - \omega_{43}) = 0$(at exact resonance of pump and coupler fields $\Delta_c = \Delta_m = 0$).

Coupling between the two subsystems results in four wave mixing process with the phase-matching condition given by $\Delta k = \vec{k}_p + \vec{k}_m - \vec{k}_c - \vec{k}_s = 0$. Thus as in Chapter 3 we have to consider the theory for a scheme of four-level atomic systems in ◊ (diamond) configuration interacting with four laser fields in a closed-loop geometry.

4.2.2. Interaction Hamiltonian

Using Eq.(1.15) the interaction Hamiltonian in the interaction picture and under rotating wave approximation is obtained as

$$V^{int} = -\hbar[\Omega_p e^{i(\vec{k}_p\cdot\vec{r}-\Delta_p t)}\,|2\rangle\langle 1| + \Omega_s e^{i(\vec{k}_s\cdot\vec{r}-\Delta_s t)}\,|3\rangle\langle 1| + \Omega_c e^{i(\vec{k}_c\cdot\vec{r}-\Delta_c t)}\,|4\rangle\langle 3| + \Omega_m e^{i(\vec{k}_m\cdot\vec{r}-\Delta_m t)}\,|4\rangle\langle 2| + H.c.]. \quad (4.3)$$

Here $\Omega_\ell = \vec{\mu}_{ij} \cdot \varepsilon_\ell/\hbar$, ($\ell$ = p, s, c, m) are the Rabi frequencies and $|i\rangle\langle j|$ (i, j =1, 2, 3, 4) are the atomic raising or lowering operators.

4.2.3. Steady-state solution of density matrix-equations of motion

The time evolution of the density matrix elements ρ_{jk} with phenomenological inclusion of various relaxation processes such as spontaneous emissions from upper and intermediate levels $2\gamma_{ij}$ (i, j = 1 – 4) and Doppler broadening can be determined using Eqs.(4.3) and (1.18b) in Eq.(1.21) as shown in Chapter 3. As usual for the EIT problems, we make an expansion of the density matrix to all orders in the pump (coupling) field amplitudes and to first order in the probe (signal) amplitude and using appropriate transformations to eliminate fast oscillating (exponential) terms, the equation of motion for the slowly varying components $\dot{\rho}_{jk}$ of density-matrix elements for the double ladder (◊) system can be obtained in the interaction picture. The dispersion and absorption properties of the probe and generated FWM signal in the inhomogeneous double ladder system are given by the real and imaginary part of velocity averaged one-photon coherences $I_{ij}^{(\Omega_k)}$ in the Schrodinger picture. Following the formalism outlined in Chapter 3 we obtain the steady-state results for the velocity averaged one-photon coherences in the Schrodinger picture as follows:

$$I_{21}^{(\Omega_p)} = e^{-i(\vec{k}_p.\vec{r}-\omega_p t)} \int \rho_{21}^{(\Omega_p)}(v)\, dv^3 = i\Omega_p \int \frac{\left(A_{41}(v)+|\Omega_c|^2/A_{31}(v)\right)M(v)dv^3}{A_{21}(v)\left(A_{41}(v)+|\Omega_c|^2/A_{31}(v)+|\Omega_m|^2/A_{21}(v)\right)}, \qquad (4.4a)$$

$$I_{31}^{(\Omega_s)} = e^{-i(\vec{k}_s.\vec{r}-\omega_s t)} \int \rho_{31}^{(\Omega_s)}(v)\, dv^3 = i\Omega_s \int \frac{\left(A_{41}(v)+|\Omega_m|^2/A_{21}(v)\right)M(v)dv^3}{A_{31}(v)\left(A_{41}(v)+|\Omega_c|^2/A_{31}(v)+|\Omega_m|^2/A_{21}(v)\right)}. \qquad (4.4b)$$

The real and imaginary parts of Eq.(4.4) describe dispersion and absorption of the probe and generated FWM signal in the inhomogeneous double ladder system. The generation of four wave mixing field and probe is governed by the nonlinear coherences given in the Schrodinger picture by

$$I_{21}^{(\Omega_s)} = e^{-i(\vec{k}_p.\vec{r}-\omega_p t)} \int \rho_{21}^{(\Omega_s)}(v)\, dv^3 = \Omega_s\Omega_c\Omega_m^* \int \frac{(-i)\, M(v)dv^3}{A_{21}(v)A_{31}(v)A_{41}(v)+A_{21}(v)|\Omega_c|^2+A_{31}(v)|\Omega_m|^2}, \qquad (4.5a)$$

$$I_{31}^{(\Omega_p)} = e^{-i(\vec{k}_s.\vec{r}-\omega_s t)} \int \rho_{31}^{(\Omega_p)}(v)\, dv^3 = \Omega_p\Omega_c^*\,\Omega_m \int \frac{(-i)\, M(v)dv^3}{A_{21}(v)A_{31}(v)A_{41}(v)+A_{21}(v)|\Omega_c|^2+A_{31}(v)|\Omega_m|^2}. \qquad (4.5b)$$

here

$$M(v) = \sqrt{\ln 2/(\pi \bar{v}^2)}\exp(-\ln 2\, v^2/\bar{v}^2) \qquad (4.6)$$

is the Maxwellian velocity distribution of atoms with $\bar{v} = \sqrt{\ln 2}\, v_{th}$ and $v_{th} = \sqrt{2k_B T/m_a}$ is the most probable thermal velocity at a temperature T of an atom of mass m_a and

$$A_{21}(v) = i\left[\Delta + \vec{k}_p.\vec{v}\right] + \gamma_{21}\,, \qquad (4.7a)$$

$$A_{31}(v) = i\left[\Delta + \vec{k}_s.\vec{v}\right] + \gamma_{31}\,, \qquad (4.7b)$$

$$A_{41}(v) = i\left[\Delta + (\vec{k}_p + \vec{k}_m).\vec{v}\right] + \Gamma_{41}\,. \qquad (4.7c)$$

4.2.4. Susceptibility and Group velocity

The susceptibility of the medium (Chapter 1 section **1.3.3**) is related to the velocity averaged one-photon coherence as

$$\chi = N\frac{|\mu_{m1}|^2}{\hbar\gamma_D}\left(\frac{I_{m1}^{(\Omega_j)}}{\Omega_j/\gamma_D}\right),\ (j = p, s;\ m = 2, 3), \qquad (4.8)$$

where N is the atomic density of the vapor and γ_D $(= k_p\bar{v})$ is the Doppler width in the system. As is well known, the imaginary $(Imag(\chi))$ and real $(Re(\chi))$ parts respectively of the susceptibility χ give the absorption and dispersion of the probe field.

The group velocity of the probe field in the medium is given by

$$v_g = \frac{d\omega_p}{dk(\omega_p)} = \frac{c}{n+\omega_p(dn/\omega_p)} = \frac{c}{1+2\pi\,(\chi_{Re}+i\,\chi_{Im}\,)+2\pi\,\omega_p\,[\frac{d}{d\omega_p}(\chi_{Re})+i\frac{d}{d\omega_p}(\chi_{Im})]} = \frac{c}{n_g}, \qquad (4.9)$$

When all the fields coupling (pump) fields and probe (signal) fields are on resonance $(\Delta_{43}(\Delta_{42}) = \Delta_{21}(\Delta_{31}) = 0)$, the probe absorption is an extremum so that $d\left[Im\left(I_{31}^{(1)}/\Omega_p\right)\right]/d\omega_p = d[\chi_{Im}]/d\omega_p = 0$, $\chi_{Re} = 0$ (on resonance) and χ_{Im} is negligible compare with other terms in the denominator. Therefore for on-resonance case the group velocity v_{gj} of the probe and signal is obtained as

$$v_{gj} = \frac{c}{1+2\pi\omega_j\frac{N|\mu_{m1}|^2}{\hbar}\frac{d}{d\omega_j}\left[Re\left(I_{m1}^{(\Omega_j)}/\Omega_j\right)\right]} = \frac{c}{\eta_{gj}}, \qquad (4.10)$$

where η_{gj} is the group index, j = p, m = 2 for probe and j = s, m = 3 for signal field. Thus in addition to absorption characteristics, dispersion spectrum is also of importance since η_{gj} is directly proportional to the derivative (slope) of the dispersion curve. A steep (positive slope) and steep (negative slope) dispersion profiles would result in a high value for η_{gj} which means that a very low group velocity and a very fast group velocity respectively in both the cases.

4.2.5. Generation and propagation of the probe and signal fields

To observe the transmission of the subluminal and superluminal light pairs of generated FWM signal and probe fields we consider propagation of the (weak) signal and probe waves through an extended medium composed of double ladder systems. Following the formalism of Chapter 3 we obtain the (on-resonance) field amplitudes for the signal, $\varepsilon_s(z)$ and the probe wave, $\varepsilon_p(z)$ in the medium as

$$\varepsilon_s(z) = \varepsilon_p(o)\frac{\beta_s}{2\Phi}\exp\left\{\left(\frac{\alpha_p+\alpha_s}{4}\right)z\right\}\sinh(\Phi z)\,, \tag{4.11a}$$

$$\varepsilon_p(z) = \varepsilon_p(o)\exp\left\{\left(\frac{\alpha_p+\alpha_s}{4}\right)z\right\}\left(\cosh(\Phi z) + \frac{(\alpha_p-\alpha_s)}{4\Phi}\sinh(\Phi z)\right), \tag{4.11b}$$

where

$$\Phi = \sqrt{\beta_s\beta_p/4 + (\alpha_p/4 - \alpha_s/4)^2}\ . \tag{4.11c}$$

The above coupled equations are obtained (as in Chapter 3) for the particular case in which all fields are on resonance, and under the boundary condition at the input $\varepsilon_p(z = 0) = \varepsilon_p(0)$ and $\varepsilon_s(z = 0) = 0$.

The real and imaginary parts of α_j (j= s, p) respectively, describe absorption and dispersion properties of the atomic medium. These are given by

$$\alpha_s = i\eta_s\left(\frac{I_{31}^{(\Omega_s)}}{\Omega_s/\gamma_D}\right), \tag{4.12a}$$

$$\alpha_p = i\eta_p\left(\frac{I_{21}^{(\Omega_p)}}{\Omega_p/\gamma_D}\right). \tag{4.12b}$$

The term β_j (j = s, p) essentially represents gain arising due to mutual coupling via nonlinear mixing between the probe field and the FWM field

$$\beta_s = i\eta_s \left(\frac{I_{31}^{(\Omega_p)}}{\Omega_p/\gamma_D} \right), \tag{4.13a}$$

$$\beta_p = i\eta_p \left(\frac{I_{21}^{(\Omega_s)}}{\Omega_s/\gamma_D} \right). \tag{4.13b}$$

where $\eta_s = \frac{8\pi^2 N|\mu_{31}|^2}{\lambda_s \hbar \gamma_D}$ and $\eta_p = \frac{8\pi^2 N|\mu_{21}|^2}{\lambda_p \hbar \gamma_D}$. It should also be noted that since $\alpha_k \propto i I_{m1}^{(\Omega_k)}$ (k = s, p; m = 2, 3), the real and imaginary parts of α_s (α_p) respectively, describe absorption and dispersion properties of the generated signal (probe) field in the medium. From Eq.(4.12) we find that the probe (and signal) dispersion vanishes at line center because the imaginary part of α_s (α_p) is zero at exact resonance. Thus it can be shown and verified numerically that the coefficients given by Eqs.(4.12) and (4.13) are purely real at line center. The coupled equations for the field amplitudes are obtained for this particular case of real coefficients α_k and β_k (where k = p, s).

4.3. Subluminal and superluminal propagation in homogeneously (radiatively) broadened medium

Before presenting numerical results it is instructive to discuss analytical results that can be obtained for homogenously broadened system. We first discuss the EIT characteristics of the probe and signal fields. Result for this case can be derived from Eq.(4.4) by dropping velocity dependent terms and performing the velocity integration using Eq.(4.6) at exact resonance of probe (signal) and pump(coupling) fields as follows:

$$I_{21}^{(\Omega_p)} = i\Omega_p \frac{\gamma_{31}\Gamma_{41} + |\Omega_c|^2}{\gamma_{21}\gamma_{31}\Gamma_{41} + \gamma_{31}|\Omega_m|^2 + \gamma_{21}|\Omega_c|^2}, \tag{4.14a}$$

$$I_{31}^{(\Omega_s)} = i\Omega_s \frac{\gamma_{21}\Gamma_{41} + |\Omega_m|^2}{\gamma_{21}\gamma_{31}\Gamma_{41} + \gamma_{31}|\Omega_m|^2 + \gamma_{21}|\Omega_c|^2}. \tag{4.14b}$$

For the transition considered in Cs atom the decay rates of intermediate levels to ground level are equal $\gamma_{21} = \gamma_{31}$ and $\gamma_{31} \gg \Gamma_{41}$. Hence for higher values of pump and coupling field amplitudes, Ω_c and Ω_m such that $|\Omega_c|^2 \gg \gamma_{31}\Gamma_{41}$ and $|\Omega_m|^2 \gg \gamma_{21}\Gamma_{41}$ the expressions (4.14) for one-photon coherences reduce to the form,

$$\frac{I_{21}^{(\Omega_p)}}{(\Omega_p/\gamma_{21})} = i\,\frac{|\Omega_c|^2}{|\Omega_m|^2+|\Omega_c|^2}, \tag{4.15a}$$

$$\frac{I_{31}^{(\Omega_s)}}{(\Omega_s/\gamma_{21})} = i\,\frac{|\Omega_m|^2}{|\Omega_m|^2+|\Omega_c|^2}\,. \tag{4.15b}$$

Dropping the velocity dependent terms in Eq.(4.5) and performing the velocity integration using Eq.(4.6) the three photon (nonlinear) coherences governing the generation of four wave mixing signal and probe fields under above conditions are obtained as,

$$\frac{I_{31}^{(\Omega_p)}}{(\Omega_p/\gamma_{21})} = -i\,\frac{\Omega_c^*\,\Omega_m}{|\Omega_m|^2+|\Omega_c|^2}\,, \tag{4.16a}$$

$$\frac{I_{21}^{(\Omega_s)}}{(\Omega_s/\gamma_{21})} = -i\,\frac{\Omega_m^*\,\Omega_c}{|\Omega_m|^2+|\Omega_c|^2}\,. \tag{4.16b}$$

It is interesting to note that for the particular case of equal Ω_c and Ω_m, the on-resonance values of one photon coherences and the nonlinear coherences given by Eq.(4.15) and Eq.(4.16) respectively, are equal in magnitude but with opposite signs, that is, $\beta_s = \eta_s/2 = -\alpha_s$ and $\beta_p = \eta_p/2 = -\alpha_p$. As the intermediate states are nearly degenerate, the spontaneous emission rates and the dipole matrix elements are nearly identical, so that, $\eta_s = \eta_p$. Hence we can use the parameters $\beta\,(=\beta_s=\beta_p)$ and $\alpha\,(=-\alpha_s=-\alpha_p)$ in Eq.(4.11c) to obtain $\Phi = \beta/2$. Again using the parameters $\alpha\,(=-\alpha_s=-\alpha_p)$, $\beta\,(=\beta_s=\beta_p)$ and in Eq.(4.11a) and Eq.(4.11b) which describe propagation of the probe and signal fields in the medium reduce to

$$\varepsilon_s(z)/\varepsilon_p(o) = \exp(-\tfrac{\alpha}{2}\,z)\,[\exp(\tfrac{\beta}{2}\,z) - \exp(-\tfrac{\beta}{2}\,z)]\,/2, \tag{4.17a}$$

$$\varepsilon_p(z)/\varepsilon_p(o) = \exp(-\tfrac{\alpha}{2}\,z)\,[\exp\left(\tfrac{\beta}{2}\,z\right) + \exp(-\tfrac{\beta}{2}\,z)]\,/2\,. \tag{4.17b}$$

The $\exp(-\frac{\alpha}{2}\,z)$ term outside the brackets in Eq.(4.17) is the usual absorption term. That is, at sufficiently large propagation distance z in the medium, the second terms in the square brackets vanish, but the first term in the square brackets which arise from nonlinear gain β cancels the absorption term outside the brackets. Under these conditions we observe that

$$|\varepsilon_s(z)/\varepsilon_p(o)|^2 = |\varepsilon_p(z)/\varepsilon_p(o)|^2 = 1/4. \tag{4.18}$$

The above results shows that the intensities of both the probe and signal are equal and they propagate in the medium with no further loss or gain. Thus despite there being only 50% EIT for both probe and signal fields, matched propagation of these fields occurs owing to compensation of the absorption by nonlinear gain of the four wave mixing process.

We now determine the nature of speed of these matched fields. For this purpose the group index of the probe and signal fields are derived from Eq.(4.4) by dropping velocity dependent terms and performing the velocity integration using Eq.(4.6), and through Eq.(4.10) under above conditions as,

$$n_{gp} = 1+ \omega_p \frac{2\pi N|\mu_{21}|^2}{\hbar \gamma_{21}^2} \frac{(\gamma_{21}^2 - 2|\Omega_m|^2)}{4|\Omega_m|^2} , \qquad (4.19a)$$

$$n_{gs} = 1+ \omega_s \frac{2\pi N|\mu_{31}|^2}{\hbar \gamma_{21}^2} \frac{(\gamma_{21}^2 - 2|\Omega_m|^2)}{4|\Omega_m|^2} . \qquad (4.19b)$$

For typical values of parameters of ^{133}Cs atomic transition λ_p=852.2×10^{-7} cm, homogeneous linewidths $\gamma_{21} \cong \gamma_{31}$=2 π ×2.6×10^6 Hz, $|\mu_{21}|^2 \cong |\mu_{31}|^2$= 130×10^{-36} esu, the group index and the group velocities of the probe and signal fields are evaluated as

$$n_{gs} \cong n_{gp} = 1+ 13.55\times 10^6 \times \frac{(1 - 2|\Omega_m|^2/\gamma_{21}^2)}{4|\Omega_m|^2/\gamma_{21}^2} . \qquad (4.20)$$

The above result predicts that for $|\Omega_m|^2/\gamma_{21}^2 < 1/2$ the group index and thereby the group velocity of the probe and signal pulse will be subluminal. Thus choosing $|\Omega_m|/\gamma_{21} = 1/2$ we find very large group index, $n_{gs} \cong n_{gp}$= 6.8 × 10^6 and the corresponding group velocities are found be

$$v_{gs} \cong v_{gp} = \frac{c}{n_{gs}} = \frac{3\times 10^8}{6.8\times 10^6} = +44 \text{ m/sec} . \qquad (4.21)$$

That is, both signal and probe propagate with ultraslow velocities in the medium.

On the other hand it is most remarkable to note from Eq.(4.20) that even within the EIT limit, when the pump and coupler field amplitudes are comparable to the homogenous linewidth i.e., $|\Omega_m|, |\Omega_s| \sim \gamma_{21}$ it is possible to observe superluminal propagation of the signal and probe fields. Choosing $|\Omega_m|/\gamma_{21} = 1$ we find from

Eq.(4.20) that $n_{gs} \cong n_{gs} \approx -3.4 \times 10^6$ and the corresponding group velocities are found be

$$v_{gs} \cong v_{gp} = \frac{C}{n_{gs}} = \frac{3\times10^8}{-3.4\times10^6} = -88 \text{ m/sec} . \quad (4.22)$$

The signal and probe velocities are negative which implies that they propagate at superluminal speed in the medium.

4.4. Numerical results and discussions

Having discussed analytical results for a homogeneously broadened medium we now present numerical results for an inhomogeneouly broadened medium. The level separation wavelengths of the lower and upper transitions are respectively, λ_{21}= 852.2 nm and λ_{42} = 794.3 nm. This large wavelength mismatch between the pump and probe fields in one or the generated signal and coupling fields in the other ladder subsystem introduces a residual Doppler width ($\delta k v_{th}$) that is of the order of 14 MHz even for counterpropagating probe-pump (signal-coupler) fields. Note also that in our double ladder system $k_p < k_m$ ($k_s < k_c$), so that the sign of the residual Doppler width $\delta k = k_p - k_m$ ($k_s - k_c$) is negative which is actually conducive to the phenomenon of EIT [30, 31].

In our numerical calculations both drive fields (coupler and pump) are fixed on resonance with their respective transitions, $\Delta_{42} = \Delta_{43} = 0$, and all other parameters are expressed in units of the Doppler width $\gamma_D/2\pi = 200$ MHz, i.e., $2\gamma_{21}/\gamma_D = 2\gamma_{31}/\gamma_D = 0.026$, $\Gamma_{41}/\gamma_D = (\gamma_{42} + \gamma_{43})/\gamma_D = 0.00015$.

As mentioned above, the dispersion (absorption) values for the probe and signal fields can be obtained numerically from the real (imaginary) part of the linear coherence, $I_{21}^{(\Omega_p)}/(\frac{\Omega_p}{\gamma_D})$ and $I_{31}^{(\Omega_s)}/(\frac{\Omega_s}{\gamma_D})$ respectively. In Figure 4.2, row (a) shows the absorption profile of the probe (signal) and row (b) depicts the dispersion characteristics of probe (signal) field, plotted as a function of probe (signal) detuning $-\Delta/\gamma_D$. The values of strong pump (coupler) fields used in Figure 4.2 are as follows: columns (i) $\Omega_m = \Omega_c = 0.3\gamma_D$, column (ii) $\Omega_m = \Omega_c = 1.0\gamma_D$ and column (iii) $\Omega_m = \Omega_c = 1.5\gamma_D$. For values $\Omega_m = \Omega_c = 0.3\gamma_D$ of Rabi frequencies respectively,

of pump and coupling fields, the absorption of both probe and signal is reduced by only 50% as compared with an isolated three level ladder system. That is, the transparency of both probe and signal is only 50% in a double ladder system as against 100% of that in an isolated three-level ladder system. The underlying physical mechanism this has already been explained in the previous Chapter 3. For this case (i) we observe from Figure 4.2(b) that probe and signal dispersion curves have steep positive slope. Hence, both probe and signal will propagate at ultraslow (subluminal) speed, in this double ladder system.

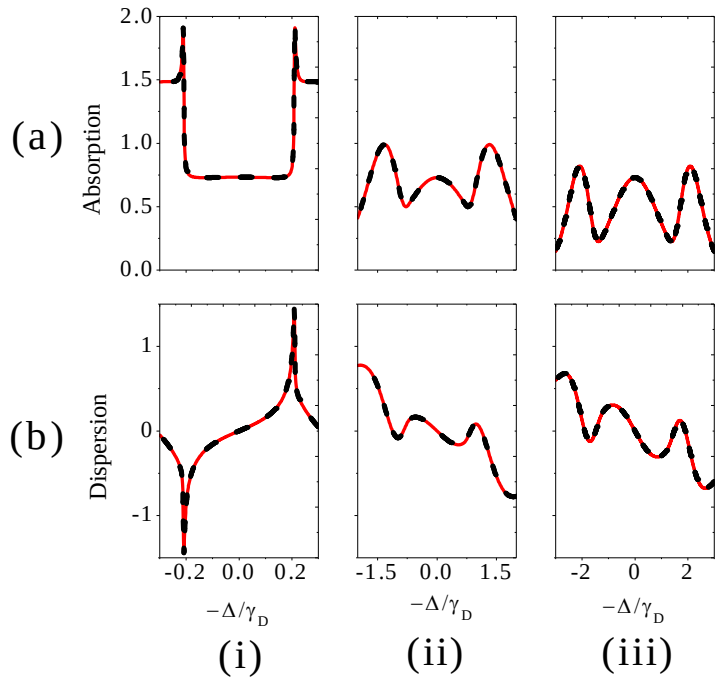

Figure 4.2: (a) Absorption profile of probe (red-solid lines) and signal (black-dashed lines) and (b) dispersion profiles probe (red-solid lines) and signal (black-dashed lines) as a function of probe (signal) detuning $(-\Delta)/\gamma_D$. *The columns correspond to the fixed values of pump and coupler field amplitudes (i)* $\Omega_m = \Omega_c = 0.3\gamma_D$, *(ii)* $\Omega_m = \Omega_c = 1.0\gamma_D$ *and (iii)* $\Omega_m = \Omega_c = 1.5\gamma_D$.

From above figure we observe for higher values of Ω_m ($= \Omega_c$) the line center values of absorption does not vary; it remains the same 50% as in the case (i), although it experiences further reduction in the wings. However for the cases (ii) and (iii) it is observed from Figure 4.2(b) that the slope of dispersion profiles of both the probe and signal fields becomes negative and steep around the line center. Hence,

both probe and signal will undergo ultrafast (superluminal) propagation, in this double ladder system. It should also be noted that as these values of pump (coupler) amplitudes are less than or comparable with the Doppler width of the dominant (inhomogeneous) broadening in the vapor, we are well within the EIT regime.

We now examine the on-resonance (i.e., $\Delta = 0$) EIT characteristics of probe and signal by plotting absorption as a function of the coupler (for fixed pump) field amplitude. These are obtained numerically from the imaginary part of the linear coherence, $I_{21}^{(\Omega_p)}/(\frac{\Omega_p}{\gamma_D})$ and $I_{31}^{(\Omega_s)}/(\frac{\Omega_s}{\gamma_D})$ for probe and signal respectively.

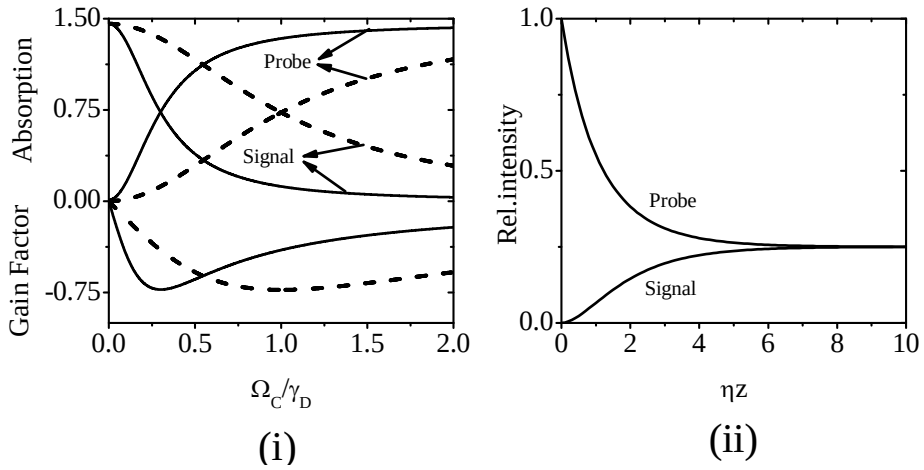

Figure 4.3: (i) On-resonance (line center) absorption values for probe and signal fields plotted as a function of the coupler amplitude Ω_c/γ_D for fixed values of the pump amplitude Ω_m/γ_D = 0.3 (solid lines) and 1.0 (dashed lines). Gain factor at line center (on-resonance) values of the imaginary part of nonlinear polarization, $I_{31}^{(\Omega_p)}/(\frac{\Omega_p}{\gamma_D})$ as a function of the coupler amplitude Ω_c/γ_D for two fixed values of the pump amplitude Ω_m/γ_D = 0.3 (solid line) 1.0 (dotted line). (ii) Variation of the relative intensity of the probe ($|\varepsilon_p(z)|^2/|\varepsilon_p(o)|^2$) and generated signal ($|\varepsilon_s(z)|^2/|\varepsilon_p(o)|^2$) as a function of the dimensionless parameter ηz where z is the propagation distance in the vapor and the value of α (and β), are evaluated on-resonance ($\Delta = 0$) for $\Omega_m/\gamma_D = \Omega_c/\gamma_D$ = 0.3 and 1. Note that the curves for these two values overlap because for both $\Omega_m/\gamma_D = \Omega_c/\gamma_D$ = 0.3 and 1 cases, the nonlinear gain term is equal and opposite to linear absorption term.

Figure 4.3(i) shows the line center (i.e., on-resonance, $\Delta = 0$) absorption profile for probe and signal as a function of the coupler field Rabi frequency Ω_c/γ_D for two fixed values of pump field Rabi frequency, $\Omega_m/\gamma_D = 0.3$ and 1.0. In this case we observe that when $\Omega_c = \Omega_m$ absorption in both ladder subsystems becomes equal and its value is half the usual absorption value (obtained in the absence of EIT). In addition to linear absorption we also plot the nonlinear gain factor, obtained from the imaginary part of the nonlinear coherence, $I_{31}^{(\Omega_p)}/(\frac{\Omega_p}{\gamma_D})$ (see (β_s)) as a function of the coupler amplitude Ω_c/γ_D for two fixed values of pump field Rabi frequency, $\Omega_m/\gamma_D = 0.3$ and 1.0. From Figure 4.3(i) we find that the contributions from nonlinear generation (gain factor) and absorption (loss) of the signal (and probe) field are opposite in sign and the magnitudes of these become equal at higher values of the pump and coupler fields. This fact is evident from the curves for $\Omega_c/\gamma_D = \Omega_m/\gamma_D = 0.3$ (and 1.0). Since other parameters appearing in the expressions for α_s , β_s (and α_p, β_p) are the same, we find that $\alpha\,(= -\alpha_p = -\alpha_s)$ and $\beta\,(= \beta_p = \beta_s)$ are nearly equal in this regime of driving fields. Thus it is expected that a balance (steady-state) will be established in the situation where the propagation loss determined by absorption coefficient α is compensated for by the effective (nonlinear) gain given by β in the medium.

To illustrate this point, we show in Figure 4.3(ii) the probe and signal light propagation characteristics for the case same as Figure 4.3(i), in which $\alpha = \beta$ and $\Omega_c/\gamma_D = \Omega_m/\gamma_D = 0.3$ and 1.0. The relative signal (probe) intensity given by $\left|\frac{\varepsilon_s(z)}{\varepsilon_p(o)}\right|^2$ $(\left|\frac{\varepsilon_p(z)}{\varepsilon_p(o)}\right|^2)$ is plotted as a function of the density-length product ηz. The density-length product ηz can be varied either by changing the atomic density or length of the vapor cell. We observe from the figure that initially the signal field is zero and probe intensity is maximum. As the fields propagate in the medium, generation of the signal field via FWM takes place due to which intensity of the probe decreases. However when the generated signal becomes sufficiently strong and comparable to the probe field strength, the reverse process also can occur in which the signal, coupler and the pump via FWM regenerate the probe field. It is thus obvious that beyond a certain values of ηz the generated signal and probe are amplitude (or

intensity) matched and consequently propagate through the medium without further dissipation since the condition $\alpha = \beta$ is satisfied. We further note that under these matched conditions $\varepsilon_s(z)/\varepsilon_p(o) = \varepsilon_p(z)/\varepsilon_p(o) = 1/2$ and thus the signal (probe) intensity relative to the incident probe is 25%.

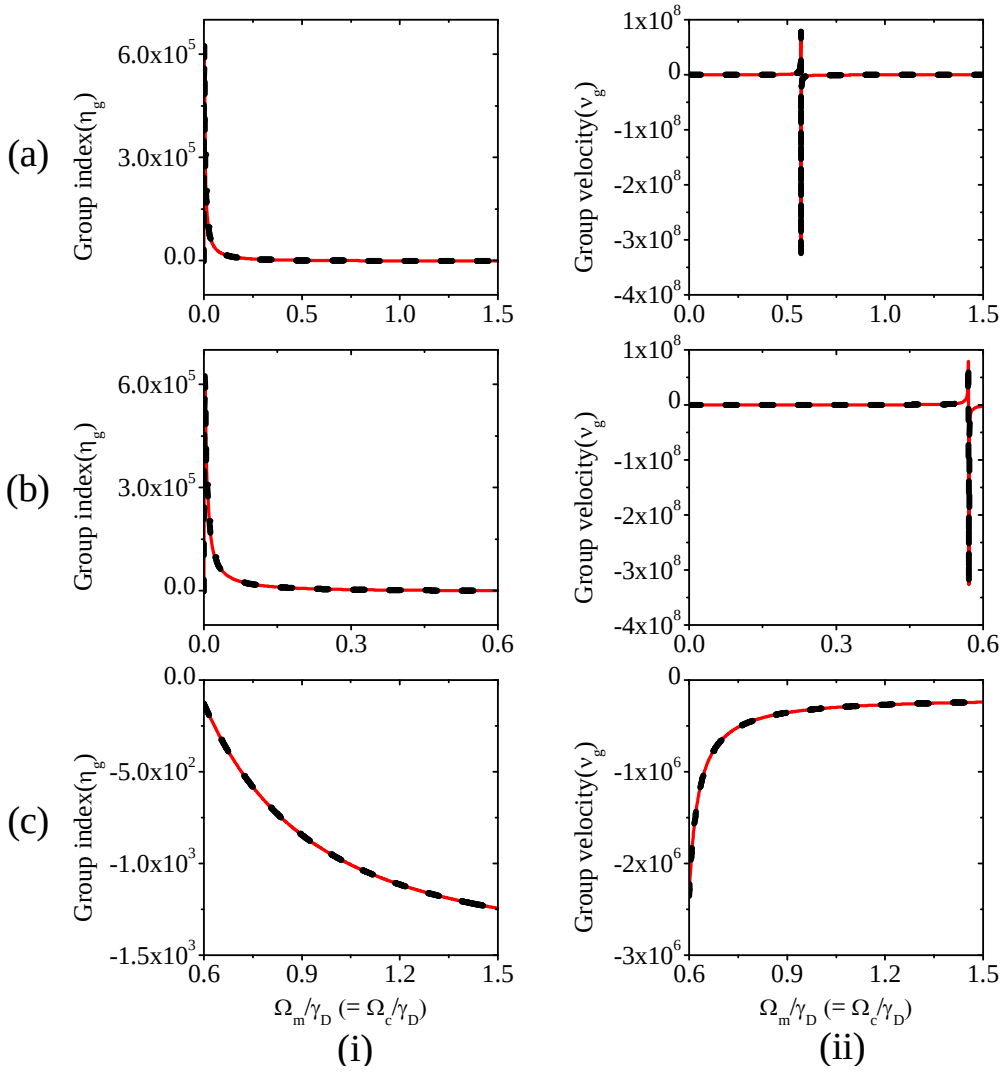

Figure 4.4: (i) Group index (η_g) (ii) Group velocity (v_g) for probe (red-solid lines) and signal (black-dashed lines) fields as a function of pump (coupling) field amplitudes $\Omega_m/\gamma_D (= \Omega_c/\gamma_D)$. The rows corresponds to the Variation of pump (coupling) field amplitudes from (a) 0.0 to 1.5γ_D, (b) 0.0 to 0.6γ_D, (c) 0.6γ_D to 1.5γ_D

Finally in Figure 4.4, we show the numerically computed group index (η_g) and group velocity (v_g) for probe and signal fields as a function of pump field

amplitude Ω_m/γ_D $(= \Omega_c/\gamma_D)$ in an inhomogeneouly broadened medium. We observe that for smaller values of pump and coupling fields, the group index (group velocity) is positive shown in Figure 4.4(b) and with increasing values of pump (coupling) fields, the group index (group velocity) becomes negative shown in Figure 4.4(c). Further we observed that the corresponding group velocities are (i) $V_g \approx 0.0003c$ and (ii) $V_g \approx -0.001c$ respectively, for the fixed values of pump (coupling) fields (i) $\Omega_m = \Omega_c = 0.3\gamma_D$ and (ii) $\Omega_m = \Omega_c = \gamma_D$. For a medium of length, L = 5cm the corresponding time delay for the subluminal propagation of the probe and signal fields is calculated as

$$t_d = \frac{L}{v_g} - \frac{L}{c} = 555\text{ns}$$

whereas the time advance, Δt of the transmitted probe (signal) field relative to a reference field propagating in vacuum is found to be $t_a = -166$ns.

4.5. Conclusion

We have demonstrated an EIT scheme to generate as well as switch between slow and fast light propagation for both probe and signal fields in degenerate double ladder system that can be regarded as two three-level ladder subsystems sharing a common ground and highest upper levels. The proposed scheme is based on appropriately choosing the intensities of the pump and coupler fields to generate sufficiently large nonlinear gain that can offset the high absorption losses in the medium. Under suitable choice of driving field strengths both the signal and probe fields are matched in intensity and propagate with the same subluminal or superluminal (group) velocity for long distance in the medium without loss or gain. We have presented a simple and practical scheme that can easily be implemented in both homogeneously as well as inhomogeneously broadened atomic media such as cold atoms or hot vapors.

4.6. References

1. S. E. Harris, J. E. Field and A. Imamoglu, Phys. Rev. Lett. **64**, 1107 (1990);

S. E. Harris, Phys. Today **50**, 36 (1997).

2. L. V. Hau, S. E. Harris, Z. Dutton and C. H. Behroozi, Nature **397**, 594 (1999).

3. M. M. Kash, V. A. Sautenkov, A. S. Zibrov, L. Hollberg, G. R. Welch, M. D. Lukin, Y. Rostovtsev, E. S. Fry and M. O. Scully, Phys. Rev. Lett. **82,** 5229 (1999); E. E. Mikhailov, Y. V. Rostovtsev and G. R. Welch, J. Mod. Opt. **50**, 2645 (2003).

4. D. Budker, D. F. Kimball, S.M. Rochesterand and V. V. Yashchuk, Phys. Rev. Lett. **83**, 1767 (1999).

5. A. M. Akulshin, S. Barreiro and A. Lezama, Phys. Rev. Lett. **83**, 4277 (1999).

6. A. I. Talukder, Y. Amaishi and M. Tomita, Phys. Rev. Lett. **86**, 3546 (2001).

7. L. J. Wang, A. Kuzmich and A. Dogariu, Nature **406**, 277 (2000); A. Dogariu, A. Kuzmich and L. J. Wang , Phys. Rev. A **63**, 053806 (2001).

8. M. S. Bigelow, N. N. Lepeshkin and R. W. Boyd, Science **301**, 200 (2003).

9. A. M. Akulshin and R. J. McLean, J. Opt. **12**, 104001(2010).

10. M. Fleischhauer and M. D. Lukin, Phys. Rev. Lett. **84**, 5094 (2000); Y. Okawachi, M. S. Bigelow, J. E. Sharping, Z. M. Zhu, A. Schweinsberg, D. J. Gauthier, R. W. Boyd and A. L. Gaeta, Phys. Rev. Lett. **94**, 153902 (2005); M. Fleischhauer, A. Imamoglu and J. P. Marangos, Rev. Mod. Phys. **77**, 633 (2005).

11. G. S. Agarwal, T. N. Dey and S. Menon, Phys. Rev. A **64**, 053809 (2001).

12. H. Sun, H. Guo, Y. F. Bai, D. A. Han, S. L. Fan and X. Z. Chen, Phys. Lett. A **335**, 68 (2005).

13. M. Mahmoudi and J. Evers, Phys. Rev. A **74**, 063827 (2006).

14. Bin Luo, Yu Liu and H. Guo, Opt. Lett. **35**, 64 (2010).

15. R. Y. Chiao and J. Boyce, Phys. Rev. Lett. **73**, 3383 (1994).

16. H. Tanaka, H. Niwa, K. Hayami, S. Furue, K. Nakayama, T. Kohmoto, M. Kunitomo and Y. Fukuda, Phys. Rev. A **68,** 035801 (2003).

17. A. M. Steinberg and R. Y. Chiao, Phys. Rev. A **49**, 2071 (1994).

18. E. Bolda, J. C. Garrison and R. Y. Chiao, Phys. Rev. A **49**, 2938 (1994).

19. M. D. Stenner and D. J. Gauthier, Phys. Rev. A **67**, 063801 (2003).

20. H. N. Yum, M. Salit, G. S. Pati, S. Tseng, P. R. Hemmer and M. S. Shahriar, Opt. Exp. **16**, 20448 (2008).

21. J. Zhang, G. Hernandez and Y. Zhu, Opt. Lett. **31**, 2598 (2006).

22. R. Y. Chiao, Phys. Rev. A **48,** R34 (1993).

23. G. S. Pati, M. Salit, K. Salit and M.S. Shahriar, Opt. Exp. **17**, 8775 (2009).

24. D. V. Kosachiov, B. G. Matisov and Y. V. Rozhdestvensky, J. Phys. B: At. Mol. Opt. Phys. **25**, 2473 (1992).

25. H. Sun, H. Guo, Y. F. Bai, D. A. Han, S. L. Fan and X. Z. Chen, Phys. Lett. A **335**, 68 (2005).

26. K. Yamamoto, K. Ichimura and N. Gemma, Phys. Rev. A **58**, 2460 (1998).

27. H. Li, V. A. Sautenkov, Y. V. Rostovtsev, G. R. Welch, P. R. Hemmer and M. O. Scully, Phys. Rev. A **80**, 023820 (2009).

28. P. S. Hsu, A. K. Patnaik and G. R. Welch, Opt. Lett. **33**, 381 (2008); P. S. Hsu, G. R. Welch, J. R. Gord and A. K. Patnaik, Phys. Rev. A **83**, 053819 (2011).

29. A. K. Patnaik, Sukesh Roy and J. R. Gord, Opt. Lett. **36**, 3272 (2011).

30. J. Gea-Banacloche, Y. Q. Li, S. Z. Jin and M. Xiao, Phys. Rev. A **51**, 576 (1995).

31. S. Shepherd, D. J. Fulton and M. H. Dunn, Phys. Rev. A **54**, 5394 (1996); J. R. Boon, E. Zekou, D. McGloin and M. H. Dunn, *ibid.* **59**, 4675 (1999).

Chapter 5

EIT in Five-Level K-type System

We investigate the electromagnetically-induced transparency (EIT) of a probe field in a five-level K-type and in four-level Y-type, inverted Y-type systems driven by strong laser (coupling) fields. Both homogeneously (radiative) and Doppler broadened mediums are considered. Effect of wave-vector mismatch (residual Doppler broadening) occurring on EIT when the frequency of coupling fields is equal $(\lambda_p = \lambda_c)$*, higher* $(\lambda_p > \lambda_c)$*or lesser* $(\lambda_p < \lambda_c)$ *than that of the probe field frequency. Depending upon the choices of control fields transitions, we consider three wave-vector mismatch regimes: (i) perfect wavelength matching regime* $(\lambda_p = \lambda_{c2} = \lambda_{c3})$ *(ii) partial wavelength mismatching regime* $(\lambda_p \neq \lambda_{c2} = \lambda_{c3})$ *and (iii) complete wavelength mismatching regime* $(\lambda_p \neq \lambda_{c2} \neq \lambda_{c3})$*. We observed the typical collective and overlapping behavior of EIT characteristics on (coupler-atom) resonance in the Doppler broadened atomic vapor in the partial and complete wavelength mismatching regimes as compared to the perfect wavelength matching regime. Furthermore we observed under the influence of the coherent coupling fields, the steady-state linear susceptibility of the probe laser shows that the system can have single, double or triple EIT windows whose width, depth, and location depends upon the wave-vector mismatch, Rabi frequencies and atom field detuning of the coupling fields.*

5.1. Introduction

An absorbing atomic medium is rendered transparent to a resonant probe field by a strong control field. This phenomenon, which is termed as electromagnetically induced transparency (EIT), has been studied in all kinds of simple three level atomic configurations including lamda (Λ), vee (V) and cascade (ladder - Ξ) schemes [1]. As stated earlier it is expected that more complicated levels structure of atomic system might generate further interesting effects. According to this nowadays there is considerable interest in the study of EIT in multilevel atomic systems formed by including extra, optical fields driven resonant transitions, to the three-level systems. This complicated level structure admitting additional fields and additional active atomic states enriches the dynamics and opens new possibilities for its external control. For example, the induced atomic coherences in multi-level atomic systems generates some interesting effects such as, four-wave mixing (FWM) process and enhanced frequency conversion [2], polarization qubit phase gate [3], Suppression of two-photon absorption [4] in a ladder-type four-level atomic system and suppression of two-photon absorption by quantum interference in inverted Y-system [5] and more recently a theoretical study of complete wavelength mismatching effect in a Doppler broadened six-level EIT atomic medium [6] is reported.

These interesting theoretical and experimental studies have motivated us to further explore the EIT characteristics in five-level and four-level atomic system with various types of configurations. The five-level K-type configuration are consisting of two or more than two different EIT sub-systems so that it becomes interesting to look at collective behaviors of these sub-systems as well as to control the collective EIT characteristics by various system and field parameters. Pertinent to the present work is on five-level K-type system interacting with three strong laser (coupling) fields and a low-intensity probe field. Recently, this kind five level K-type atomic structure has been utilized in some studies such as, effect of spontaneously generated coherence on EIT [7], Double electromagnetically induced two-photon transparency [8] and observation of dressed odd-order multi-wave mixing [9]. The Five-level (K-type) atomic medium where the intermediate level in a ladder-type atom is coupled with a

higher-excited and ground levels by two strong laser (coupling) fields as shown in Figure 5.1.

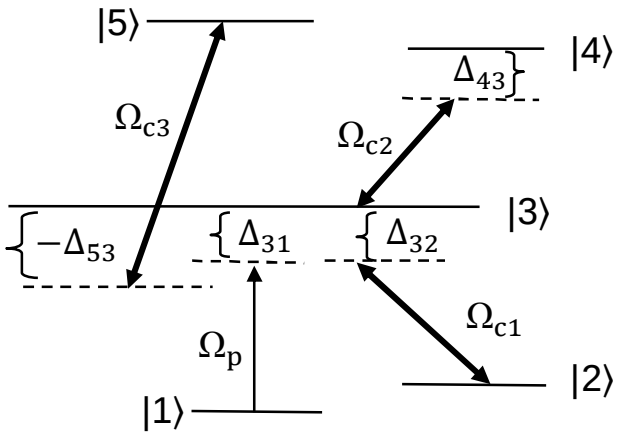

Figure 5.1: EIT scheme in five-level K-type atomic system. Here Ω_p is Rabi frequency of the (weak) probe and Ω_{c1}, Ω_{c2} and Ω_{c3} respectively are the (strong) coupling field Rabi frequencies. The detunings of the probe and coupling fields from their respective atomic transitions are $\Delta_{31} = \omega_{31} - \omega_p$,$\Delta_{32} = \omega_{32} - \omega_{c1}$,$\Delta_{43} = \omega_{43} - \omega_{c2}$ and $\Delta_{53} = \omega_{53} - \omega_{c3}$ respectively.

As mentioned earlier, in Doppler broadened EIT systems the probe absorption and dispersion characteristics are governed by nature of the residual (two-photon) Doppler broadening originating from thermal motion of atoms and mismatch $k_p - k_c$, of applied probe and coupling field wave-vectors k_p and k_c respectively [1 ,10, 11]. In three level ladder system it was found that the $k_p < k_c$the negative wave-vector mismatch case is actually conducive to observation of reduced probe absorption [10, 11]. It therefore would be of interest to study the influence of the various broadening mechanisms and different regimes of wave vector mismatches in the Doppler broadened medium depending upon the choices of control fields transitions (particularly when $k_p < k_c$) on probe absorption characteristics in multilevel atomic systems such as five level (K- type) and four level (Y-type, inverted Y-type) systems.

We study transparency of a weak probe field in a Doppler broadened five level K-type system interacting with three strong laser (coupling) fields, it can also consider as a coupling (control) field couple the intermediate level of the Y-type (inverted-Y type) atom with another ground (or excited) level and that the ground level and

excited levels of the coupling transitions in a five-level K-type atomic system are nearly degenerate or non degenerate. For comparison and contrasting, analysis for a homogeneously (radiatively) broadened five level K-type systems is also presented. Here we deals with density matrix formulation, solve for the steady-state density matrix-equations for the K-type system to first order in amplitude of a (weak) probe field. Expressions are derived for one-photon (probe) coherence, susceptibility from which absorption and dispersion characteristics of the probe field can be determined. Analytical results are derived so as to explain the influence of various broadening mechanisms. It is shown that depending on the amplitude and the detuning of the coupling lasers, the absorption profile of a weak probe field shows single, double or triple EIT windows whose location, width, and depth can be controlled by manipulating the parameters of the coupling fields. Present the numerical results for probe absorption and dispersion considering the transitions $5S_{1/2}(F=1)\rightarrow 5P_{3/2}\rightarrow 5D_{3/2}\begin{Bmatrix}5S_{1/2}(F=1)\rightarrow 5P_{3/2}\rightarrow 5D_{5/2}(7S_{1/2})\\5S_{1/2}(F=1)\rightarrow 5P_{3/2}\rightarrow 5S_{1/2}(F=2)\end{Bmatrix}$ in Rubidium atom.

5.2. Theory for the five level K-type system

5.2.1. Formulation

We consider a five level K-type atomic system interacting with four laser fields $\vec{E}_p$, $\vec{E}_{c1}$ and $\vec{E}_{c2}(\vec{E}_{c3})$ as shown in Figure 5.1. The spontaneous emission rates from the two nearly degenerate or non degenerate upper states $|4\rangle(|5\rangle)$, to intermediate level $|3\rangle$ are $2\gamma_{43}(2\gamma_{53})$ and that from level $|3\rangle$ to ground level $|2\rangle(|1\rangle)$, is $2\gamma_{32}(2\gamma_{31})$. The four laser fields are given by $\vec{E}_p = \vec{\varepsilon}_p \exp[i(\vec{k}_p.\vec{r}-\omega_p t)] + c.c.$, $\vec{E}_{c1} = \vec{\varepsilon}_{c1}\exp[i(\vec{k}_{c1}.\vec{r}-\omega_{c1}t)] + c.c$ and $\vec{E}_{c2}(\vec{E}_{c3}) = \vec{\varepsilon}_{c2}\exp[i(\vec{k}_{c2}.\vec{r}-\omega_{c2}t)] + c.c, (\vec{\varepsilon}_{c3}\exp[i(\vec{k}_{c3}.\vec{r}-\omega_{c3}t)] + c.c.,)$. The weak probe laser field $\vec{E}_p$ of frequency ω_p, wave vector $\vec{k}_p$ and Rabi frequency $\Omega_p = (\vec{\mu}_{31}.\vec{\varepsilon}_p)/\hbar$ is applied to the $|1\rangle \rightarrow |3\rangle$ transition. The transition $|2\rangle \rightarrow |3\rangle$ is being driven by coupling laser field $\vec{E}_{c1}$ of frequency ω_{c1}, wave vector $\vec{k}_{c1}$ with Rabi frequency $\Omega_{c1} = (\vec{\mu}_{32}.\vec{\varepsilon}_{c1})/\hbar$ and transitions $|3\rangle \rightarrow |4\rangle(|3\rangle \rightarrow |5\rangle)$ are driven by $\vec{E}_{c2}(\vec{E}_{c3})$ of frequency ω_{c2} (ω_{c3}),

wave vector $\vec{k}_{c2}$ ($\vec{k}_{c3}$) and Rabi frequency $\Omega_{c2}(\Omega_{c3}) = (\vec{\mu}_{34}.\vec{\varepsilon}_{c2})/\hbar((\vec{\mu}_{35}.\vec{\varepsilon}_{c3})/\hbar)$. Here $\vec{\mu}_{31}, \vec{\mu}_{32}$and $\vec{\mu}_{34}(\vec{\mu}_{35})$ are dipole moments of $|3\rangle \rightarrow |1\rangle, |3\rangle \rightarrow |2\rangle$ and $|4\rangle \rightarrow |3\rangle$ ($|5\rangle \rightarrow |3\rangle$) transitions respectively.

5.2.2. Interaction Hamiltonian

Using Eq.(1.15) the interaction Hamiltonian in the interaction picture and under rotating wave approximation is obtained as

$$V^{int} = -\hbar[\Omega_p e^{i(\vec{k}_p.\vec{r}+\Delta_{31}t)}|3\rangle\langle 1| + \Omega_{c1}e^{i(\vec{k}_{c1}.\vec{r}+\Delta_{32}t)}|3\rangle\langle 2| + \Omega_{c2}e^{i(\vec{k}_{c2}.\vec{r}+\Delta_{43}t)}|4\rangle\langle 3| + \Omega_{c3}e^{i(\vec{k}_{c3}.\vec{r}+\Delta_{53}t)}|5\rangle\langle 3| + H.c.], \quad (5.1)$$

where $\Delta_{31} = \omega_{31} - \omega_p$, $\Delta_{32} = \omega_{32} - \omega_{c1}$, $\Delta_{43}(\Delta_{53}) = \omega_{43} - \omega_{c2}(\omega_{53} - \omega_{c3})$ denote the detuning of probe and coupling fields frequencies from the atomic resonance frequencies ω_{31}, ω_{32} , $\omega_{43}(\omega_{53})$ respectively, and $|i\rangle\langle j|$, (i, j =1-5) are the atomic raising or lowering operators.

5.2.3. Density matrix-equations of motion

The equations describing time evolution of the slowly varying components of the density matrix elements $\tilde{\rho}_{jk}$ can now be written using Eqs.(5.1) and (1.18b) in Eq.(1.21) and the following transformations to remove fast oscillating (exponential) terms,

$$\tilde{\rho}_{31}=\rho_{31}e^{-i(k_p.r+\Delta_{31}t)}, \quad (5.2a)$$

$$\tilde{\rho}_{32}=\rho_{32}e^{-i(k_{c1}.r+\Delta_{32}t)}, \quad (5.2b)$$

$$\tilde{\rho}_{43}=\rho_{43}e^{-i(k_{c2}.r+\Delta_{43}t)}, \quad (5.2c)$$

$$\tilde{\rho}_{53}=\rho_{53}e^{-i(k_{c3}.r+\Delta_{53}t)}, \quad (5.2d)$$

$$\tilde{\rho}_{21}=\rho_{21}e^{-i\{(k_p-k_{c1}).r+(\Delta_{31}-\Delta_{32})t\}}, \quad (5.2e)$$

$$\tilde{\rho}_{41}=\rho_{41}e^{-i\{(k_p+k_{c2}).r+(\Delta_{31}+\Delta_{43})t\}}, \quad (5.2f)$$

$$\tilde{\rho}_{42}=\rho_{42}e^{-i\{(k_{c1}+k_{c2}).r+(\Delta_{32}+\Delta_{43})t\}}, \quad (5.2g)$$

$$\tilde{\rho}_{51}=\rho_{51}e^{-i\{(k_p+k_{c3}).r+(\Delta_{31}+\Delta_{53})t\}}, \quad (5.2h)$$

$$\tilde{\rho}_{52}=\rho_{52}e^{-i\{(k_{c1}+k_{c3}).r+(\Delta_{32}+\Delta_{53})t\}}. \quad (5.2i)$$

with phenomenological incorporation of the spontaneous decay in the equations of motion for diagonal and in off-diagonal (coherence) matrix elements, the equations for time evolution of the slowly varying components of the density matrix $\rho(v)$ for atoms with velocity v are obtained as

$$\dot{\tilde{\rho}}_{21}=-[i(\Delta_{31}-\Delta_{32}+(\vec{k}_p-\vec{k}_{c1}).\vec{v})+2\gamma_{21}]\tilde{\rho}_{21}-i\Omega_p\tilde{\rho}_{23}+i\Omega_{c1}^{*}\tilde{\rho}_{31}, \quad (5.3a)$$

$$\dot{\tilde{\rho}}_{31}=-[i(\Delta_{31}+\vec{k}_p.\vec{v})+(\gamma_{31}+\gamma_{32})]\tilde{\rho}_{31}+i\Omega_p(\rho_{11}-\rho_{33}) +i\Omega_{c1}\tilde{\rho}_{21}+i\Omega_{c2}^{*}\tilde{\rho}_{41}+i\Omega_{c3}^{*}\tilde{\rho}_{51}, \quad (5.3b)$$

$$\dot{\tilde{\rho}}_{41}=-[i(\Delta_{31}+\Delta_{43}+(\vec{k}_p+\vec{k}_{c2}).\vec{v})+\gamma_{43}]\tilde{\rho}_{41}-i\Omega_p\tilde{\rho}_{43}+i\Omega_{c2}\tilde{\rho}_{31}+i\Omega_{c3}\tilde{\rho}_{51}, \quad (5.3c)$$

$$\dot{\tilde{\rho}}_{51}=-[i(\Delta_{31}+\Delta_{53}+(\vec{k}_p+\vec{k}_{c3}).\vec{v})+\gamma_{53}]\tilde{\rho}_{51}-i\Omega_p\tilde{\rho}_{53}+i\Omega_{c3}\tilde{\rho}_{31}, \quad (5.3d)$$

$$\dot{\tilde{\rho}}_{32}=-[i(\Delta_{32}+\vec{k}_{c1}.\vec{v})+(\gamma_{31}+\gamma_{32})]\tilde{\rho}_{32}+i\Omega_p\tilde{\rho}_{12} +i\Omega_{c1}(\rho_{22}-\rho_{33})+i\Omega_{c2}^{*}\tilde{\rho}_{42}+i\Omega_{c3}^{*}\tilde{\rho}_{52}, \quad (5.3e)$$

$$\dot{\tilde{\rho}}_{42}=-[i(\Delta_{32}+\Delta_{43}+(\vec{k}_{c1}+\vec{k}_{c2}).\vec{v})+2\gamma_{21}+\gamma_{43}]\tilde{\rho}_{42}-i\Omega_{c1}\tilde{\rho}_{43}+i\Omega_{c2}\tilde{\rho}_{32}, \quad (5.3f)$$

$$\dot{\tilde{\rho}}_{52}=-[i(\Delta_{32}+\Delta_{53}+(\vec{k}_{c1}+\vec{k}_{c3}).\vec{v})+\gamma_{53}]\tilde{\rho}_{52}-i\Omega_{c1}\tilde{\rho}_{53}+i\Omega_{c3}\tilde{\rho}_{32}, \quad (5.3g)$$

$$\dot{\tilde{\rho}}_{43}=-[i(\Delta_{43}+\vec{k}_{c2}.\vec{v})+(\gamma_{43}+\gamma_{32}+\gamma_{31})]\tilde{\rho}_{43}-i\Omega_p^{*}\tilde{\rho}_{41}-i\Omega_{c1}^{*}\tilde{\rho}_{42} +i\Omega_{c2}(\rho_{33}-\rho_{44})-i\Omega_{c3}\tilde{\rho}_{45}, \quad (5.3h)$$

$$\dot{\tilde{\rho}}_{53}=-[i(\Delta_{53}+\vec{k}_{c3}.\vec{v})+(\gamma_{53}+\gamma_{32}+\gamma_{31})]\tilde{\rho}_{53}-i\Omega_p^{*}\tilde{\rho}_{51} -i\Omega_{c1}^{*}\tilde{\rho}_{52}+i\Omega_{c3}(\rho_{33}-\rho_{55})-i\Omega_{c2}\tilde{\rho}_{54}, \quad (5.3i)$$

$$\dot{\rho}_{11}=2\gamma_{21}\rho_{22}+2\gamma_{31}\rho_{33}+i\Omega_p^{*}\tilde{\rho}_{31}-i\Omega_p\tilde{\rho}_{13}, \quad (5.3j)$$

$$\dot{\rho}_{22}=2\gamma_{32}\rho_{33}-2\gamma_{21}\rho_{22}+i\Omega_{c1}^{*}\tilde{\rho}_{32}-i\Omega_{c1}\tilde{\rho}_{23}, \quad (5.3k)$$

$$\dot{\rho}_{33}=2\gamma_{43}\rho_{44}+2\gamma_{53}\rho_{55}-2\gamma_{32}\rho_{33}-\gamma_{31}\rho_{33}+i\Omega_p\tilde{\rho}_{13}+i\Omega_{c1}\tilde{\rho}_{23}+i\Omega_{c2}^{*}\tilde{\rho}_{43} -i\Omega_p^{*}\tilde{\rho}_{31}-i\Omega_{c1}^{*}\tilde{\rho}_{32}-i\Omega_{c2}\tilde{\rho}_{34}-i\Omega_{c3}\tilde{\rho}_{35}+i\Omega_{c3}^{*}\tilde{\rho}_{53}, \quad (5.3l)$$

$$\dot{\rho}_{44}=-2\gamma_{54}\rho_{55}-2\gamma_{43}\rho_{44}-i\Omega_{c2}^{*}\tilde{\rho}_{43}+i\Omega_{c2}\tilde{\rho}_{34}, \quad (5.3m)$$

$$\dot{\rho}_{55}=-2\gamma_{53}\rho_{55}-2\gamma_{45}\rho_{55}-i\Omega_{c3}^{*}\tilde{\rho}_{53}+i\Omega_{c3}\tilde{\rho}_{35}. \quad (5.3n)$$

Our aim is to determine the velocity averaged first-order one-photon coherence $I_{31}=\int\tilde{\rho}_{31}(v)dv^{3}$; the imaginary and the real parts of which describes probe absorption and dispersion respectively, in five level K-type system. We solve the above set of density-matrix equations in the usual limit of a weak probe and an arbitrarily strong coupling (or 'control') fields using the following approach. Initially all the population is in the ground level $|1\rangle$ with a Maxwellian velocity distribution.

We assume the probe to be sufficiently weak so as not to induce any population transfer to upper levels. Thus the zeroth-order solution obtained from Eq.(5.3) in the absence of probe (i.e., putting $\Omega_p = 0$) is

$$\rho_{11}^{0} = M(v), \tag{5.4}$$

and all other zeroth-order matrix elements vanish.

where

$$M(v) = \frac{1}{\bar{v}}\sqrt{\frac{\ln 2}{\pi}}\exp(-\ln 2\frac{v^2}{\bar{v}^2}) \tag{5.5}$$

is the Maxwellian velocity distribution of atoms with $\bar{v} = \sqrt{\ln 2}\, v_{th}$ and $v_{th} = \sqrt{\frac{2k_B T}{m_a}}$ is the most probable thermal velocity at a temperature T of an atom of mass m_a.The relevant first-order (i.e., to leading order in probe amplitude) density-matrix equations are found as

$$\dot{\tilde{\rho}}_{21}^{(1)} = -[i(\Delta_{31} - \Delta_{32} + (\vec{k}_p - \vec{k}_{c1}).\vec{v}) + 2\gamma_{21}]\tilde{\rho}_{21}^{(1)} + i\Omega_{c1}^{*}\tilde{\rho}_{31}^{(1)}, \tag{5.6a}$$

$$\dot{\tilde{\rho}}_{31}^{(1)} = -[i(\Delta_{31} + \vec{k}_p.\vec{v}) + (\gamma_{31}+\gamma_{32})]\tilde{\rho}_{31}^{(1)} + i\Omega_p M(v) + i\Omega_{c1}\tilde{\rho}_{21}^{(1)} + i\Omega_{c2}^{*}\tilde{\rho}_{41}^{(1)} + + i\Omega_{c3}^{*}\tilde{\rho}_{51}^{(1)}, \tag{5.6b}$$

$$\dot{\tilde{\rho}}_{41}^{(1)} = -[i(\Delta_{31} + \Delta_{43} + (\vec{k}_p + \vec{k}_{c2}).\vec{v}) + \gamma_{43}]\tilde{\rho}_{41}^{(1)} + i\Omega_{c2}\tilde{\rho}_{31}^{(1)}, \tag{5.6c}$$

$$\dot{\tilde{\rho}}_{51}^{(1)} = -[i(\Delta_{31} + \Delta_{53} + (\vec{k}_p + \vec{k}_{c3}).\vec{v}) + \gamma_{53}]\tilde{\rho}_{51}^{(1)} + i\Omega_{c3}\tilde{\rho}_{31}^{(1)}, \tag{5.6d}$$

The steady-state solution obtained by setting the time derivates to zero on the left-hand side of Eq.(5.6) yields the one dimensional velocity averaged one-photon coherence as,

$$I_{31}^{(1)} = \int \tilde{\rho}_{31}^{(1)}(v)\, dv^3 = i\,\Omega_p \times \int dv^3\, M(v) \frac{A_{21}(v)A_{41}(v)A_{51}(v)}{A_{21}(v)A_{31}(v)A_{41}(v)A_{51}(v) + A_{41}(v)A_{51}(v)|\Omega_{c1}|^2 + A_{21}(v)A_{51}(v)|\Omega_{c2}|^2 + + A_{21}(v)A_{41}(v)|\Omega_{c3}|^2} \tag{5.7}$$

where

$$A_{21}(v) = i\{\Delta_{31} - \Delta_{32} + (\vec{k}_p - \vec{k}_{c1}).\vec{v}\} + 2\gamma_{21}, \tag{5.8a}$$

$$A_{31}(v) = i(\Delta_{31} + \vec{k}_p.\vec{v}) + (\gamma_{31}+\gamma_{32}), \tag{5.8b}$$

$$A_{41}(v) = i\{\Delta_{31} + \Delta_{43} + (\vec{k}_p + \vec{k}_{c2}).\vec{v}\}+\gamma_{43}, \quad (5.8c)$$

$$A_{51}(v) = i\{\Delta_{31} + \Delta_{53} + (\vec{k}_p + \vec{k}_{c3}).\vec{v}\}+\gamma_{53}. \quad (5.8d)$$

In the above equations $2\gamma_{ij}$ are the spontaneous emission rates from level $|i\rangle \rightarrow |j\rangle$ (i, j = 1- 5). In experimental situations typically one considers an arrangement of probe $\vec{E}_p$ and coupler fields $\vec{E}_{c1}$ ($\vec{E}_{c2}$ and $\vec{E}_{c3}$) co (counter)-propagating along z axis. For this experimental configuration we can henceforth set the terms $(\vec{k}_p - \vec{k}_{c1}).\vec{v} = (k_p - k_{c1})v_z$, $(\vec{k}_p + \vec{k}_{cj}).\vec{v} = (k_p - k_{cj})v_z$, (where j = 2,3) and $\vec{k}_p.\vec{v} = k_p v_z$ in Eq.(5.8) and consequently the velocity integration in Eq.(5.7) reduces to a one-dimensional integral over velocity v_z.

5.2.4. Susceptibility and Absorption coefficient

The susceptibility of the medium is related to the velocity averaged one-photon coherence as follows:

$$\chi = N\frac{|\mu_{31}|^2}{\hbar\gamma_D}\left(\frac{I_{31}^{(1)}}{\Omega_p/\gamma_D}\right), \quad (5.9)$$

where N is the atomic density of the vapor and $\gamma_D (= k_p\bar{v})$ is the Doppler width in the system. As is well known, the imaginary ($Imag(\chi)$) and real ($Re(\chi)$) parts respectively of the susceptibility χ give the absorption and dispersion of the probe field. The probe absorption coefficient is given by

$$\alpha_p = -\frac{8\pi^2}{\lambda_p} Imag(\chi). \quad (5.9a)$$

5.3. Analytical Results

5.3.1. Radiatively (homogenously) broadened medium

We analyze probe absorption (transparency) characteristics to arrive at conditions for EIT in a radiatively (homogenously) broadened medium. Result for this case can be derived from Eq.(5.9) by dropping velocity dependent terms and performing the velocity integration using Eq.(5.5) as follows:

$$\frac{I_{31}^{(1)}}{\Omega_p} = \frac{i}{(\gamma_{31}+\gamma_{32}) + i\Delta_{31} + \frac{|\Omega_{c1}|^2}{2\gamma_{21}+i(\Delta_{31}-\Delta_{32})} + \frac{|\Omega_{c2}|^2}{\gamma_{43}+i(\Delta_{31}+\Delta_{43})} + \frac{|\Omega_{c3}|^2}{\gamma_{53}+i(\Delta_{31}+\Delta_{53})}} \quad (5.10)$$

The above expression reveals the existence of *three* two-photon resonances in probe absorption profile as a function of probe detuning. Evidently the one occurring at $\Delta_{31} = \Delta_{32}$ corresponds to $|1\rangle \rightarrow |3\rangle \rightarrow |2\rangle$ transitions of Λ-type atom, whereas the other occurring at $\Delta_{31} = -\Delta_{43}(-\Delta_{53})$ corresponds to $|1\rangle \rightarrow |3\rangle \rightarrow |4\rangle$ ($|1\rangle \rightarrow |3\rangle \rightarrow |5\rangle$) transitions of the two distinct ladder systems. Thus the five level K-system derives contributions from three-level lamda (Λ) system and two distinct three-level cascade subsystems which can be strongly coupled or decoupled by manipulating the coupling field detunings or Rabi frequencies. For instance let us consider the case, in which all the three coupling fields have same detuning given by, $\Delta\,(= \Delta_{32} = -\Delta_{43}(-\Delta_{53}))$. In this case a single two photon resonance that occurs at $\Delta_{31} = \Delta$ has contributions from all the three subsystems. For this case it is also clear from expression Eq.(5.10) that if the Rabi frequencies of the coupling fields are sufficiently large, so that the following criterion is met:

$$(\gamma_{31} + \gamma_{32}) \ll \frac{|\Omega_{c1}|^2}{2\gamma_{21}} + \frac{|\Omega_{c2}|^2}{\gamma_{43}} + \frac{|\Omega_{c3}|^2}{\gamma_{53}}, \tag{5.11}$$

the probe absorption is considerably reduced at the position of the two photon resonance $\Delta_{31} = \Delta$. Furthermore, in the exact resonance case, that is, when the coupling fields are tuned to exact resonance $\Delta_{32} = \Delta_{43}(\Delta_{53}) = 0$, the EIT resonance is centered around the probe detuning $\Delta_{31} = 0$. Implementation of the criterion specified in Eq.(5.11) would require choosing either very large $|\Omega_{c1}|^2$, $|\Omega_{c2}|^2(|\Omega_{c3}|^2)$ or very small γ_{21} and $\gamma_{43}(\gamma_{53})$. Since at higher powers of the coupling fields, resolution of the Autler Townes (AT) doublet [12] which arise from splitting of the intermediate level $|3\rangle$ tends to obfuscate EIT effects, it is essential to choose systems in which two photon dephasing parameters $2\gamma_{21}$ and $\gamma_{43}(\gamma_{53})$ are very small in order to enable observation of EIT.

On the other hand when detuning of the coupling fields are different, corresponding to lamda and equal detuning of two ladder systems i.e., $\Delta_{32} \neq \Delta$, $\Delta_{43} = \Delta_{53} = -\Delta$, the K-system reduces to four-level inverted Y-type system composed of three-level lamda system driven by Rabi frequency Ω_{c1} and a typical three-level ladder system driven by the effective Rabi frequency $\Omega_c = \sqrt{|\Omega_{c2}|^2 + |\Omega_{c3}|^2}$ respectively. The inverted Y-type system decouples into two

distinct subsystems because tuning the probe frequency detuning to two-photon resonance of a particular (say Λ) subsystem will render the other (Ξ) subsystem non-resonant with a large detuning.

When detuning of all the three coupling fields are different, $\Delta_{32} \neq \Delta_{43} \neq \Delta_{53}$ the three subsystems are decoupled [13, 14, 15] because tuning the probe frequency detuning to a particular two-photon resonance will render the other two subsystems non-resonant with a large detuning. Eq.(5.10) shows that then the contribution from non-resonant term can be ignored and consequently the K system reduces to a single three level lamda and two distinct three level cascade systems with absorption and dispersion properties governed by the Rabi frequency and two-photon dephasing rate in that corresponding system.

5.3.2. Doppler broadened medium

When the medium is Doppler broadened the two photon detuning is affected by residual Doppler broadening. The result for a Doppler broadened K system is obtained from Eqs.(5.7) and Eq.(5.8) for co and counter-propagating (along z axis) coupling and probe fields configuration as

$$\frac{I_{31}^{(1)}}{\Omega_p} = \int \tilde{\rho}_{31}^{(1)}(v_z)\, dv_z = \int dv_z M(v_z) \times \frac{i}{(\gamma_{31}+\gamma_{32}) + i(\Delta_{31}+k_p v_z) + \frac{|\Omega_{c1}|^2}{2\gamma_{21}+i(\Delta_{31}-\Delta_{32})+i(k_p-k_{c1})v_z} + \frac{|\Omega_{c2}|^2}{\gamma_{43}+i(\Delta_{31}+\Delta_{43})+i(k_p-k_{c2})v_z} + \frac{|\Omega_{c3}|^2}{\gamma_{53}+i(\Delta_{31}+\Delta_{53})+i(k_p-k_{c3})v_z}} \quad (5.12)$$

Comparing above result (Eq.(5.12)) with that of a radiatively broadened case given by Eq.(5.10), we can draw the following inferences:

(A). Various wave-vector mismatch regimes:

(i). Perfect wave-vector matching:

For the case of perfect wave-vector matching the two photon resonances are Doppler free, i.e., $(k_p - k_{c1})v_z = (k_p - k_{c2})v_z = (k_p - k_{c3})v_z = 0$. Under this case the Eq.(5.12) reduced to

$$\frac{I_{31}^{(1)}}{\Omega_p} = \int \tilde{\rho}_{31}^{(1)}(v_z)\, dv_z = \int dv_z M(v_z) \times \frac{i}{(\gamma_{31}+\gamma_{32}) + i(\Delta_{31}+k_p v_z) + \frac{|\Omega_{c1}|^2}{2\gamma_{21}+i(\Delta_{31}-\Delta_{32})} + \frac{|\Omega_{c2}|^2}{\gamma_{43}+i(\Delta_{31}+\Delta_{43})} + \frac{|\Omega_{c3}|^2}{\gamma_{53}+i(\Delta_{31}+\Delta_{53})}} \quad (5.13)$$

The criterion for observing of probe transparency at the location of two photon resonance$(\Delta = \Delta_{32} = -\Delta_{43}(-\Delta_{53}))$ is still given by Eq.(5.11) but with radiative width $(\gamma_{31} + \gamma_{32})$ replaced by the Doppler width γ_D, i. e.,

$$\gamma_D \ll \frac{|\Omega_{c1}|^2}{2\gamma_{21}} + \frac{|\Omega_{c2}|^2}{\gamma_{43}} + \frac{|\Omega_{c3}|^2}{\gamma_{53}}, \quad (5.14)$$

(ii). Partial wave-vector mismatch case:

It however remains to be seen what happens when the probe and coupling wave-vectors differ from each other. Inspection of Eq.(5.12) shows that if we consider a system in which the upper levels $|4\rangle$ and $|5\rangle$ are very close with similar decay rates, we can approximately write $\Delta_c\ (= \Delta_{43} \cong \Delta_{53})$, $k_c\ (= k_{c2} \cong k_{c3})$ and $\gamma_c\ (= \gamma_{43} \cong \gamma_{53})$. We can also neglect the small two-photon residual Doppler width of the lamda subsystem $(k_p - k_{c1})v_z$ compared with a large two-photon residual Doppler width created by dual ladder subsystem in five level K-type system. Using these facts in Eq.(5.8) and through Eq.(5.7) we obtain

$$\frac{I_{31}^{(1)}}{\Omega_p} = \int \tilde{\rho}_{31}^{(1)}(v_z)\, dv_z = \int dv_z M(v_z) \times \frac{i}{(\gamma_{31}+\gamma_{32}) + i(\Delta_{31}+k_p v_z) + \frac{|\Omega_{c1}|^2}{2\gamma_{21}+i(\Delta_{31}-\Delta_{32})} + \frac{|\Omega_{c2}|^2+|\Omega_{c3}|^2}{\gamma_c+i(\Delta_{31}+\Delta_c)+i(k_p-k_c)v_z}} \quad (5.15)$$

Inspection of above Eq.(5.15) reveals as anticipated above that the five level K-type system reduces to four level inverted Y-type system composed of lamda subsystem interacting with coupling field Ω_{c1} and a typical ladder subsystem interacting with effective Rabi frequency $\Omega_c = \sqrt{|\Omega_{c2}|^2 + |\Omega_{c3}|^2}$.

(iii). Complete wave-vector mismatch case:

For the case of complete wave-vector mismatch, the two photon resonances are not Doppler-free in both the ladder subsystems and are distinct i.e.,$(k_p - k_{c2})v_z \neq (k_p - k_{c3})v_z \neq 0$. In this case from Eq.(5.12) we observe that the five-level

K-type system can be considered as a combination of two four level subsystems of: either a Y and an inverted-Y type configurations or inverted-Y-type configurations.

(B). Detuning of the coupling fields:

(i) When detuning of the coupling fields are same (exact resonance case), that is, when the coupling fields are tuned to exact resonance $\Delta_{32} = \Delta_{43} = \Delta_{53} = 0$, the EIT resonance is centered around the probe detuning $\Delta_{31} = 0$. (a) In perfect wave-vector matching case a single transparency window which accrue around the exact probe resonance ($\Delta_{31} = 0$). (b) In partial wave-vector mismatch case overlapping of a narrow transparency window caused by lamda system in a wide transparency widow caused by ladder system. (c) In complete wave-vector mismatch case overlapping of a narrow transparency window caused by lamda system in a further splitting wide transparency widow caused by dual cascade system.

(ii) When detuning of the coupling fields are different, $\Delta_{32} \neq \Delta_{43} \neq \Delta_{53}$the three subsystems are decoupled. The probe absorption profile then displays three distinct two-photon resonances corresponding to the individual lamda and dual cascade systems.

5.4. Numerical results and discussions

It is seen from Figure 5.1 that in a closed five-level atomic system of K-type configuration, levels $|1\rangle$, $|2\rangle$ and $|3\rangle$ form a three-level Λ- configuration. Level $|4\rangle$ ($|5\rangle$) together with levels $|1\rangle$, $|3\rangle$ are in a usual three level ladder-type configuration. In which the intermediate level ($|3\rangle$) of three level ladder-type atoms is coupled with a higher-excited ($|5\rangle$) and ground level ($|2\rangle$) by two strong laser (coupling) fields, from this structure K-type configuration can be consider as a composition of two four-level inverted-Y type systems. (And also in the absence of field acting between $|3\rangle \rightarrow |2\rangle$ the system reduced to four level systems in Y type configuration and in the absence of field acting between $|4\rangle \rightarrow |3\rangle$ ($|5\rangle \rightarrow |3\rangle$) the system reduced to four level systems in inverted Y type configuration). This situation can be realized, for example, considering the transitions $5S_{1/2}(F=1) \rightarrow 5P_{3/2} \rightarrow 5S_{1/2}$ (F=2) forms three

level lamda system and $5S_{1/2}(F=1) \rightarrow 5P_{3/2} \rightarrow 5D_{3/2}$ ($5S_{1/2}(F=1) \rightarrow 5P_{3/2} \rightarrow 5D_{5/2}$ /$7S_{1/2}$) forms three level ladder systems in five-level K-type configuration in Rubidium atom. The level separation wavelength of the lower levels $5S_{1/2}$ (F=1) ($5S_{1/2}$ (F=2)) and intermediate level $5P_{3/2}$ is λ_p = 780.0268nm ($\lambda_{c1} \simeq$ 780.0268nm) (D2 transition) and those of the intermediate and upper transitions $5D_{3/2}$ ($5D_{5/2}$) are λ_{c2} (λ_{c3}) = 775.9436nm (775.7650nm), in case of upper transition $7S_{1/2}$ the level separation wavelength is λ_{c3} = 740.817 nm. The wavelength mismatch between the counter-propagating coupling ($\vec{E}_{c2}$ and $\vec{E}_{c3}$) and probe ($\vec{E}_p$) fields when the upper transitions are $5D_{3/2}(5D_{5/2})$ in five level K-type EIT system introduces a residual Doppler width $(k_p - k_{cj})\bar{v} / k_p\bar{v} \simeq -0.005$ (where j = 2, 3), in case of upper transition $7S_{1/2}$ the residual Doppler width $(k_p - k_{c3})\bar{v} / k_p\bar{v} \simeq -0.05$. For comparison purpose the other case of matched $(k_p - k_{cj})$ wave-vector is also considered hypothetically for this K-type atomic system. In our numerical calculation all parameters are expressed in units of Doppler width $\gamma_D / 2\pi = 250MHz$, i.e., $2\gamma_{21} / \gamma_D = 0.000004$, $2\gamma_{31} / \gamma_D = 2\gamma_{32} / \gamma_D = 0.012$, $2\gamma_{43} / \gamma_D = 0.0003$ and the spontaneous decay rate $2\gamma_{53} / \gamma_D = 0.00171(0.00286)$ in case of $5D_{5/2}$ ($7S_{1/2}$).

Various four and five level EIT systems

Depending on the choice of coupling (control) fields acting between the atomic transition levels we consider the following different four and five level EIT systems.

(i) Four level Y-type system:

From Figure 5.1 we observe that in a closed five-level atomic system of K-type configuration, absence of field acting between levels $|3\rangle \rightarrow |2\rangle$ the system reduces to four-level systems of Y-type configuration. The four-level Y-type system has one stable ground state $|1\rangle$, an intermediate level $|3\rangle$ and two either nearly degenerate or non degenerate $|4\rangle$ ($|5\rangle$) states. The intermediate state $|3\rangle$ is coupled to the excited state $|4\rangle$ ($|5\rangle$) by a strong coupling field with the Rabi frequency Ω_{c2}(Ω_{c3}) while the ground level $|1\rangle$ is coherently connected to the intermediate level $|3\rangle$ by a weak probe field with the Rabi frequency Ω_p.

In Figure 5.2 Probe absorption $\left[\mathrm{Im}\left(I_{31}^{(1)}\gamma_D/\Omega_p\right)\right]$ is plotted as a function of the probe field detuning for various cases of coupling and probe field wave-vector mismatches. The coupling fields are on resonance ($\Delta_{43} = \Delta_{53} = 0$) and the Rabi frequencies are chosen equal ($\Omega_{c2} = \Omega_{c3}$).

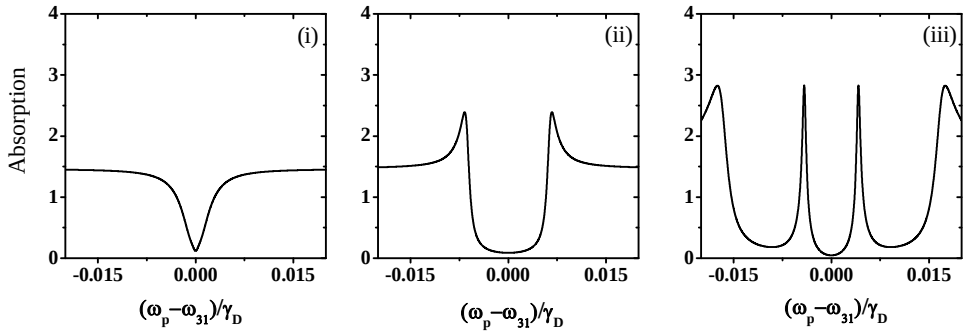

Figure 5.2: Probe absorption as a function of the probe field detuning ($\omega_p - \omega_{31})/\gamma_D$ with coupling field Rabi frequencies $\Omega_{c1} = 0.0$, $\Omega_{c2} = \Omega_{c3} = (2\pi \times 8\,MHz)$ for various wave-vector mismatch case which occur in dual cascade (i) $k_p = k_{c2} = k_{c3}$ (ii) $k_p - k_{c2} = k_p - k_{c3} = -0.005\,k_p$ (iii) $k_p - k_{c2} = -0.005\,k_p$, $k_p - k_{c3} = -0.05\,k_p$. The coupling fields are at exact resonance, $\Delta_{32} = \Delta_{43} = \Delta_{53} = 0$.

From above figure we observe the No complete transparency occurs in (i) perfect wave-vector matching $(k_p = k_{c2} = k_{c3})$ case where the level separation wavelengths are assumed equal for probe and both the coupling fields. For (ii) partial wave-vector mismatch $(k_p \neq k_{c2} = k_{c3})$, the wavelength of both the coupling fields are taken equal and differing with probe wavelength. In this case we observe a wide and almost complete transparency window compared with earlier case. In both the cases ((i) and (ii)) the four level Y-type system reduces to typical three-level cascade system interacting with effective Rabi frequency $\Omega_c = \sqrt{|\Omega_{c2}|^2 + |\Omega_{c3}|^2}$, the former is Doppler-free and the latter residual Doppler broadened typical three level cascade medium. (iii) In complete wave-vector mismatching $(k_p \neq k_{c2} \neq k_{c3})$, the wavelength of both the coupling fields are not equal and differ from probe wavelength. In this case we observe an interesting result where the single wide transparency window of case (ii) splits into three windows with large transparency at

exact resonance of the probe field. This structure arises as the narrower transparency window of the ladder subsystem (with smaller negative wavevector) occurs between the much wider transparency window of the large negative wavevector mismatched ladder subsystem.

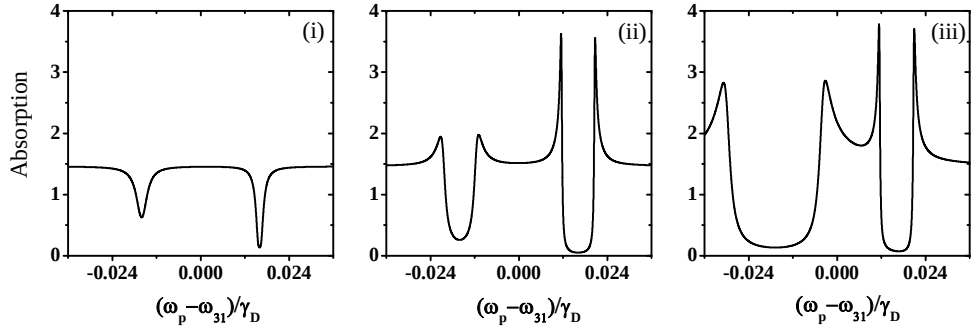

Figure 5.3: Probe absorption as a function of the probe field detuning ($\omega_p - \omega_{31})/\gamma_D$ with coupling field Rabi frequencies $\Omega_{c1} = 0.0$, $\Omega_{c2} = \Omega_{c3} = (2\pi \times 8\,MHz)$ for various wave-vector mismatch case which occur in dual cascade, (i) $k_p = k_{c2} = k_{c3}$ (ii) $k_p - k_{c2} = k_p - k_{c3} = -0.005\,k_p$, (iii) $k_p - k_{c2} = -0.005k_p$, $k_p - k_{c3} = -0.05k_p$. The coupling fields detuning chosen are ($\Delta_{43} = -\Delta_{53} = (2\pi \times 4MHz)$).

We now consider the finite detuning case when the coupling fields are detuned on either side of the intermediate level ($|3\rangle$). Figure 5.3 shows the probe absorption $\left[\mathrm{Im}\,(I_{31}^{(1)}\gamma_D/\Omega_p)\right]$ variation as the probe frequency is tuned through the coupling field detuning for various wave-vector mismatch cases, (i) $k_p = k_{c2} = k_{c3}$ (ii) $k_p - k_{c2} = k_p - k_{c3} = -0.005k_p$ (iii) $k_p - k_{c2} = -0.005k_p$, $k_p - k_{c3} = -0.05k_p$. The probe absorption profile for this case splits into two distinct transparency windows corresponding to two distinct cascade subsystems. The transparency window occurring at the two-photon resonance $\Delta_{31} + \Delta_{43}$ corresponds to the $5S_{1/2}(F=1)\rightarrow 5P_{3/2}\rightarrow 5D_{3/2}$ transition, whereas the other occurring at $\Delta_{31} + \Delta_{53}$ corresponds to the $5S_{1/2}(F=1)\rightarrow 5P_{3/2}\rightarrow 5D_{5/2}/7S_{1/2}$ transitions. Since these two cascade subsystems are decoupled, the depth and width of each transparency window is now governed by the two-photon dephasing rate parameter and the coupling field Rabi frequency in that particular subsystem. The asymmetry in the depth and width of

the transparency in the two windows occurs as the two-photon decay rates, two-photon residual Doppler width present in each of the subsystems of the Y-system.

(ii) Four level inverted Y-type system:

Figure 5.1 shows that in a closed five-level atomic system of K-type configuration, absence of field acting between the transition $|4\rangle \rightarrow |3\rangle$ ($|5\rangle \rightarrow |3\rangle$) reduces the system to four-level systems in inverted Y type configuration. The levels $|1\rangle$, $|2\rangle$ and $|3\rangle$ form a three-level Λ- configuration and level $|4\rangle/|5\rangle$ together with levels $|1\rangle$, $|3\rangle$ are in a usual three level ladder-type configuration. The intermediate state $|3\rangle$ is coupled to the hyperfine splitting of a ground state (excited) $|2\rangle$ ($|4\rangle/|5\rangle$) by a strong coupling field with the Rabi frequency Ω_{c1} (Ω_{c2}/Ω_{c3}) while another hyperfine splitting of a ground state $|1\rangle$ is coherently connected to the intermediate state $|3\rangle$ by a low-intensity (weak) probe field with the Rabi frequency Ω_p.

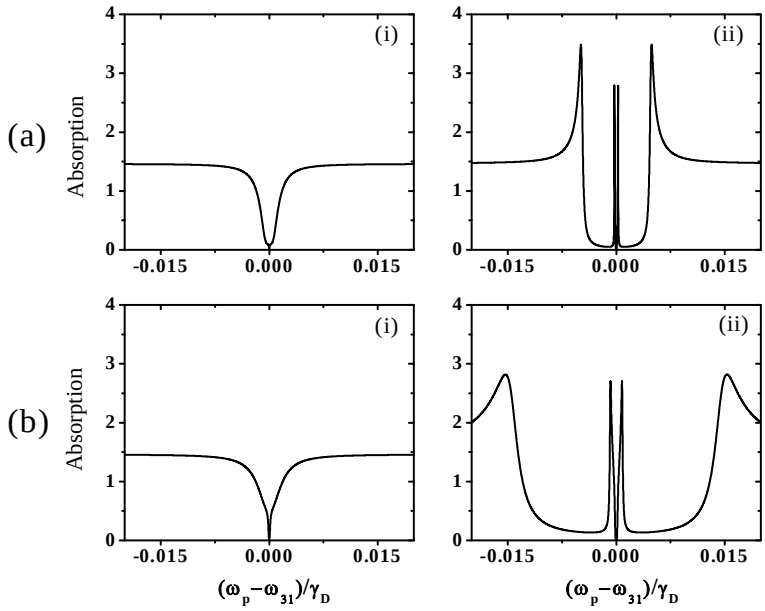

*Figure 5.4: Probe absorption as a function of the probe field detuning ($\omega_p - \omega_{31})/\gamma_D$ with coupling field Rabi frequencies **(a).** $\Omega_{c1} = (2\pi \times 4\,MHz)$, $\Omega_{c2} = (2\pi \times 8\,MHz)$, $\Omega_{c3} = 0.0$ **(b).** $\Omega_{c1} = (2\pi \times 4\,MHz)$, $\Omega_{c2} = 0.0$, $\Omega_{c3} = (2\pi \times 8\,MHz)$, for various wave-vector mismatch cases which occur in cascade subsystem of inverted Y-system, (i) $k_p = k_{c2}$ ($k_p = k_{c3}$), (ii) $k_p - k_{c2} = -0.005k_p$ ($k_p - k_{c3} = -0.05k_p$). The coupling fields are on resonance ($\Delta_{32} = \Delta_{43}(\Delta_{53}) = 0$).*

In Figure 5.4 probe absorption $\left[\mathrm{Im}\left(I_{31}^{(1)}\gamma_D/\Omega_p\right)\right]$ is plotted as a function of the probe field detuning for various cases of coupling and probe field wave-vector mismatches which occur through three level cascade subsystem in inverted Y system. Here two higher excited states $5D_{3/2}/5D_{5/2}$ and $7S_{1/2}$ form two ladder subsystems with the ground state $5S_{1/2}$(F=1) through the intermediate level $5P_{3/2}$. For ladder subsystem with excited state $5D_{3/2}/5D_{5/2}$ the wave-vector mismatch between probe and coupling field is, $k_p - k_{c2} = -0.005k_p$, whereas for the other ladder subsystem with excited state $7S_{1/2}$, the wave-vector mismatch is, $k_p - k_{c3} = -0.05k_p$. The absorption profiles are shown for excited state $5D_{3/2}/5D_{5/2}$ in Figure 5.4(a) and for excited state $7S_{1/2}$ in Figure 5.4(b). The coupling fields are on resonance ($\Delta_{32} = \Delta_{43} = \Delta_{53} = 0$) and the Rabi frequencies are chosen as $\Omega_{c1}\,(= \Omega_{c2}/2 = \Omega_{c3}/2\,)$ in Figures 5.4a and 5.5b. A complete and single transparency window (i) in perfect wave-vector matching $k_p = k_{c2} = k_{c3}$, in this case we assume the level separation wavelengths for probe and coupling fields are equal. (ii) In wave-vector mismatching $\left(k_p \neq k_{c2}(k_{c3})\right)$, the wavelength of the coupling field differing with probe wavelength. In this case we observe a splitting of a wide transparency window into three windows, the middle transparency at exact resonance of the probe field is due three level lamda system formed by $5S_{1/2}$(F=1)$\rightarrow 5P_{3/2} \rightarrow 5S_{1/2}(F = 2)$ transitions which occurs around probe resonance within the wide transparency window of the three level ladder system formed by the transitions $5S_{1/2}$(F=1) $\rightarrow 5P_{3/2} \rightarrow 5D_{3/2}/5D_{5/2}(7S_{1/2})$.

Figure 5.5 shows the probe absorption $\left[\mathrm{Im}\left(I_{31}^{(1)}\gamma_D/\Omega_p\right)\right]$ variation as the probe frequency is tuned through the coupling field detuning for various wave-vector mismatch cases (i) $k_p = k_{c2}$ $(k_p = k_{c3})$, (ii) $k_p - k_{c2} = -0.005k_p$ $(k_p - k_{c3} = -0.05k_p)$ occurred in inverted Y-type system. The transitions levels considered same as in Figure 5.4, the absorption profiles shown for excited state $5D_{3/2}/5D_{5/2}$ in Figure 5.5(a) and for excited state $7S_{1/2}$ in Figure 5.5(b). Consider the coupling fields detuning are, $\Delta_{32} = \Delta_{43}(\Delta_{53}) = 2\pi \times 3\mathrm{MHz}(2\pi \times 15\mathrm{MHz})$ and the Rabi frequencies are chosen as $\Omega_{c1}\,(= \Omega_{c2}/2 = \Omega_{c3}/2)$ in Figures 5.5a and 5.5b. The

probe absorption profile for this case splits into two distinct transparency windows corresponding to two distinct three level subsystems in lamda and ladder configurations.

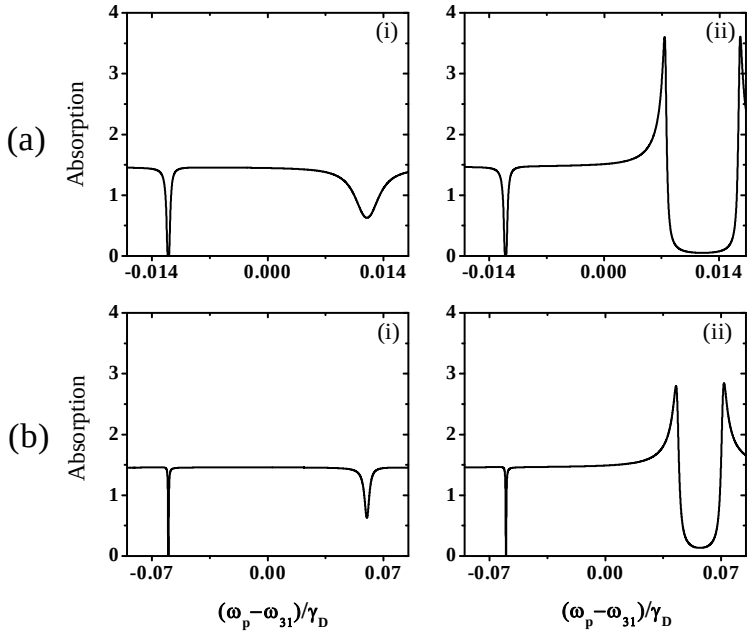

Figure 5.5: Probe absorption as a function of the probe field detuning ($\omega_p - \omega_{31})/\gamma_D$ with coupling field Rabi frequencies ***(a).*** *$\Omega_{c1} = (2\pi \times 4\,MHz)$, $\Omega_{c2} = (2\pi \times 8\,MHz)$, $\Omega_{c3} = 0.0$ **(b).** $\Omega_{c1} = (2\pi \times 4\,MHz)$, $\Omega_{c2} = 0.0$, $\Omega_{c3} = (2\pi \times 8\,MHz)$, for various wave-vector mismatch cases which occur in cascade subsystem of inverted Y-system, (i) $k_p = k_{c2}$ $(k_p = k_{c3})$, (ii) $k_p - k_{c2} = -0.005k_p$ $(k_p - k_{c3} = -0.05k_p)$. The coupling fields detuning chosen are $(\Delta_{32} = \Delta_{43}(\Delta_{53}) = 2\pi \times 3MHz(2\pi \times 15MHz)$.*

In above figure the transparency window occurring at the two-photon resonance $\Delta_{31} - \Delta_{32}$ corresponds to the $5S_{1/2}$(F=1)→$5P_{3/2}$→$5S_{1/2}$(F = 2) transition, whereas the other occurring at $\Delta_{31} + \Delta_{43}(\Delta_{53})$ corresponds to the $5S_{1/2}$(F=1)→$5P_{3/2}$→$5D_{3/2}/5D_{5/2}(7S_{1/2})$ transitions. Since these two subsystems are decoupled, the depth and width of each transparency window is now governed by the two-photon dephasing rate parameter, two-photon residual Doppler width and the coupling field Rabi frequency in that particular subsystem.

(iii) Five level K-type system:

The Five-level (K-type) atomic medium where the intermediate level in a ladder-type atom is coupled with a higher-excited and ground levels by two strong laser (coupling) fields as shown in Figure 5.1. The intermediate state $|3\rangle$ is coupled to the excited state $|4\rangle$ ($|5\rangle$) by a strong coupling field with the Rabi frequency $\Omega_{c2}(\Omega_{c3})$ and also coupled to the hyperfine splitting of a ground state $|2\rangle$ by a strong coupling field with the Rabi frequency Ω_{c1}, while another hyperfine splitting of a ground state $|1\rangle$ is coherently connected to the intermediate state $|3\rangle$ by a weak probe field with the Rabi frequency Ω_p.

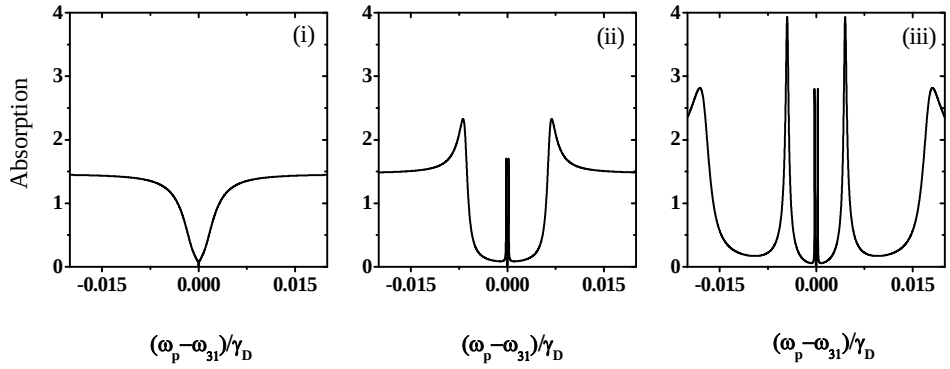

Figure 5.6: Probe absorption as a function of the probe field detuning ($\omega_p - \omega_{31})/\gamma_D$ with coupling field Rabi frequencies $\Omega_{c1} = (2\pi \times 4\,MHz)$, $\Omega_{c2} = \Omega_{c3} = (2\pi \times 8\,MHz)$ for various wave-vector mismatch case which occur in dual cascade of K-type system, (i) $k_p = k_{c2} = k_{c3}$ (ii) $k_p - k_{c2} = k_p - k_{c3} = -0.005k_p$ (iii) $k_p - k_{c2} = -0.005k_p, k_p - k_{c3} = -0.05k_p$.The coupling fields are on resonance ($\Delta_{32} = \Delta_{43} = \Delta_{53} = 0$).

In Figure 5.6 Probe absorption $\left[\mathrm{Im}\,(I_{31}^{(1)}\gamma_D/\Omega_p)\right]$ is displayed as a function of the probe field detuning for various cases of coupling and probe field wave-vector mismatches. The coupling fields are on resonance ($\Delta_{32} = \Delta_{43} = \Delta_{53} = 0$) and the Rabi frequencies are chosen as $\Omega_{c1} = \Omega_{c2}/2 = \Omega_{c3}/2$. A complete and single transparency window is observed (i) in perfect wave-vector matching $(k_p = k_{c2} = k_{c3})$ case where it is assumed that the level separation wavelengths for probe and both the coupling fields are equal. (ii) In partial wave-vector mismatching $(k_p \neq k_{c2} = k_{c3})$, the wavelength of both the coupling fields equal and differing with probe wavelength. In

this case we observe a wide and almost complete transparency window splitting in to three windows. In this case the five level K-type system reduces to typical four level inverted Y-type system interacting with effective Rabi frequency $\Omega_c = \sqrt{|\Omega_{c2}|^2 + |\Omega_{c3}|^2}$ between upper transitions and intermediate level, $|\Omega_{c1}|$ coupling field interacting between intermediate level ($|3\rangle$) and hyperfine splitting of ground state ($|2\rangle$). (iii) In complete wave-vector mismatching $(k_p \neq k_{c2} \neq k_{c3})$, the wavelength of both the coupling fields are not equal and differ from probe wavelength. In this case we observe an interesting result where the single wide transparency window splitting into five windows with large transparency at exact resonance of the probe field.

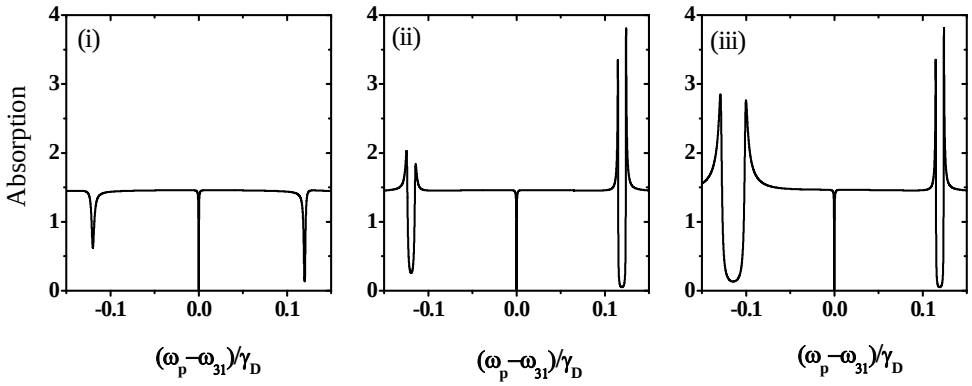

Figure 5.7: Probe absorption as a function of the probe field detuning ($\omega_p - \omega_{31})/\gamma_D$ with coupling field Rabi frequencies $\Omega_{c1} = (2\pi \times 4\,MHz)$, $\Omega_{c2} = \Omega_{c3} = (2\pi \times 8\,MHz)$ for various wave-vector mismatch case which occur in dual cascade of K-type system, (i) $k_p = k_{c2} = k_{c3}$ (ii) $k_p - k_{c2} = k_p - k_{c3} = -0.005k_p$ (iii) $k_p - k_{c2} = -0.005k_p, k_p - k_{c3} = -0.05k_p$. The coupling fields detuning chosen are ($\Delta_{32} = 0.0, \Delta_{43} = -\Delta_{53} = (2\pi \times 30MHz)$.

We now consider the finite detuning case when the coupling fields Ω_{c2}, Ω_{c3} are detuned on either side of the intermediate level ($|3\rangle$), Figure 5.7 shows the probe absorption $\left[\mathrm{Im}\,(I_{31}^{(1)}\gamma_D/\Omega_p)\right]$ variation as the probe frequency is tuned through the coupling field detuning for various wave-vector mismatch cases, (i) $k_p = k_{c2} = k_{c3}$ (ii) $k_p - k_{c2} = k_p - k_{c3} = -0.005k_p$ (iii) $k_p - k_{c2} = -0.005k_p, k_p - k_{c3} = -0.05k_p$. The probe absorption profile for this case splits into three distinct transparency

windows corresponding to three level lamda subsystem and two distinct three level cascade subsystems. The transparency window corresponding to three level lamda subsystem occurring at the two-photon resonance $\Delta_{31} - \Delta_{32}$ corresponds to the $5S_{1/2}(F=1) \rightarrow 5P_{3/2} \rightarrow 5S_{1/2}(F = 2)$ transition and the other transparency windows corresponding to cascade subsystems occurring at the two-photon resonance $\Delta_{31} + \Delta_{43}(\Delta_{31} + \Delta_{53})$ corresponds to the $5S_{1/2}(F=1) \rightarrow 5P_{3/2} \rightarrow 5D_{3/2}$ ($5S_{1/2}(F=1) \rightarrow 5P_{3/2} \rightarrow 5D_{5/2}/7S_{1/2}$) transition. Since these three subsystems are decoupled, the depth and width of each transparency window is now governed by the two-photon dephasing rate parameter and the coupling field Rabi frequency in that particular subsystem. The asymmetry in the depth and width of the transparency windows either side of middle window occurs as the two-photon decay rates, two-photon residual Doppler width dissimilar in the dual cascade of present K-system.

5.5. Conclusion

We have studied the electromagnetically-induced transparency (EIT) of a probe field in both homogeneously (radiative) and Doppler broadened five-level K-type atomic system driven by three strong laser (coupling) fields and in four-level systems Y-type, inverted Y-type driven by two strong laser (coupling) fields. Effect of wave-vector mismatch on EIT occurring when the frequency of coupling fields is equal, higher or lesser than that of the probe field frequency. Depending upon the choices of control fields transitions in multilevel atomic systems, we consider three wave-vector mismatch regimes: (i) perfect wavelength matching regime ($\lambda_p = \lambda_{c2} = \lambda_{c3}$) (ii) partial wavelength mismatching regime ($\lambda_p \neq \lambda_{c2} = \lambda_{c3}$) and (iii) complete wavelength mismatching regime ($\lambda_p \neq \lambda_{c2} \neq \lambda_{c3}$). The multilevel atomic systems such as five-level and four-level configurations are consisting of two or more than two different EIT sub-systems, yet we find that on (coupler-atom) resonance, the EIT response of the composite system can be dramatically distinct and more complicated than those of the constituent systems. For large field frequency detuning, we get the two or three well-separated usual EIT profiles of the constituent systems of multilevel atomic systems. This suggests that this unusual behavior at exact resonance is due to further interference between the regimes of overlap of the very narrow absorption

profile of the Λ-type system with the very wide transparency window created by the ladder type constituent systems of multi-level atomic configurations. Such systems might be useful in any EIT-based optical switching device as control and variation of EIT are the main features of these systems.

5.6. References

1. D. J. Fulton, S. Shepherd, R. R. Moseley, B. D. Sinclair and M. H. Dunn, Phys. Rev. A **52**, 2302 (1995).

2. S. E. Harris, J. E. Field and A. Imamoglu, Phys. Rev. Lett. **64**, 1107 (1990)*;* P. R. Hemmer, D. P. Katz, J. Donoghue, M. Cronin-Golomb, M. S. Shahriar and P. Kumar, Opt. Lett. **20**, 982 (1995).

3. C. Ottaviani, D. Vitali, M. Artoni, F. Cataliotti and P. Tombesi, Phys. Rev. Lett. **90**, 197902 (2003).

4. G.S. Agarwal and W. Harshawardhan, Phys. Rev. Lett. **77**,1039 (1996); J. Y. Gao, S. H. Yang, D. Wang, X. Z. Guo, K. X. Chen, Y. Jiang and B. Zhao, Phys. Rev. A **61**, 023401(2000).

5. M. Yan, E. G. Rickey and Y. Zhu, Phys. Rev. A **64**, 043807 (2001).

6. V. Bharti and A. Wasan, Opt. Comm. **324**, 238 (2014).

7. K. I. Osman, S. S. Hassan and A. Joshi, Eur. Phys. J. D **54**, 119 (2009).

8. B. P. Hou, S. J. Wang, W. L. Yu and W. L. Sun, Phys. Lett. A **352**, 462 (2006).

9. N. Li, Z. Zhao, H. Chen, P. Li, Y. Li, Y. Zhao, G. Zhou, S. Jia and Y. Zhang, Opt. Ex. **20**, 1912 (2012).

10. J. Gea-Banacloche, Y. Q. Li, S. Z. Jin and M. Xiao, Phys. Rev. A **51**, 576 (1995); J. R. Boon, E. Zekou, D. McGloin and M. H. Dunn, *ibid.* **59**, 4675 (1999).

11. S. Shepherd, D. J. Fulton and M. H. Dunn, Phys. Rev. A **54**, 5394 (1996); A. B. Mirza and Suneel Singh, Phys. Rev. A **85**, 053837 (2012).

12. S. H. Autler and C. H. Townes, Phys. Rev. **100**, 703 (1955).

13. G. S. Agarwal and W. Harshawardhan, Phys. Rev. Lett. **77**, 1039 (1996).

14. Y. Zhang, A. W. Brown and M. Xiao, Phys. Rev. Lett. **99**, 123603 (2007).

15. Y. Zhang, B. Anderson, A.W. Brown and M. Xiao, Appl. Phys. Lett. **91**, 061113 (2007).

Chapter 6

Conclusions and Future scope

6.1. Summary and Conclusions

In this thesis, we have studied the phenomenon of electromagnetically induced transparency (EIT) and EIT assisted process of nonlinear generation such as four wave mixing (FWM) in multilevel atomic systems formed by inclusion of an additional level in three level lamda (Λ), vee (V) and cascade (ladder- Ξ) systems, such as four level Y-type atomic system, four-level double-ladder and five level K-type systems. We have studied the modification of EIT and its applications due to effect of various broadening mechanisms: homogeneous (radiative) and Doppler broadening that are present in a medium.

In this context we have shown explicitly how different types of residual Doppler widths of two-photon coherence as well as the Doppler broadening of one-photon coherences arising due to random thermal motion of atoms in a gaseous medium can significantly affect EIT and the associated nonlinear processes. Considering thermal motion of atoms (with velocity component v_z) along the z-direction of propagation of the counter-propagating probe and coupler fields. More specifically, the effect of residual Doppler broadening on EIT is demonstrated for various wave-vector mismatches occurring when the wavenumber k_c (or k_m) of strong coupling (or pump) field is equal ($k_c = k_p$), higher ($k_c > k_p$), or lesser ($k_c < k_p$) than that of the probe field wavenumber. The first chapter of this thesis

provides the literature review and theoretical background concepts related to the present work.

In Chapter 2, we have study the transparency of a weak probe field in a four-level Y-type atomic system with dual ladder-type EIT scheme, interacting with two strong coupling laser fields. The crucial dependence of the nature of EIT on the type of the wave-vector mismatch, originating from the wavelength (frequency) difference between the probe and coupling fields in Doppler broadening medium is illustrated in detail. We have demonstrated that negative residual Doppler broadening case (i.e.,$k_c > k_p$) is actually conducive for the observation of transparency in Doppler broadened four level Y-type atomic systems. The absorption profile of a weak probe field displays very wide and almost complete single or double EIT windows whose width, depth and location depend upon the wave-vector mismatch, Rabi frequencies, and atom field detuning of the coupling fields. Analytical results are also obtained to explain these interesting features.

In Chapter 3, we explore the feasibility of attaining simultaneous electromagnetically induced transparency and efficient nonlinear generation in a different configuration of Doppler broadened diamond (double-cascade) systems. We presented the systematic study of the influence of various system parameters (dipole moments, level decay rates, transition frequencies) and driving (pump and coupling) field strength and wavenumber mismatch on absorption (loss) and nonlinear generation (gain) coefficients, which govern the propagation characteristics of the weak (probe and signal) fields in the Doppler broadened medium. We show that EIT and nonlinear generation efficiency depend critically on the type of residual Doppler broadenings present in each of the two cascade subsystems constituting the diamond system. Further it is observed that nonlinear generation with perfect EIT simultaneously in both subsystems is not possible as the process of nonlinear generation actually tends to oppose EIT. Furthermore we show how with suitable choice of the driving field strengths, sufficiently large nonlinear gain can be produced to offset the high absorption losses and create a steady state (equilibrium) situation in the medium. Under these conditions both probe and the signal fields propagate in the medium without further attenuation or gain.

In Chapter 4, we propose a simple and easy to implement scheme for generating superluminal (and subluminal) light propagation of both probe and signal fields in a radiative and Doppler broadened double ladder system driven by two strong laser (pump and coupler) fields. The proposed scheme is easier to implement compared with other existing schemes for superluminal propagation as it is based on generation of nonlinear gain large enough to compensate for the absorption losses. This can be done simply by appropriate choice of strengths of the strong pump and coupler fields. Under these conditions similar to that in Chapter 3 we observe that a steady state (equilibrium) situation in the medium is created where both probe and signal fields are matched in intensity and propagate at either superluminal or subluminal speeds without attenuation or gain in the medium.

In Chapter 5, we investigate the electromagnetically-induced transparency (EIT) of a probe field in a five-level K-type and in four-level Y-type, inverted Y-type systems driven by strong laser (coupling) fields. We consider the three wave-vector mismatch regimes: (i) perfect wavelength matching regime ($\lambda_p = \lambda_{c2} = \lambda_{c3}$) (ii) partial wavelength mismatching regime ($\lambda_p \neq \lambda_{c2} = \lambda_{c3}$) and (iii) complete wavelength mismatching regime ($\lambda_p \neq \lambda_{c2} \neq \lambda_{c3}$). We observed the typical collective and overlapping behavior of EIT characteristics on (coupler-atom) resonance in the Doppler broadened atomic vapor in the partial and complete wavelength mismatching regimes as compared to the perfect wavelength matching regime. Furthermore we observed under the influence of the coherent coupling fields, the steady-state linear susceptibility of the probe laser shows that the systems can have single, double or triple EIT windows whose width, depth, and location depend upon the wave-vector mismatch, Rabi frequencies and atom field detuning of the coupling fields.

6.2. Future scope

The formulation presented in this thesis may be extended to other complicated EIT systems and their utilization for practical applications. The dependence of absorption profiles on the wavelength mismatch of laser fields can be studied in various multi-level systems. Especially in negative wavevector mismatch case; which is essential for propagation of very short laser pulses through an inhomogeneously

broadened medium. The reported multi-level atomic systems in this thesis may present the single, double or triple EIT windows, it might be useful in any EIT-based optical switching device as control and variation of EIT which are the main features of these systems.

The multi-level systems reported in this thesis can be studied with the inclusion of spontaneously generated coherence (SGC) and vacuum-induced coherence (VIC) effects, which may affect the absorption properties of multi-level systems. The various systems studied in this thesis were under weak probe conditions where they behave like a closed system. These studies on the considered systems can also be extended under strong probe field conditions where the systems behave like open systems. This open system may affect the optical properties of multi-level atomic systems. Such studies can be of our future interests as an extension to this work.

The multi-level systems which are reported in this thesis may also be realized in solid state materials, such as quantum dots and rare earth doped $LaCl_3$ and LaF_3, which have properties similar to atomic vapors. So it is possible to study the optical properties of such solid state materials.

List of Publications

Journal Publications:

1. **Azeem B. Mirza** and Suneel Singh "Wave-vector mismatch effects in electromagnetically induced transparency in Y-type systems" Phys. Rev. A **85**, 053837 (2012).
2. **Azeem B. Mirza** and Suneel Singh "Electromagnetically induced transparency and steady-state propagation characteristics in Doppler broadened diamond systems" J. Mod. Opt. **62**, 16 (2015).
3. **Azeem B. Mirza** and Suneel Singh "Electromagnetically induced transparency in Doppler broadened five-level systems" Pramana **82**, 295 (2014).
4. **Azeem B. Mirza** and Suneel Singh "Subluminal and Superluminal light propagation in double ladder configuration" to be submitted

Conference Proceedings:

1. **Azeem B. Mirza** and Suneel Singh "Electromagnetically induced transparency in Doppler broadened inverted Y-type systems" in International Conference on Fiber Optics and Photonics, OSA Technical Digest (online) (Optical Society of America, 2012), paper TPo.40

International and National Conference Attended:

1. **Azeem B. Mirza** and Suneel Singh "Electromagnetically induced transparency and four wave mixing in a Doppler broadened diamond system" International Conference on Quantum Optics and Quantum Computing (ICQOQC-2011) conference held on March 24-26 of 2011 at Noida in Delhi.[Poster Presentation]
2. **Azeem B. Mirza** and Suneel Singh "Electromagnetically induced transparency in a Doppler broadened Y-type system" Proc of XXXVI OSI Symposium on Frontiers in Optics and Photonics (FOP11), Symposium held on December 3-5, 2011 at New Delhi. [Poster Presentation]

3. **Azeem B. Mirza** and Suneel Singh "Electromagnetically induced transparency and four wave mixing in a Doppler broadened diamond system" Frontiers in Physics Symposium held on October 28 – 29, 2011 at School of Physics, University of Hyderabad, India.[Poster Presentation]
4. **Azeem B. Mirza** and Suneel Singh "Electromagnetically induced transparency in Doppler broadened inverted Y-type systems" Photonics-2012(International Conference on Fiber Optics and Photonics) conference, held on December 9-12, 2012 at IIT-Madras, India.[Poster Presentation]
5. **Azeem B. Mirza** and Suneel Singh "Electromagnetically induced transparency in Doppler broadened five-level systems" 21st DAE-BRNS National Laser Symposium (NLS-21) Symposium, held on February 6-9, 2013 at BARC-Mumbai.[Poster Presentation]